

International Ocean Discovery Program

Expedition 374 Preliminary Report

Ross Sea West Antarctic Ice Sheet History

**Ocean-ice sheet interactions and West Antarctic Ice Sheet
vulnerability: clues from the Neogene and Quaternary record
of the outer Ross Sea continental margin**

4 January–8 March 2018

Robert M. McKay, Laura De Santis, Denise K. Kulhanek, and the Expedition 374 Scientists



Publisher's notes

Core samples and the wider set of data from the science program covered in this report are under moratorium and accessible only to Science Party members until 10 August 2019.

This publication was prepared by the *JOIDES Resolution* Science Operator (JRSO) at Texas A&M University (TAMU) as an account of work performed under the International Ocean Discovery Program (IODP). Funding for the program is provided by the following international partners:

National Science Foundation (NSF), United States
Ministry of Education, Culture, Sports, Science and Technology (MEXT), Japan
European Consortium for Ocean Research Drilling (ECORD)
Ministry of Science and Technology (MOST), People's Republic of China
Korea Institute of Geoscience and Mineral Resources (KIGAM)
Australian/New Zealand Consortium (ANZIC)
Ministry of Earth Sciences (MoES), India
Coordination for Improvement of Higher Education Personnel (CAPES), Brazil

Portions of this work may have been published in whole or in part in other IODP documents or publications.

Disclaimer

Any opinions, findings, and conclusions or recommendations expressed in this publication are those of the author(s) and do not necessarily reflect the views of the participating agencies, TAMU, or Texas A&M Research Foundation.

Copyright

Except where otherwise noted, this work is licensed under the Creative Commons Attribution 4.0 International (CC BY 4.0) license (<https://creativecommons.org/licenses/by/4.0/>). Unrestricted use, distribution, and reproduction are permitted, provided the original author and source are credited.



Citation

McKay, R.M., De Santis, L., Kulhanek, D.K., and the Expedition 374 Scientists, 2018. *Expedition 374 Preliminary Report: Ross Sea West Antarctic Ice Sheet History*. International Ocean Discovery Program, 374.
<https://doi.org/10.14379/iodp.pr.374.2018>

ISSN

World Wide Web: 2372-9562

Expedition 374 participants

Expedition 374 scientists

Robert M. McKay

Co-Chief Scientist

Antarctic Research Centre
Victoria University of Wellington
New Zealand
robert.mckay@vuw.ac.nz

Laura De Santis

Co-Chief Scientist

Geophysics Division
Istituto Nazionale di Oceanografia e di Geofisica Sperimentale
(OGS)
Italy
ldesantis@inogs.it

Denise K. Kulhanek

Expedition Project Manager/Staff Scientist

International Ocean Discovery Program
Texas A&M University
USA
kulhanek@iodp.tamu.edu

Jeanine L. Ash

Sedimentologist

Department of Earth, Environmental and Planetary Sciences
Rice University
USA
jeanine.ash@rice.edu

François Beny

Physical Properties Specialist

Laboratoire d'Océanologie et de Géosciences
Université de Lille I
France
beny.francois@gmail.com

Imogen M. Browne

Physical Properties Specialist

College of Marine Science
University of South Florida, St. Petersburg
USA
imogenbrowne@mail.usf.edu

Giuseppe Cortese

Paleontologist (radiolarians)

Paleontology Department
GNS Science
New Zealand
g.cortese@gns.cri.nz

Isabela M. Cordeiro de Sousa

Sedimentologist

Instituto de Geociencias
Universidade de Brasília
Brazil
isabelasousa@unb.br

Justin P. Dodd

Inorganic Geochemist

Geology and Environmental Geosciences
Northern Illinois University
USA
jdodd@niu.edu

Oliver M. Esper

Palynologist

Marine Geology
Helmholtz Centre for Polar and Marine Research
Alfred Wegener Institute
Germany
oliver.esper@awi.de

Jenny A. Gales

Physical Properties Specialist/Downhole Measurements

School of Biological & Marine Sciences
Plymouth University
United Kingdom
jenny.gales@plymouth.ac.uk

David M. Harwood

Paleontologist (diatoms)

Earth and Atmospheric Sciences
University of Nebraska, Lincoln
USA
dharwood1@unl.edu

Saki Ishino

Sedimentologist

Department of Earth and Planetary Sciences
Nagoya University
Japan
ishino.saki@b.mbox.nagoya-u.ac.jp

Benjamin A. Keisling

Sedimentologist

Department of Geosciences
University of Massachusetts, Amherst
USA
bkeisling@geo.umass.edu

Sookwan Kim

Physical Properties Specialist

Division of Polar-Earth System Sciences
Korea Polar Research Institute
Republic of Korea
skwan@kopri.re.kr

Sunghan Kim

Sedimentologist

Division of Polar Climate Change
Korea Polar Research Institute
Republic of Korea
delongksh@kopri.re.kr

Jan Sverre Laberg
Sedimentologist

Department of Geosciences
 University of Tromsø - the Arctic University of Norway
 Norway
jan.laberg@uit.no

R. Mark Leckie
Paleontologist (foraminifers)

Department of Geosciences
 University of Massachusetts, Amherst
 USA
mleckie@geo.umass.edu

Juliane Müller
Organic Geochemist

Marine Geology
 Helmholtz Centre for Polar and Marine Research
 Alfred Wegener Institute
 Germany
juliane.mueller@awi.de

Molly O. Patterson
Sedimentologist

Geological Sciences and Environmental Studies
 Binghamton University, State University of New York
 USA
patterso@binghamton.edu

Brian W. Romans

Physical Properties Specialist/Downhole Measurements

Department of Geosciences
 Virginia Tech
 USA
romans@vt.edu

Oscar E. Romero

Paleontologist (diatoms)

MARUM—Center for Marine Environmental Sciences
 University of Bremen
 Germany
oromero@uni-bremen.de

Francesca Sangiorgi

Palynologist

Department of Earth Sciences
 Utrecht University
 The Netherlands
f.sangiorgi@uu.nl

Osamu Seki

Organic Geochemist

Institute of Low Temperature Science
 Hokkaido University
 Japan
seki@pop.lowtem.hokudai.ac.jp

Observer

John L. Powell
Weather/Ice Observer

Canada
jpowell@ns.sympatico.ca

Amelia Shevenell
Sedimentologist

College of Marine Science
 University of South Florida, St. Petersburg
 USA
ashevenell@usf.edu

Shiv M. Singh
Sedimentologist

Polar Biology Lab
 National Centre for Antarctic and Ocean Research (NCAOR)
 India
smsingh@ncaor.gov.in
 Also at:
 Department of Botany
 Institute of Science
 Banaras Hindu University
 India
drshivmohansingh@gmail.com

Saiko Sugisaki
Paleomagnetist

Marine Geology Research Group
 Geological Survey of Japan, AIST
 Japan
s.sugisaki@aist.go.jp

Tina van de Flierdt
Inorganic Geochemist

Department of Earth Science & Engineering
 Imperial College London
 United Kingdom
tina.vandeflierdt@imperial.ac.uk

Tim E. van Peer
Paleomagnetist

National Oceanography Centre Southampton
 University of Southampton
 United Kingdom
T.E.vanPeer@soton.ac.uk

Wenshen Xiao

Paleontologist (diatoms)

State Key Laboratory of Marine Geology
 Tongji University
 China
wxiao@tongji.edu.cn

Zhifang Xiong

Inorganic Geochemist

First Institute of Oceanography
 State Oceanic Administration
 China
zhfxiong@fio.org.cn

Education and outreach

Rosa Hughes-Currie

Educator

Massey High School

New Zealand

rosahughescurrie@gmail.com

Kimberly A. Kenny

Videographer

USA

kimberlyannekenny@gmail.com

Agnès Pointu

Educator

Lycée Louis de Broglie

France

agnes.pointu@gmail.com

Operational and technical staff

Siem Offshore AS officials

Terry Skinner

Master of the Drilling Vessel

James Samuel McLelland

Drilling Supervisor

JRSO shipboard personnel and technical representatives

Gary D. Acton

Manager of Technical and Analytical Services

Margaret Hastedt

Assistant Laboratory Officer

Alexis Armstrong

X-ray Laboratory

Brittany Martinez

Curatorial Specialist

Heather Barnes

Assistant Laboratory Officer

Zenon Mateo

Underway Geophysics Laboratory

Timothy Blaisdell

Application Developer

Stephen Midgley

Operations Superintendent

Michael Cannon

Marine Computer Specialist

Erik Moortgat

Chemistry Laboratory

Etienne Claassen

Marine Instrumentation Specialist

Chieh Peng

Laboratory Officer

William Crawford

Senior Imaging Specialist

Vincent Percuoco

Chemistry Laboratory

Seth Frank

Thin Section Laboratory

Kerry Swain

Schlumberger Logging Engineer

Sheryl Frazier

Physical Properties Laboratory

Steven Thomas

Marine Computer Specialist

Edwin Garrett

Paleomagnetism Laboratory

Rui Wang

Applications Developer

Rachael Gray

Core Laboratory

Jean Wulfson

Publications Specialist

Abstract

The marine-based West Antarctic Ice Sheet (WAIS) is currently retreating due to shifting wind-driven oceanic currents that transport warm waters toward the ice margin, resulting in ice shelf thinning and accelerated mass loss of the WAIS. Previous results from geologic drilling on Antarctica's continental margins show significant variability in marine-based ice sheet extent during the late Neogene and Quaternary. Numerical models indicate a fundamental role for oceanic heat in controlling this variability over at least the past 20 My. Although evidence for past ice sheet variability has been collected in marginal settings, sedimentologic sequences from the outer continental shelf are required to evaluate the extent of past ice sheet variability and the associated oceanic forcings and feedbacks. International Ocean Discovery Program Expedition 374 drilled a latitudinal and depth transect of five drill sites from the outer continental shelf to rise in the eastern Ross Sea to resolve the relationship between climatic and oceanic change and WAIS evolution through the Neogene and Quaternary. This location was selected because numerical ice sheet models indicate that this sector of Antarctica is highly sensitive to changes in ocean heat flux. The expedition was designed for optimal data-model integration and will enable an improved understanding of the sensitivity of Antarctic Ice Sheet (AIS) mass balance during warmer-than-present climates (e.g., the Pleistocene "super interglacials," the mid-Pliocene, and the late early to middle Miocene). The principal goals of Expedition 374 were to

- Evaluate the contribution of West Antarctica to far-field ice volume and sea level estimates;
- Reconstruct ice-proximal atmospheric and oceanic temperatures to identify past polar amplification and assess its forcings and feedbacks;
- Assess the role of oceanic forcing (e.g., sea level and temperature) on AIS stability/instability;
- Identify the sensitivity of the AIS to Earth's orbital configuration under a variety of climate boundary conditions; and
- Reconstruct eastern Ross Sea paleobathymetry to examine relationships between seafloor geometry, ice sheet stability/instability, and global climate.

To achieve these objectives, we will

- Use data and models to reconcile intervals of maximum Neogene and Quaternary Antarctic ice advance with far-field records of eustatic sea level change;
- Reconstruct past changes in oceanic and atmospheric temperatures using a multiproxy approach;
- Reconstruct Neogene and Quaternary sea ice margin fluctuations in datable marine continental slope and rise records and correlate these records to existing inner continental shelf records;
- Examine relationships among WAIS stability/instability, Earth's orbital configuration, oceanic temperature and circulation, and atmospheric $p\text{CO}_2$; and
- Constrain the timing of Ross Sea continental shelf overdeepening and assess its impact on Neogene and Quaternary ice dynamics.

Expedition 374 was carried out from January to March 2018, departing from Lyttelton, New Zealand. We recovered 1292.70 m of high-quality cores from five sites spanning the early Miocene to late Quaternary. Three sites were cored on the continental shelf (Sites

U1521, U1522, and U1523). At Site U1521, we cored a 650 m thick sequence of interbedded diamictite, mudstone, and diatomite, penetrating the Ross Sea seismic Unconformity RSU4. The depositional reconstructions of past glacial and open-marine conditions at this site will provide unprecedented insight into environmental change on the Antarctic continental shelf during the early and middle Miocene. At Site U1522, we cored a discontinuous upper Miocene to Pleistocene sequence of glacial and glaciomarine strata from the outer shelf, with the primary objective to penetrate and date seismic Unconformity RSU3, which is interpreted to represent the first major continental shelf-wide expansion and coalescing of marine-based ice streams from both East and West Antarctica. At Site U1523, we cored a sediment drift located beneath the westerly flowing Antarctic Slope Current (ASC). Cores from this site will provide a record of the changing vigor of the ASC through time. Such a reconstruction will enable testing of the hypothesis that changes in the vigor of the ASC represent a key control on regulating heat flux onto the continental shelf, resulting in the ASC playing a fundamental role in ice sheet mass balance.

We also cored two sites on the continental slope and rise. At Site U1524, we cored a Plio–Pleistocene sedimentary sequence on the continental rise on the levee of the Hillary Canyon, which is one of the largest conduits of Antarctic Bottom Water delivery from the Antarctic continental shelf into the abyssal ocean. Drilling at Site U1524 was intended to penetrate into middle Miocene and older strata but was initially interrupted by drifting sea ice that forced us to abandon coring in Hole U1524A at 399.5 m drilling depth below seafloor (DSF). We moved to a nearby alternate site on the continental slope (U1525) to core a single hole with a record complementary to the upper part of the section recovered at Site U1524. We returned to Site U1524 3 days later, after the sea ice cleared. We then cored Hole U1524C with the rotary core barrel with the intention of reaching the target depth of 1000 m DSF. However, we were forced to terminate Hole U1524C at 441.9 m DSF due to a mechanical failure with the vessel that resulted in termination of all drilling operations and a return to Lyttelton 16 days earlier than scheduled. The loss of 39% of our operational days significantly impacted our ability to achieve all Expedition 374 objectives as originally planned. In particular, we were not able to obtain the deeper time record of the middle Miocene on the continental rise or abyssal sequences that would have provided a continuous and contemporaneous archive to the high-quality (but discontinuous) record from Site U1521 on the continental shelf. The mechanical failure also meant we could not recover sediment cores from proposed Site RSCR-19A, which was targeted to obtain a high-fidelity, continuous record of upper Neogene and Quaternary pelagic/hemipelagic sedimentation. Despite our failure to recover a shelf-to-rise transect for the Miocene, a continental shelf-to-rise transect for the Pliocene to Pleistocene interval is possible through comparison of the high-quality records from Site U1522 with those from Site U1525 and legacy cores from the Antarctic Geological Drilling Project (ANDRILL).

Introduction

Drilling Ross Sea outer continental shelf-to-rise sedimentary sequences recovered a direct record of Neogene to Quaternary Antarctic Ice Sheet (AIS) evolution to improve understanding of climate forcings/feedbacks relating to ice sheet variability. In combination with model sensitivity tests, tectonic considerations, and the well-developed seismic stratigraphic framework of the Ross Sea,

the cores will enable researchers to determine if estimates of large far-field Neogene sea level variability (20–60 m) (cf. Miller et al., 2005, 2012; Naish and Wilson, 2009) reflect changes in Antarctic ice volume (Figures F1, F2, F3). The continental shelf-to-rise transect in an area of demonstrated climate sensitivity (Figure F4) will allow for improved understanding of ocean–ice sheet interactions on orbital to million year timescales.

The onset of the Neogene (23 Ma; Oligocene/Miocene [O/M] boundary) is characterized by an abrupt increase in Antarctic ice volume attributed to changes in Earth's orbital parameters (Zachos et al., 1997; Naish et al., 2001) and declining atmospheric CO₂ (Figure F1) (Pagani et al., 2005; Foster and Rohling, 2013). Following a period of cooler climates in the early Miocene relative to the Oligocene, both near- and far-field proxy records indicate a period of sustained (~3°C warmer than present; You et al., 2009) warmth and carbon cycle reorganization (e.g., Vincent and Berger, 1985; Foster et al., 2012) referred to as the Middle Miocene Climatic Optimum (MMCO; ~17–15 Ma) (Flower and Kennett, 1994; Shevenell et al., 2004), and significant polar amplification of temperature is suggested (Shevenell et al., 2004, 2008; Lewis et al., 2008; Warny et al., 2009; Feakins et al., 2012; Sangiorgi et al., 2018). The MMCO was immediately followed by an interval of Antarctic ice growth and cooling termed the Middle Miocene Climate Transition (MMCT; 14.2–13.8 Ma), which can be observed in both far-field benthic foraminifer δ¹⁸O records and ice-proximal data (Figure F1B) (Kennett, 1977; Flower and Kennett, 1994; Zachos et al., 2001; Shevenell et al., 2004, 2008; Holbourn et al., 2007; Cramer et al., 2009; John et al., 2011; Sangiorgi et al., 2018). The MMCT may have resulted in the extinction of the Antarctic tundra vegetation (Lewis et al., 2008). Although ice expansion has traditionally been inferred in East Antarctica, Ross Sea seismic evidence also suggests West Antarctic Ice Sheet (WAIS) expansion during the MMCT (Bart, 2003). However, the timing of the Ross Sea event, WAIS development, and forcings and feedbacks involved in the MMCT remain enigmatic, as does the subsequent climate and ice sheet history of the sparsely sampled late Miocene (De Santis et al., 1995; Zachos et al. 2001). During the mid-Pliocene, global sea levels were thought to be ~20 ± 10 m above present-day levels, indicating a reduction/collapse of both the Greenland Ice Sheet and the WAIS (Miller et al., 2012). Ice-proximal sedimentary facies indicate orbitally paced advances and retreats of the WAIS from the early Pliocene (Figures F4) that occur until at least 1.0 Ma. However, equivocal evidence exists for WAIS collapse as recently as the last interglacial, and obtaining paleoclimate records of the late Pleistocene in the Ross Sea was a high priority for International Ocean Discovery Program (IODP) Expedition 374 (Scherer et al., 1998; Kopp et al., 2009; Naish et al., 2009; McKay et al., 2012b; Dahl-Jensen et al., 2013).

Background

Oceanographic setting

Much of the abyssal ocean is presently filled with cold, dense water produced in the large polynyas of the Weddell and Ross Seas and mixed with ambient water. Thus, changes in temperature and/or meltwater input to the Ross Sea could disrupt global meridional overturning circulation (MOC) (Jacobs et al., 2002; Orsi and Wiederwohl, 2009; Purkey and Johnson, 2010). Over the past 40 y, Ross Sea–derived Antarctic Bottom Water (AABW) has freshened as a result of increased meltwater input to the Amundsen and Bellingshausen Seas from melting ice shelves/glacial systems (Jacobs et al., 2002, 2011).

Unlike the Amundsen and Bellingshausen Seas, where the Antarctic Circumpolar Current (ACC) impinges the continental shelf and cross-shelf bathymetry encourages the presence of relatively warm Circumpolar Deep Water (CDW) on the inner shelf, the eastern limb of the Ross Gyre brings cooler Modified Circumpolar Deep Water (MCDW) to the Ross Sea along the lower continental slope (Whitworth et al., 1995; Orsi and Wiederwohl, 2009). The strong westward-flowing Antarctic Slope Current (ASC), which has a sharp subsurface front (Antarctic Slope Front), separates Antarctic Surface Water (AASW) on the shelf from MCDW on the lower continental slope (Figure F5). This front serves as a dynamic barrier that limits the transfer of CDW and MCDW onto the Ross Sea continental shelf (Ainley and Jacobs, 1981). Thus, ASC vigor and the formation of fresh AASW regulate the volume of MCDW on the Ross Sea continental shelf.

Geological setting and previous drilling

The breakup of Gondwana during the Middle Jurassic began with the initiation of the West Antarctic Rift, which led to the opening of the Ross Sea (Behrendt et al., 1991) and the development of three sedimentary basins (Figures F2, F3) (Cooper et al., 1991). The westernmost Victoria Land Basin (VLB) was the focus of previous regional geological drilling (e.g., Dry Valley Drilling Project [DVDP], McMurdo Sound Sediments and Tectonics Study [MSSTS-1], Cenozoic Investigations in the Western Ross Sea [CIROS-1 and CIROS-2], Cape Roberts Project [CRP], and the Antarctic Geological Drilling Project [ANDRILL]). Expedition 374 focused on the Eastern Basin, which encompasses the Glomar Challenger Basin and contains as much as 6 km of Cenozoic sediment infill (Figure F3).

The basement geology of the Ross Sea Central High adjacent to the Eastern Basin was penetrated at Deep Sea Drilling Project (DSDP) Site 270 and consists of high-grade Paleozoic calcareous metamorphic rocks (Ford and Barrett, 1975) that were mylonitized during Late Cretaceous uplift (Siddoway et al., 2004). Upper Cretaceous mylonites were also recovered from the western part of the Eastern Basin (Luyendyk et al., 2001). The lack of basement younger than Devonian at CRP-3 and Site 270 suggests that younger Permian–Triassic Beacon Supergroup strata are likely absent in the western (and eastern) Ross Sea. This interpretation is supported by paleogeographic maps from Barrett (1981), which suggest that the western (and eastern) Ross Sea was likely an area of uplift and erosion through much of the Permian–Triassic, although these maps are poorly constrained. The Devonian (lower part) of the Beacon Supergroup is dominated by coarse clastics (Barrett, 1981). The tectonic models for the formation of the Ross Sea, through the thinning of thickened (~40 km) crust that covered the entire Transantarctic Mountain (TAM)–Ross Sea–Marie Byrd Land region (Karner et al., 2005; Decesari et al., 2007), would also tend to argue against the preservation of younger Beacon strata because uplift and erosion of large amounts of strata would be predicted during early rifting, and this rifting would likely include the removal of any upper Beacon Supergroup strata even if they had been present. Consequently, this rifting would result in a very different provenance signature for glacial deposits transported from the western Ross Sea compared with the eastern Ross Sea.

The Antarctic Offshore Stratigraphy (ANTOSTRAT) seismic stratigraphic scheme defines eight seismic units (RSS-1 through RSS-8) in the sediment infill lying above the basement that are bounded by six major shelf-wide unconformities (RSU1 through RSU6) (Figures F3, F6; Table T1) (Brancolini et al., 1995; De Santis

et al., 1995), but their ages were only partially constrained by drilling (see synthesis by Bart and De Santis, 2012). In the eastern Ross Sea, CIROS-1 and CRP-3 indicate marine-terminating glaciation in the TAM by the earliest Oligocene (Barrett, 1989, 2007). In the central Ross Sea, seismic-based reconstructions suggest ice caps nucleated on the subaerially elevated basement highs in the central Ross Sea during the Oligocene. The adjacent deep-water basins in the outer Ross Sea appear to have remained free of grounded ice until the late Oligocene, although they were probably influenced by voluminous sediment-laden meltwater discharge under a more temperate style of glacial sedimentation, resulting in progressive shoaling of the Eastern Basin as accommodation space was filled (Shipboard Scientific Party, 1975a; De Santis et al., 1995). Expedition 374 seeks to constrain the ages of Unconformities RSU4 through RSU1 to understand how they relate to the evolution of the marine-based WAIS.

Strata (Unit RSS-1) underlying seismic Unconformity RSU6 are the oldest and deepest basin infill sedimentary packages in the central Ross Sea. Unit RSS-1 is divided into a lower and upper package. The lower part of Unit RSS-1 has not been drilled, whereas the upper part was drilled in the western Ross Sea (CRP and CIROS-1) and consists of upper Eocene to Oligocene high-energy fluvial, deltaic, and shallow-shelf rift-fill strata with a glacial influence in its upper parts (Fielding et al., 2000; Galeotti et al., 2016). The lithology and age of the lowermost strata under Unconformity RSU6 are uncertain because this interval has not been sampled, but it likely consists of coarse-grained fluvial facies deposited in the initial phases of Late Cretaceous to Paleocene rifting in the central Ross Sea (Wilson and Luyendyk, 2009).

The units overlying Unconformity RSU6 have all been partially sampled by drilling, and the stratigraphic architecture in the Ross Sea is relatively well constrained, although most drill holes are located in isolated basins in the VLB of the western Ross Sea (Figures F2, F6), and thus basin-to-basin correlations remain uncertain. Direct correlation of Unconformity RSU6 from across the various Ross Sea basins is not possible because the unconformity onlaps the basement flanks (Figures F3, F6). However, an inferred correlation can be made based on the distinctive acoustic character of the unconformity, which generally appears as a high-amplitude continuous reflector that is very distinct from the underlying seismic facies.

Upper Oligocene (~28 Ma) to lower Miocene (~20 Ma) strata at Site 270 consist of a 365 m sequence of lithified glaciomarine mudstones with iceberg-rafted debris (IBRD) and common macro- and microfossils (Hayes et al., 1975; Leckie and Webb, 1986), suggesting a shallow continental shelf environment with periods of abundant terrestrial runoff. Above 100 meters below seafloor (mbsf), many of the units (originally classified as mudstone) are lower Miocene diamictites (i.e., >25% sand) that were eroded and transported by glacial ice (Barrett, 1975).

Two ANDRILL sites drilled on the inner continental shelf of the western Ross Sea (98% recovery) contain an unprecedented record of marine-based ice sheet variability in the Ross Sea (Naish et al., 2009; Fielding et al., 2011; Wilson et al., 2012; Patterson and Ishman, 2013; Levy et al., 2016) over the past 20 My, although both of these sites are heavily influenced by the East Antarctic Ice Sheet (EAIS). Drilling at Site AND-2A recovered a ~20–14 Ma sequence interpreted to reflect TAM tidewater outlet glaciers overriding and/or calving near the site (Fielding et al., 2011; Passchier et al., 2011; Levy et al., 2016). A diatomite (dated to 15.7 Ma) with abundant diatoms, dinoflagellate cysts, foraminifers, pollen, and other biomarkers suggests a warmer-than-present (~11°C mean surface temperature)

and hydrologically active climate during the MMCO (Warny et al., 2009; Feakins et al., 2012). At 300 mbsf, a 300 ky disconformity is thought to be equivalent to Unconformity RSU4, suggesting a shelf-wide advance of the marine-based ice sheet during the MMCT (Figures F6, F7) (De Santis et al., 1999; Passchier et al., 2011).

The first unequivocal seismic evidence of a glacially carved trough in the central Ross Sea (key target of Site U1521) occurs at Unconformity RSU4 (mid-Miocene) and is interpreted as an expansion of a grounded marine-based ice stream originating from the EAIS to the west (Figures F7, F8) (De Santis et al., 1995; Ten Brink et al., 1995; Anderson, 1999). At DSDP Site 272, a ~400 m thick middle–upper Miocene sequence of glaciomarine mudstone was recovered (Shipboard Scientific Party, 1975b) (Figure F6). Combined with the presence of numerous outwash channels above Unconformity RSU4, as much as 250 m of till foreset and aggrading bottomset strata suggest that glaciomarine sedimentation was dominated by the release of abundant erosive sediment-laden meltwater during the middle Miocene (~14 Ma; Figure F8) (Anderson and Bartek, 1992; Chow and Bart, 2003). This meltwater release was likely associated with extensive channel-levee systems above Unconformity RSU4 on the continental slope and rise (De Santis et al., 1995, 1999).

The Miocene cooling that followed the MMCO caused multiple erosional episodes of the shallow central Ross Sea, so the upper Miocene to Pliocene record is poorly preserved. Till foreset strata that thicken toward the Central High within a thick tilted section that dips gently seaward were drilled at Site 272, suggesting that middle Miocene glaciation records may be preserved on the eastern Ross Sea sector (cf. Figures F7, F8). Evidence for glacial erosion and deposition in the southeasternmost sector of the Ross Sea is derived from an ice cap already located on Marie Byrd Land in the Oligocene (Sorlien et al., 2007). However, in the mid- to late Miocene, the eastern Ross Sea was still a wide embayment gently sloping seaward surrounded by grounded ice on the shallow shelf that was delivering sediments to the slope from the Central High and from Marie Byrd Land.

Unconformity RSU3 (key target of Site U1522) provides the first evidence for a major cross-shelf paleotrough eroded by an expanded WAIS, although the age of this event(s) was poorly constrained (~4–14 Ma; Figures F6, F7) (De Santis et al., 1995, 1999; Bart, 2003). Large meltwater and outwash features are absent, and laminated seismic facies are progressively thinner/less common in strata younger than Unconformity RSU3, suggesting sediment starvation and a transition to a colder glacial regime. Site AND-1B sediments indicate that this transition may not have occurred until the Pliocene (McKay et al., 2009), although evidence for meltwater outburst features is lacking in the TAM after 12.4 Ma (Lewis et al., 2006). High-velocity seismic units above Unconformities RSU3 and RSU2 suggest overcompaction by ice loading during WAIS expansion (Böhm et al., 2009). Bathymetric reconstructions suggest overdeepening with a transition to a landward-deepening continental shelf occurred by the Unconformity RSU2 event during the early Pliocene to early Pleistocene(?) (Figure F7) (De Santis et al., 1995, 1999). A trough-mouth fan on the upper slope and a sediment-starved continental rise (typical of the Plio–Pleistocene Antarctic margin) coincided with overdeepening (Bart et al., 1999; Cooper and O'Brien, 2004; Rebisco et al., 2006; Bart and Iwai, 2012).

At Site AND-1B, ~58 sedimentary cycles of ice sheet advance and retreat can be observed in the Ross Embayment over the past 13 My (McKay et al., 2009). Diatomites indicate frequent collapses of the WAIS in the Pliocene (2.6–5.3 Ma), during which diatom assem-

blages and geochemical paleothermometry indicate ocean temperatures up to 4°C warmer than present (McKay et al., 2012a; Naish et al., 2009). However, sedimentary lithofacies indicate that meltwater discharge was reduced during Pliocene interglacials compared with the late Miocene (5.3–11 Ma). By the mid-Pleistocene (1.0 Ma), the Ross Ice Shelf persisted through most interglacials (McKay et al., 2009).

Seismic facies above Unconformity RSU2 are indicative of till sheets bound by erosional unconformities in an aggrading shelf margin caused by shelf-wide advances of the WAIS (Figure F7) (Alonso et al., 1992; Bart et al., 2011; Brancolini et al., 1995). Unlike other sectors of the Antarctic, the eastern Ross Sea trough mouth contains thick (~2000 m) sedimentary sequences on the shelf and upper continental slope that may contain a detailed WAIS history. Above Unconformity RSU1 (0.7? Ma), shelf-edge sediments are aggrading or backstepping (rather than prograding), indicating that most sediment delivered from land was sequestered on the outer shelf or bypassed the continental shelf to pass directly into the deep sea.

Site survey data

Multichannel seismic (MCS) and single-channel seismic (SCS) profiles have been collected in the Ross Sea by several nations since 1980. MCS data are available through the Antarctic Seismic Data Library System, which works under the auspices of the Scientific Committee on Antarctic Research and the Antarctic Treaty (ATCM XVI-12). Prestack data are available only from the Italian cruises (1988, 1989, 1991, 1994, and 2006) and recently also from the BGR80 cruise.

We selected sites based on maximum thickness of target sequence, better potential for dating sediments, and acoustic facies and geometry, which usually can be seen much better on high-resolution profiles. In most cases, high-resolution profiles are single channel or, in the case of the TAN060_08 profile, they have a very short streamer (200 m) compared with the water depth (>1000 m). In some cases, crossing lines are not available, and the remoteness of Antarctic water and presence of sea ice prevent the easy collection of new site survey data. New MCS Profiles KSL14-02 and KSL14-04 (Kim et al., 2018) were collected in February 2013 and in 2015 by the Korea Polar Research Institute (KOPRI) with the aim of providing cross-lines for several proposed sites. Another SCS survey cruise was conducted in 2017 (EU/FP7 EUROFLEETS2 ANTSSS project and Programma Nazionale di Ricerche in Antartide WHISPERS and ODYSSEA projects) with the aim to collect additional cross-lines of the proposed sites and identify alternate sites.

SCS data, collected by National Science Foundation (NSF) Cruises 1990 and 1994–1995, were made available by John Anderson (Rice University, Texas) in the format of digital SEGY data (Cruise PD90) and paper copies (Cruise NBP 94-95). We made the conversion of the TIFF or JPG image to SEGY format to depth-convert the sections and load the data in the IHS Kingdom interpretation software with the other available data sets. The supporting site survey data for Expedition 374 are archived at the IODP Site Survey Data Bank (<https://ssdb.iodp.org/SSDBquery/SSDBquery.php>; select P751 for proposal number).

Scientific objectives

1. Evaluate the contribution of West Antarctica to far-field ice volume and sea level estimates.

Far-field benthic foraminifer $\delta^{18}\text{O}$ and sequence stratigraphic records suggest that large global ice volume and sea level (20–60 m) variations occurred during the Miocene and Pliocene (Figures F1, F6) (Zachos et al., 2001; Miller et al., 2005, 2012; Cramer et al., 2009; Raymo et al., 2011). Miocene–Pliocene sea level reconstructions could potentially be reconciled without invoking Northern Hemisphere contributions if Antarctica's ice sheets expanded to the continental shelf edge (~14 m sea level equivalent [SLE]) (Figure F4). The modeled difference between the glacial maxima states and loss of the marine-based WAIS (assuming present bathymetry) represents ~21 m SLE (with some minor loss of the EAIS), although changes in Ross Sea bathymetry could increase this value (Figure F4) (see Objective 5). Expedition 374 records will help constrain the timing of the first WAIS advances to the shelf edge, and integration with ANDRILL records will allow assessment of the WAIS contribution to Neogene sea level estimates.

Sedimentologic and micropaleontologic analyses at the continental shelf Sites U1521 and U1522, combined with seismic stratigraphic correlations, will identify deposition under grounded-ice, glaciomarine, and open-marine conditions following ANDRILL/CRP methodology (Fielding et al., 2000, 2011; McKay et al., 2009; Passchier et al., 2011; Powell and Cooper, 2002). Magneto-, bio-, and tephrachronology will enable identification of orbital-scale ice sheet variations and have been employed in discontinuous Antarctic margin sequences (Florindo et al., 2003, 2005; Tauxe et al., 2012; Wilson et al., 2012) (Figure F4). Furthermore, new quantitative techniques have greatly enhanced the biostratigraphic framework of the Southern Ocean (Cody et al., 2008, 2012; Crampton et al., 2016). Glacially reworked volcanic clasts (Wilson et al., 2012) and radiometrically datable felsic ashes from Marie Byrd Land may be used to provide maximum ages (Wilch et al., 1999). Climate snapshots near magnetic reversals will be targeted (e.g., the M2 glacial in Figure F4) because these events can be traced to more continuous records from the continental rise (Site U1524) and global sea level records. Sediment provenance studies (clast/sand petrology, mineral thermochronology, and radiogenic isotope analysis) at Sites U1521 and U1522 will enable understanding of the changes in the origin of sediments (e.g., local ice caps versus ice sheet expansion and provenance from East versus West Antarctic sources) (Figure F7) (Licht et al., 2005, 2014; Talarico et al., 2012; Cook et al., 2013). As with all objectives, data integration with modeling studies will be undertaken (cf. Figure F4) (Golledge et al., 2012; Wilson et al., 2013; DeConto and Pollard, 2016; Gasson et al., 2016).

2. Reconstruct ice-proximal atmospheric and oceanic temperatures to identify past polar amplification and assess its forcings/feedbacks.

Obtaining atmospheric and ocean temperatures from the Expedition 374 drill sites will enable the paleoclimate community to address the following key scientific questions:

- Were polar temperatures sensitive to the low-amplitude variations in Neogene atmospheric $p\text{CO}_2$?
- Were Neogene ocean and atmospheric temperatures at the Antarctic margin amplified relative to the global mean, and if so, what were the forcings?
- How did ocean temperatures evolve as Antarctica's ice sheets expanded and contracted during major Neogene climate transitions and on orbital timescales?

Although the ANDRILL records provide important archives of high-latitude oceanic conditions, they only provide snapshots of temperature and sea ice conditions through interglacials, when these sites were not covered by ice (Warry et al., 2009; McKay et al., 2012a; Levy et al., 2016). In contrast, Sites U1521 and U1522 provide intervals of more continuous sedimentation (albeit with some periods of erosion during large glaciations) because they are in paleobathymetric depressions that provided the accommodation space needed for preservation after ice expansion (De Santis et al., 1995). These sites are also farther out on the continental shelf, near the paleoshelf break (Figure F7), and are therefore less likely to be frequently overridden by grounded ice (Pollard and DeConto, 2009; Bart et al., 2011). Near-continuous records of oceanographic change were recovered at Sites U1523–U1525, providing high-latitude information on Neogene and Quaternary ocean and atmospheric temperatures, meltwater input, and bottom water production.

Lithofacies analysis will be used to reconstruct glacial thermal regimes and glacial cyclicity (cf. Naish et al., 2009; McKay et al., 2009), whereas diatom and radiolarian census counts, marine and terrestrial palynology, organic biomarkers (e.g., TEX_{86} , branched and isoprenoid tetraether [BIT] index, and methylation of branched tetraether [MBT]/cyclization of branched tetraether [CBT] proxy; cf. McKay et al., 2012a; Levy et al., 2016; Sangiorgi et al., 2018), and redox-sensitive metals (e.g., Mn, U, Re, and Mo) provide records for paleoproductivity, high-latitude marine and terrestrial climate, and oceanography. Lithofacies analysis is also relevant to monitoring alteration of the biomarkers by methanogenesis and shifting redox boundaries. Biogenic carbonate (e.g., calcareous nannofossils/foraminifers) is also present in Expedition 374 Neogene and upper Pleistocene interglacial sequences, as well as at other circum-Antarctic sites (e.g., Theissen et al., 2003; Scherer et al., 2008; Villa et al., 2008; Expedition 318 Scientists, 2011). In the lower to middle Miocene, biogenic carbonate is more common in the Southern Ocean and Antarctic margins (Hayes et al., 1975; Kennett and Barker, 1990; Shipboard Scientific Party, 2001; Shevenell et al., 2004; Expedition 318 Scientists, 2011; Fielding et al., 2011), making stable isotope ($\delta^{18}\text{O}$ and $\delta^{13}\text{C}$), trace element (e.g., Mg/Ca, Li/Ca, U/Ca, Ba/Ca, and B/Ca), and clumped isotope analyses possible. However, for all of the proxies discussed above, careful consideration of strengths/weaknesses in a marginal marine setting should be made.

3. Assess the role of oceanic forcing (e.g., sea level and temperature) on WAIS stability/instability.

WAIS collapse events during past warmer-than-present climates may be the consequence of intensified ocean-cryosphere interactions (Naish et al., 2009; Pollard and DeConto, 2009). Interactions between the wind-driven upwelling of warm CDW and the ice shelves that buttress the WAIS appear to play a significant role in modern ice mass loss in West Antarctica (Mercer, 1978; Joughin et al., 2012; Pritchard et al., 2012; Shepherd et al., 2012). Observations and numerical ice sheet models suggest that changes in ocean heat flux are a key factor influencing the stability/instabil-

ity of the WAIS (Golledge et al., 2012; Pritchard et al., 2012; DeConto and Pollard, 2016). We postulate that changes in either the formation of AASW and AABW or the vigor of the wind-driven ASC control incursions of CDW onto the Ross Sea continental slope and shelf and the resultant retreat of the WAIS (Figure F5). The records from Expedition 374 will allow us to test this hypothesis by assessing changes in these two variables (from grain size and lithofacies analysis of sediment mounds on the continental shelf bank, slope, and rise; e.g., Sites U1523–U1525) and ice sheet extent in the Ross Embayment (Sites U1521, U1522, DSDP Site 272, and ANDRILL).

The Ross Sea is also one of the three main sources of AABW that feeds the abyssal ocean (to become Southern Component Water [SCW]). In the middle Miocene, benthic foraminifer $\delta^{13}\text{C}$ indicates changes in the relative input of SCW and Northern Component Water (NCW) into the global ocean (Woodruff and Savin, 1985; Wright et al., 1991; Shevenell et al., 2004; Cramer et al., 2009). Newer proxies, such as Nd isotopes, are now used to further refine the geographic source (e.g., van de Flierdt et al., 2004; Scher and Martin, 2006; Newkirk and Martin, 2009; see also Huck et al., 2017). Thus, the records obtained during Expedition 374 and comparison with far-field records will provide insight into temporal changes in SCW production through the Neogene (Vincent and Berger, 1985; Flower and Kennett, 1994; Hodell and Venz-Curtis, 2006).

Paleocurrent strength associated with past ASC changes and the history of AABW formation through the Hillary Canyon will be reconstructed by examining the sedimentologic (e.g., lithofacies analysis and grain size) and magnetic characteristics of Sites U1523–U1525 (e.g., Bianchi et al., 1999; Hall et al., 2001; Prins et al., 2002; Joseph et al., 2004). Micropaleontological, geochemical, and sedimentologic records from drill cores from all Expedition 374 sites will provide reconstructions of changing regional surface and seafloor conditions (e.g., sea ice, surface stratification, sea-surface temperatures [SSTs], polynya mixing, glacial meltwater discharge, nutrient uptake, and supercooling of dense waters by ice shelves) proximal to the AISs (e.g., Shevenell et al., 2011; McKay et al., 2012a; Houben et al., 2013; Levy et al., 2016; Sangiorgi et al., 2018) and thus AASW (and SCW) formation. Additionally, downslope currents resulting from the transfer of High-Salinity Shelf Water into the abyssal ocean can also be assessed (and distinguished from ASC flow) by integrated lithofacies analysis, geochemistry, micropaleontology, and seismic profiles (e.g., Hepp et al., 2006; Lucchi and Rebesci, 2007; Caburlotto et al., 2010; Kim et al., 2018) at Sites U1523–U1525. Carbonate-based paleotemperature and carbonate ion proxies (e.g., foraminiferal Mg/Ca, Li/Ca, U/Ca, and clumped isotopes) will also be applied where appropriate species are preserved (see Objective 2).

4. Identify the sensitivity of WAIS to Earth's orbital configuration under a variety of climate boundary conditions.

Fundamental questions remain about the orbital pacing of AIS development and variability. The Ross Sea Expedition 374 sequences will shed light on the absence of the 20 ky precession cycle in benthic $\delta^{18}\text{O}$ records (Figure F4) (Lisicki and Raymo, 2005; Huybers, 2006; Raymo et al., 2006) and the origin of transient shifts in the sensitivity of Earth's climate system to orbital forcing (e.g., 40–100 ky dominated frequencies) in the middle Miocene (Shevenell et al., 2004) and Plio–Pleistocene (Tzedakis et al., 2017).

A recent hypothesis suggests that the last such shift in Earth history (the mid-Pleistocene transition) was initiated by an abrupt in-

crease in Antarctic ice volume (Elderfield et al., 2012). This hypothesis may be tested by identifying and dating grounding events on the outer Ross Sea continental shelf. If the dominant frequency of AIS advance and retreat shifted from 40 to 100 ky at 0.8 Ma, records from this sensitive region will likely record this transition.

Recent evidence from ice-proximal drill sites indicates that Antarctic ice sheets did advance and retreat with 40 and 100 ky cyclicity in the Neogene (Grützner et al., 2003; Williams and Handwerger, 2005; Naish et al., 2009; Patterson et al., 2014). We envision a more complete picture of the forcings and feedbacks involved with ice advance and retreat from our outer shelf to slope/rise transect. Sedimentologic analyses (complemented by downhole logs) will enable development of an orbital-scale continental shelf-to-rise sequence stratigraphy of glacial advance and retreat (all Expedition 374 sites; see Objective 1). Additional micropaleontologic data, inorganic and organic geochemistry (e.g., $\delta^{18}\text{O}$, $\delta^{13}\text{C}$, $\delta^{30}\text{Si}$, Mg/Ca, and ε_{Nd}), minor and trace elements (X-ray fluorescence and discrete samples), and organic biomarkers may be used to assess associated frequencies of change in the continental slope and rise sites (U1523–U1525).

5. Reconstruct eastern Ross Sea bathymetry to examine relationships between seafloor geometry, ice sheet stability/instability, and global climate.

The transition from a terrestrial (or shallow marine) West Antarctica with a seaward-dipping shallow continental shelf to that of the modern overdeepened (i.e., landward dipping) continental shelf would have a first order control on AIS volume and mass balance (Wilson et al., 2013; Gasson et al., 2016). The cooling threshold for the development of a terrestrial-based ice sheet is lower than that of a marine-based ice sheet, which is highly sensitive to changes in oceanic heat flux (Figure F4) (Pollard and DeConto, 2009; Golledge et al., 2012). A terrestrial (or shallow marine) West Antarctica may have supported a larger ice sheet in warmer-than-present climates, whereas overdeepening of the continental shelves may have resulted in a smaller ice sheet with less frequent ice sheet advances, as hypothesized for the Antarctic Peninsula (e.g., Bart and Iwai, 2012). Ice sheet models indicate that a largely terrestrial West Antarctica could accommodate an extra ~13 million km³ of grounded ice in the warmer-than-present climate of the Eocene (~30 m SLE; Figure F4) (Wilson et al., 2013). Therefore, constraining the timing of overdeepening in the Ross Sea is critical to reconcile far-field records of eustatic sea level variance into the late Neogene and Quaternary (see Objective 1).

The timing of Ross Sea shelf overdeepening is currently unconstrained. However, the Ross Sea has the most developed seismic framework in Antarctica and the highest resolution history of WAIS variability currently available (ANDRILL), making this location ideal for achieving this objective. Dating and providing information about the depositional environment at the time of formation of Unconformities RSU3 and RSU2 (Figure F6) at Sites U1521 and U1522 in the eastern Ross Sea (by methodologies in Objective 1) will constrain the timing of this overdeepening (Figure F7).

Site summaries

Site U1521

Background and objectives

Site U1521 (proposed Site EBOCS-01D) is located in the Pennell Basin at 75°41.0351'S, 179°40.3108'W at 562 m water depth (Figure F9). The site is on the mid- to outer continental shelf near a north-

east–southwest-oriented Miocene paleotrough identified by mapping regional unconformities in seismic profiles. The primary objective at Site U1521 was to sample and date strata above and below the Ross Sea Unconformity RSU4, which was previously identified in seismic stratigraphic studies (Hinz and Block, 1984; Anderson and Bartek, 1992; Cooper et al., 1997) (Figure F10). Unconformity RSU4 has been mapped over most of the Ross Sea and is interpreted to represent a cross-shelf expansion of the EAIS in the central regions of the Ross Sea (Brancolini et al., 1995; De Santis et al., 1995). Strata above Unconformity RSU4 are interpreted to be a MMCO record (~17–15 Ma) deposited on the Ross Sea continental shelf. Coring through Unconformity RSU4 should improve on the broad age constraints provided for Unconformity RSU4 by DSDP Sites 272 and 273 (Bart, 2003).

Records from this site will directly address all five primary Expedition 374 objectives. The record of ice advance and retreat from Site U1521, when integrated with seismic stratigraphy, provenance studies, and numerical modeling, will allow for a fuller assessment of Antarctic contributions to numerous inferred (~30 m amplitude) variations in far-field Miocene sea level (Objective 1) (Miller et al., 2005; John et al., 2011). The magnitude of polar amplification during the MMCO will be assessed through proxies for atmospheric and marine temperatures derived from both the in situ marine organic matter and terrestrial organic matter transported off shore by meltwater (e.g., micropaleontology and lipid biomarkers) (Objective 2). Insights into the oceanic drivers for retreat of middle Miocene marine-terminating ice sheets and subsequent readvances in the late Miocene can be achieved by detailed lithofacies analysis to reconstruct physical changes in the paleoenvironment. This information can be paired with paleontological and geochemical proxies to identify the magnitude of the oceanic change through these intervals, and to understand the effect of ocean heat flux on ice sheet stability/instability (Objective 3). Similarly, these methods will identify the sensitivity of middle Miocene ice sheets to orbital variability based on the presence of cyclicity in the open-marine, glaciomarine, and glacial proximal sediments when combined with downhole logging results to complete the stratigraphy (Objective 4). Finally, a “backstripped” paleobathymetry through accurate dating and depth estimates of the Unconformity RSU4 surface and other unconformities at Site U1521, in combination with previous drilling constraints from other locations in the Ross Sea, will allow for a fuller assessment of bathymetric controls on AIS evolution.

Operations

After a 2014 nmi transit from Lyttelton, the vessel arrived at Site U1521 at 0954 h (UTC + 13 h) on 16 January 2018. The original operations plan for Site U1521 called for a single rotary core barrel (RCB) hole to 950 m drilling depth below seafloor (DSF) and down-hole logging with the triple combination (triple combo), Formation MicroScanner (FMS)-sonic, and Versatile Seismic Imager (VSI) tool strings. We ultimately cored Hole U1521A to 650.1 m DSF (Cores 374-U1521A-1R through 71R) (Table T2). Coring proceeded without incident to Core 37R (0–352.5 m DSF); however, after poor recovery in Cores 32R through 37R (14.49 m; 25%) caused by jamming of the core barrel with clasts, we switched to cutting half-length cores to improve core recovery. Cores 38R through 43R (352.5–381.3 m DSF) were collected using a 4.8 m advance (instead of 9.6 m), significantly improving recovery (80%). We switched back to 9.6 m advances after the formation became less indurated and continued to core with the RCB system from Core 44R through 71R (381.3–650.1 m DSF). We terminated coring at that depth after

meeting the primary scientific objectives. At the end of coring operations, we displaced the hole with heavy (10.5 lb/gal) mud and logged with all three tool strings, all of which reached to within ~1 m of the bottom of the hole. Operations at Site U1521 concluded at 2245 h on 21 January. A total of 132.75 h (5.5 days) were spent at Site U1521. RCB coring in Hole U1521A penetrated to 650.1 m DSF, recovering 411.50 m of core (63%).

Principal results

The 648 m succession of lower Miocene to recent sediment recovered at Site U1521 is divided into seven lithostratigraphic units (I–VII). Unit VI is further divided into Subunits VIA–VIC (Figure F11). Contacts between lithostratigraphic units at Site U1521 range from sharp to gradational. Diatomite, mudstone, and diamictite account for ~90% of the core recovered, whereas minor lithofacies include chert and conglomerate (Figure F11). The assemblage of facies reflects open-marine to subglacial depositional environments at this location in the central Ross Sea basin since at least the early Miocene.

Lithostratigraphic Unit I (0–7.4 m core depth below seafloor, Method A [CSF-A]) consists of a sequence of unconsolidated olive to light olive gray diatom ooze, dark grayish brown diatom-rich mud with dispersed clasts, and gray sandy mud. Unit II is ~80 m thick and consists of dark gray massive clast-poor muddy diamictite interbedded with heavily bioturbated diatomite and diatom-rich/bearing mudstone with dispersed clasts. There are several intervals of physically intermixed diatomite/mudstone and diamictite with microfaulting and soft-sediment deformation features. Unit III (~124 m thick) consists of bioturbated olive gray to greenish gray diatomite and diatom-rich/bearing mudstone. Some intervals are faintly laminated, and whole bivalve shells and shell fragments are present throughout. Unit IV consists of ~70 m of dark gray massive diatom-bearing clast-rich sandy diamictite with clasts of basalt and granodiorite. Mudstone and diamictite are interbedded at the top and bottom of the unit, and a conglomerate composed of elongated mudstone intraclasts is observed at the base of the unit. Unit V is a 40 m interval of poorly recovered chert nodules interbedded with silica cemented mudstone. Unit VI (~245 m thick) is characterized by interbedded mudstone and diamictite that is divided into three subunits based on the style of interbedding. Subunit VIA (~56 m thick) consists of interbedded dark gray massive diamictite with silica-cemented intervals and mudstone, whereas Subunit VIB (~60 m thick) consists of massive to stratified dark gray sandy diamictite with three intervals of clast-supported conglomerate. Subunit VIC (~128 m thick) is a sequence of interbedded mudstone with dispersed clasts and sandy diamictite with carbonate concretions and shell fragments. Unit VII consists of ~70 m of interbedded massive to stratified sandy diamictite.

Micropaleontological investigation at Site U1521 included examination of core catcher samples and additional samples from split core sections for diatoms, radiolarians, foraminifers, calcareous nannofossils, and palynomorphs (including dinoflagellate cysts, pollen, and spores) to obtain biostratigraphic ages and preliminary paleoenvironmental information. The presence and abundances of the microfossil groups vary significantly throughout the recovered sediment column (Figure F11). Rich assemblages of diatoms, silicoflagellates, and ebridians are present in the upper ~280 m CSF-A. Below that depth, diatoms are altered to opal-CT or are poorly preserved and offer minimal biostratigraphic constraint. Radiolarians are rare in the upper ~30 m CSF-A, and their abundance decreases significantly downhole. Foraminifers and palynomorphs are gener-

ally sparse throughout the hole, and calcareous nannofossils are only present in trace numbers deeper than ~525 m CSF-A. All microfossil group assemblages represent a combination of in situ and reworked taxa of different ages.

Although all investigated microfossil groups provide valuable age and/or paleoenvironmental information, diatoms provide the best age constraint, particularly in the upper ~280 m CSF-A (Figure F11). Shallower than 75 m CSF-A, age assignment is difficult due to reworking; however, diatom and radiolarian assemblages suggest a Pliocene to Pleistocene/recent age for the uppermost 25 m. An unconformity at ~25 m CSF-A separates Pliocene sediment from middle Miocene sediment. Age diagnostic diatoms are present between ~75 and 280 m CSF-A and allow assignment of that interval to the *Actinocyclus ingens* and *Denticulopsis maccollumii* Zones (middle to early Miocene). Dinoflagellate cysts and other aquatic palynomorphs confirm this age. Between ~280 and 380 m CSF-A, siliceous microfossils are altered to opal-CT. From ~380 to 580 m CSF-A, diatoms are present but preservation is poor, with valves occurring as silicified casts. Despite this lithology, the presence of *Thalassiosira* sp. cf. *Thalassiosira bukryi* and absence of *Thalassiosira praefraga* indicate an early Miocene age. Dinocysts are present over this interval, but the assemblage contains a mix of in situ and reworked taxa. Siliceous microfossils are absent deeper than 580 m CSF-A, whereas dinocysts and calcareous nannofossils are present and could indicate an early Miocene age if not reworked.

Foraminifers are generally sparse, and the assemblages are dominated by calcareous benthic species. The foraminifer assemblages represent distinct biofacies that vary in parallel with the lithofacies recovered at Site U1521. Well-preserved diatoms and dinocysts indicate a highly productive and seasonally stratified water column between ~75 and 280 m CSF-A (early to early middle Miocene). All microfossils will greatly contribute to constraining paleoceanographic and paleoproductivity changes that occurred through the early to middle Miocene in the Ross Sea.

Paleomagnetic investigations at Site U1521 focused on measurements of archive-half core sections and oriented discrete (cube) samples. Natural remanent magnetization (NRM) measurements of archive-half core sections were conducted before and after progressive alternating field (AF) demagnetization, commonly in 5 mT increments up to 20 mT peak AF. After 20 mT peak AF demagnetization, NRM intensities usually range between $\sim 10^{-4}$ and 10^{-2} A/m and vary with lithology. Selected discrete samples were also used for initial NRM measurement, followed by NRM measurements after progressive AF demagnetization in 2–5 mT increments up to a peak AF of 80 mT. Principal component analysis (PCA) of these measurements reveals a stable characteristic remanent magnetization (ChRM) component in most of the samples, yielding normal and reversed polarities based on inclination data. Steep upward or downward inclinations are also present in most intervals of archive-half core data and agree with directions from discrete samples, suggesting a stable and reliable magnetic carrier that can be used for magnetostratigraphic interpretation. The identified normal and reversed polarity zones can be correlated to the geomagnetic polarity timescale (GPTS) with the aid of biostratigraphic datums.

Discrete samples were also used to measure the anisotropy of magnetic susceptibility (AMS) and mean bulk magnetic susceptibility. The AMS agrees well with variability in the lithostratigraphic units. For instance, AMS shows an oblate fabric that reflects sedimentary compaction in the diatom-rich to diatom-bearing mudstone of lithostratigraphic Unit III.

Physical property measurements were conducted on whole-round cores, split core sections, and discrete samples. In general, the whole-round core gamma ray attenuation (GRA) bulk density and magnetic susceptibility measurements show trends similar to those from discrete moisture and density (MAD) samples and point measurements of magnetic susceptibility on the section halves (Figure F11). A downhole increase in *P*-wave caliper (PWC) values generally coincides with an increase in bulk density and a decrease in porosity. Downhole variations in natural gamma radiation (NGR) also correlate well to changes in bulk density. Downhole changes in physical property characteristics are in good overall agreement with the lithostratigraphic units, which are defined based on sedimentologic characteristics. In general, diatom ooze, diatom-rich mud/mudstone, and mudstone lithofacies (lithostratigraphic Units I, III, and V) correspond with low magnetic susceptibility, NGR, thermal conductivity (<1 W/[m·K]), and bulk density and high porosity. The lowest grain density and highest porosity correspond with diatom-rich/bearing mudstone that is the dominant facies in lithostratigraphic Unit III (Figure F11). In contrast, intervals that are predominantly diamictite (Units II, IV, VI, and VII) are characterized by increased NGR; high bulk density, *P*-wave velocity, and thermal conductivity; moderate to high magnetic susceptibility; and low to moderate porosity. Variations in magnetic susceptibility for clast-poor diamictite (low to moderate) and clast-rich diamictite (variable and generally high) suggest that magnetic susceptibility is an indicator of the abundance of glacially transported clasts or coarse sand in the sediment (Figure F11).

Headspace gas analyses show low methane and ethane concentrations in the upper 40 m CSF-A, increasing downhole to 67,000 ppmv for methane and 264 ppmv for ethane. Interstitial water analyses on 15 samples from the uppermost 360 m CSF-A show a typical diagenetic profile with sulfate reduction and increasing ammonium concentration in the uppermost 75 m CSF-A. Alkalinity follows a similar profile to ammonium, whereas iron and manganese concentrations in the interstitial water were below detection limit. A range of major and trace elements have smooth downhole profiles with changes that are generally well correlated with lithostratigraphic units. Total organic carbon (TOC), total nitrogen (TN), and carbonate (CaCO_3) content in Site U1521 sediments are generally low (<1.2, 0.1, and <6 wt%, respectively) (Figure F11). TOC content is slightly higher in the mudstone facies in the upper 300 m CSF-A and decreases in the diamictite between ~330 and 640 m CSF-A. TOC/TN ratios suggest mixed input of terrestrial- and marine-derived organic matter with no clear downhole trend. Elevated CaCO_3 content was only observed in the sandy diamictites of lithostratigraphic Unit IV, Subunit VIA, and Unit VII, which also have higher magnetic susceptibility. Elemental ratios obtained by portable handheld X-ray fluorescence (pXRF) scans show good agreement with major lithostratigraphic units but also suggest some deviations between chemical and lithologic boundaries.

Downhole logging in Hole U1521A consisted of three separate tool runs (triple combo, FMS-sonic, and VSI), all of which reached the bottom of the hole and proceeded without issue due to favorable borehole conditions. The triple combo measured NGR, density, porosity, resistivity, magnetic susceptibility, and borehole diameter. The caliper data show that the borehole was in excellent condition, with only one washed out interval between 221 and 226 m wireline matched depth below seafloor (WMSF). The NGR, bulk density, and porosity data match well with data from core measurements, whereas magnetic susceptibility data do not correlate as well, possibly as a result of temperature drift or other issues with the magnetic

susceptibility sonde (MSS). The second logging run consisted of the FMS-sonic tool string to measure resistivity borehole images and acoustic velocity. The latter shows good correlation with the data measured with the PWC, especially shallower than ~300 m CSF-A. The FMS images are extremely well resolved and clearly show clasts in the diamictite intervals, as well as a poorly recovered layered interval of chert and mudstone in lithostratigraphic Unit V. The third logging run was with the VSI tool string (geophone) to conduct a vertical seismic profile (VSP) experiment. Raw check shot data were used in preliminary velocity models for an initial seismic-core-log correlation.

Site U1522

Background and objectives

Site U1522 (proposed Site EBOCS-03C) is located in the Glomar Challenger Basin at 76°33.2262'S, 174°45.4652'W at 558 m water depth (Figure F12). During the middle Miocene, this site was located near the western edge of a wide embayment ~80 km southeast of the shelf break. Coring at this site was anticipated to recover a sedimentary sequence that spans the middle Miocene to the Pleistocene (coinciding with seismic Unconformities RSU3–RSU1). Coring targeted laminated and massive acoustic facies interpreted to be interlayered stratified diamictite/mudstone and diatomite (glaciomarine/open marine) and massive diamictite (till), respectively (Figure F13).

The upper ~400 m (1.2 s two-way traveltime [TWT]) of sediment consists of tabular units that are interpreted to be aggradational subglacial till sheets deposited by a grounded ice sheet (i.e., compacted sediments) during the late Pleistocene (Alonso et al., 1992; De Santis et al., 1995). Underlying the till sheets is ~300 m of acoustically laminated facies interbedded with lens-shaped layers that are more transparent and interpreted to be glaciomarine or hemipelagic sediments and ice-proximal deposits (Böhm et al., 2009) (Figure F13). This site will enable us to determine if ice sheet-overriding events observed at the ANDRILL AND-1B site beneath the modern Ross Ice Shelf advanced to the shelf edge and will therefore help constrain the contribution of AISs to Pliocene sea level lowstands (Objective 1) (Naish et al., 2009; Miller et al., 2012). During periods of glaciomarine deposition, this site will provide an opportunity to reconstruct the paleooceanographic and paleoecological conditions at the outermost Ross Sea continental shelf (Objective 2). These sequences, combined with downhole logging to fill in unrecovered sections, are anticipated to provide insights into the orbital controls on marine-based ice sheet extent (Objective 4).

Operations

After an 88 nmi transit from Site U1521 that averaged 10.7 kt, the vessel arrived at Site U1522 at 0629 h (UTC + 13 h) on 22 January 2018. The original operations plan consisted of a single RCB hole to 545 m DSF; however, after requesting and receiving approval from the Environmental Protection and Safety Panel (EPSP) and Texas A&M Safety Panel, we ultimately cored Hole U1522A to 701.8 m DSF (Cores 374-U1522A-1R through 76R) (Table T2). Core recovery was very poor from 0 to 203.2 m DSF, was moderate from 203.2 to 424.5 m DSF, and improved significantly below that depth. Hole cleaning became problematic near the end of coring operations, and off-bottom torque steadily increased despite multiple heavy mud sweeps to clean the hole. At the end of coring operations, the hole was displaced with heavy mud (10.5 lb/gal) and logged with three tool strings: a modified triple combo, the VSI, and the FMS. The Dipole Sonic Imager (DSI) was run on the triple

combo instead of with the FMS, and the Hostile Environment Litho-Density Sonde (HLDS) was run without the source to measure borehole diameter with the caliper. Operations at Site U1522 concluded at 1311 h on 28 January. A total of 149.25 h (6.2 days) were spent at Site U1522. RCB coring in Hole U1522A penetrated to 701.8 m DSF and recovered 279.57 m of core (40%).

Principal results

The 695.74 m succession of upper Miocene to recent sediment cored at Site U1522 is divided into four lithostratigraphic units (I–IV). Unit III is further divided into Subunits IIIA–IIIC (Figure F14). Several intervals are characterized by very poor recovery that consists primarily of washed gravel and fall-in, which compromises our ability to identify the lithologic variations in some units but may indicate the presence of unrecovered sand- or gravel-rich beds. The dominant facies throughout the cores is massive diatom-bearing diamictite, although some intervals have thin beds of laminated mudstone, carbonate-cemented mudstone, and mud-rich diatomite.

Lithostratigraphic Unit I consists of ~200 m of Pleistocene diatom-bearing sandy mud, muddy sand, and muddy diamict. The upper ~3 m of the unit consists of unconsolidated diatom-rich sandy mud to diatom-bearing sandy mud with dispersed clasts. Recovery is mostly poor between ~3 and ~200 m CSF-A and consists primarily of washed cobble and gravel resulting from drilling disturbance. A few recovered intervals contain massive clast-rich diatom-bearing muddy diamict. The base of Unit I is defined by increased lithification of the diamict. Lithostratigraphic Unit II consists of ~195 m of Pliocene massive diatom-bearing sandy to muddy diamictite, with clast-rich and clast-poor intervals interbedded over 10s of meters. Diatom-bearing mudstone and deformed (physically intermixed during deposition) discontinuous laminae to centimeter-scale beds are occasionally present in the muddy diamictite. Lithostratigraphic Unit III (~250 m) includes upper Miocene diatomite and diatom-bearing/rich diamictite and is divided into three sub-units based on the style of interbedding and presence of lithologic accessories. Clasts occur throughout, but clast assemblage and composition changes between subunits. Subunit IIIA consists of massive bioturbated diatomite with glauconite and interbedded massive diatom-rich sandy and muddy diamictite with predominantly small (<1 cm) mudstone clasts. Subunit IIIB consists of interbedded diatom-bearing sandy and muddy diamictite with common chert clasts. Subunit IIIC consists of diatom-bearing sandy diamictite. Some intervals contain stratification characterized by thin beds of laminated mudstone and changes in matrix color, whereas massive diamictite beds are heavily bioturbated. Although the recovered succession contains diverse clast lithologies throughout, basalt clasts are only common in this interval, suggesting a switch in provenance at this time. The base of Subunit IIIC is defined by interbeds of stratified and massive diamictite and diatomite. Lithostratigraphic Unit IV consists of ~50 m of upper Miocene interbedded diatom-bearing sandy diamictite, diatomite, and massive sandy diamictite.

Micropaleontological investigations were performed on all core catcher samples and two additional samples from split core sections to obtain biostratigraphic ages and preliminary paleoenvironmental information through examination of diatom, radiolarian, foraminifer, and palynomorph assemblages. Abundance and preservation of the different microfossil groups strongly varies throughout the sequence. In general, all microfossil groups are rare and comprise a combination of in situ and reworked taxa in the upper ~200 m CSF-

A. Diatoms and radiolarians are more abundant between ~200 and 400 m CSF-A, and dinoflagellates are common in the lower part of that interval. Deeper than ~400 m CSF-A, radiolarians are absent, and palynomorphs and foraminifers are sparse. The diatom assemblage between ~400 and 480 m CSF-A is poorly preserved and primarily reworked, whereas below ~480 m CSF-A, diatom assemblages are mixed, with a few intervals of well-preserved diverse assemblages interspersed with mostly fragmented sparse assemblages (Figure F14).

The mudline sample contains a modern low-diversity radiolarian assemblage that is typical of the Antarctic continental shelf, including mainly *Antarctissa* spp. together with significant numbers of *Rhizopylema boreale* and the *Phormacantha hystrix/Plectacantha oikiskos* group. Below the mudline sample, the upper ~200 m CSF-A is tentatively assigned a Pleistocene age; however, the combination of sparse microfossils and mix of in situ and reworked taxa hinders straightforward age assignment and environmental reconstructions (Figure F14). Calcareous benthic foraminifers are represented by few specimens of typical late Neogene Ross Sea shelf species, although many of the specimens are likely reworked. One sample at ~135 m CSF-A contains a well-preserved assemblage that includes the planktonic foraminifer *Neogloboquadrina pachyderma*.

The interval between ~200 and 400 m CSF-A is assigned a Pliocene age based on diatoms and radiolarians, which were critical for providing age constraints at this site (Figure F14). One sample from ~400 m CSF-A contains well-preserved diatom, radiolarian, and dinocyst taxa that are indicative of high-productivity environmental conditions that were warmer than today. From ~400 to 480 m CSF-A, microfossil assemblages are sparse and poorly preserved, and reworking makes age assignment and environmental reconstructions difficult. Deeper than ~490 m CSF-A, the absence of the diatom *Thalassiosira torokina* indicates a late Miocene age >9 Ma. From ~490 m CSF-A to the base of the cored interval at 695.74 m CSF-A, diatom and dinocyst assemblages suggest an expanded upper Miocene sequence. A few samples from this interval contain well-preserved, diverse dinocyst assemblages that include the late Miocene species *Selenopemphix bothrion* (Harland and Pudsey, 2002). This assemblage suggests high productivity, likely with reduced sea ice relative to present day.

Paleomagnetic investigations primarily focused on measurements of archive-half core sections to determine ChRM and construct a magnetostratigraphy. The NRM of most archive-half core sections was measured before and after progressive AF demagnetization, usually in 5 mT increments to 20 mT. NRM intensity commonly decreases by approximately one order of magnitude throughout this demagnetization sequence and in general agrees with magnetic susceptibility measured with the Whole-Round Multisensor Logger (WRMSL) and Section Half Multisensor Logger (SHMSL). NRM inclinations are predominantly positive prior to demagnetization and reveal scattered clusters of normal and reversed polarity after 20 mT peak AF demagnetization.

Discrete samples were used to test the fidelity of the archive-half NRM measurements by progressive demagnetization in 2 mT steps to 20 mT, 5 mT increments to 60 mT, and 10 mT steps to 80 mT. The NRM directions of a majority of these discrete samples quickly become erratic, but several samples contain a stable direction that matches the archive-half directions. The normal and reversed polarity zones identified in both archive halves and discrete samples cannot yet be confidently correlated to the GPTS with the available biostratigraphic age control; postcruise work to refine the biostra-

tigraphy should improve the correlation. Discrete samples were also used to measure the AMS to determine magnetic fabric characteristics.

Physical property measurements were conducted on all cores collected. In general, the whole-round core bulk density and magnetic susceptibility measurements show trends similar to those from discrete MAD samples and point measurements of magnetic susceptibility on the section halves (Figure F14). Overall, downhole trends in magnetic susceptibility, NGR, bulk density, *P*-wave velocity, and porosity correspond well with the defined lithostratigraphic units. In general, higher magnetic susceptibility corresponds to higher NGR, bulk density, and *P*-wave velocity and lower porosity and is likely related to the dominance of a mud-rich matrix in the diamict/diamictite recovered at this site. NGR, density, and *P*-wave velocity are lower in lithostratigraphic Unit II (diatom-bearing sandy and muddy diamictite) relative to Units III and IV, possibly indicating a change in the clast or matrix composition. In Subunits IIIB and IIIC and Unit IV, variations in physical properties are related to lithology (muddy diamictite versus sandy diamictite) and the relative abundance of diatoms, mud clasts, carbonate nodules, and basalt clasts. In these units, higher magnetic susceptibility, NGR, density, and *P*-wave velocity and lower porosity correspond to higher proportions of basalt and/or metasedimentary clasts and diatom-bearing lithologies. Lower magnetic susceptibility, NGR, density, and *P*-wave velocity and higher porosity correspond to higher proportions of mud clasts, carbonate nodules, and diatom-rich lithologies.

Headspace gases are low in the uppermost ~200 m CSF-A but display variable methane and increasing ethane concentrations from ~200 m CSF-A to the bottom of the hole. Interstitial water analyses of the mudline and five whole-round samples indicate early diagenesis immediately below the sediment/water interface, with sulfate reduction in the upper 100 m CSF-A and manganese reduction downhole to 215.4 m CSF-A. TOC and CaCO₃ contents are generally low (<0.6 and <3.5 wt%, respectively). Carbonate content increases slightly downhole, with values generally higher between ~400 and 630 m CSF-A (Figure F14). The slightly elevated carbonate content and decreasing TOC/TN ratio between ~400 and 630 m CSF-A may suggest more open-marine conditions during deposition of the diamictite of lithostratigraphic Unit III compared with Units I and II. Systematic variations in pXRF data indicate the potential for detailed reconstruction of sediment provenance, particularly in Units II–IV.

Downhole logging consisted of three tool strings: a modified triple combo with the sonic tool and without the source in the density tool, the VSI to conduct a VSP experiment, and the FMS. The triple combo tool string measured borehole diameter, NGR, resistivity, sonic velocity, and magnetic susceptibility. The triple combo tool string reached 650.3 m wireline logging depth below seafloor (WSF), or ~50 m above the bottom of the hole. Caliper data show that the borehole size varied significantly, with numerous washed out intervals and multiple ledges, which resulted in the VSI and FMS tool strings reaching only to 297.5 m WSF.

Despite lower quality borehole conditions than those at Site U1521, downhole data generally match well with results from core measurements. NGR data from downhole logging show good correspondence with NGR data from whole-round cores, whereas the core-based *P*-wave velocity consistently underestimates the velocity relative to the downhole log data even though the general trends are similar. Alongside other downhole logging datasets, the FMS resistivity images appear to be of reasonable quality and should help as-

sess lithologies in the poorly recovered upper part of the formation. Check shot data were successfully collected at eight depths with the VSI tool (geophone). Raw check shot data were used in preliminary velocity models for initial core-log-seismic integration.

Site U1523

Background and objectives

Site U1523 (proposed Site RSCR-14A) is located on the south-eastern flank of the Iselin Bank, ~50 km northwest of Pennell Basin, at 74°9.02'S, 179°47.70'W at 828 m water depth (Figure F15). The site is on the outermost continental shelf edge and lies beneath the modern-day ASC (Orsi and Wiederwohl, 2009). The targeted sediments are drift deposits characterized by stratified, parallel seismic reflectors with high to medium amplitudes (Figure F16). Undulations in the seafloor and subseafloor reflectors occur toward the top of the bank, 12 km west of Site U1523, and are interpreted to be from iceberg scouring. The scour marks crosscut into the youngest strata, and iceberg keels ploughing into this sediment may act to re-mobilize sediment deposited on the bank. Farther west (~80 km), seismic profiles show flat-topped ridges interpreted to represent grounding-zone wedges. Ice sheet models suggest that during the Last Glacial Maximum these likely formed as a consequence of eastward ice flow from an ice divide forming on the bathymetric high of the Pennell Bank (Golledge et al., 2013). Consequently, sediment supply at this site could arise from a combination of sources, including the following:

- Icebergs and suspended sediment from the east via the ACC,
- Downslope delivery by glacial outwash and glaciogenic debris flows at the margin of an ice sheet grounded on northernmost Pennell Bank west of the site,
- Downslope delivery by suspended sediment scoured by icebergs west of the site, and
- Pelagic/hemipelagic sedimentation.

Bottom currents associated with the ACC in this region are modeled to be between ~10 and 20 cm/s (Padman and Fricker, 2005), and winnowing of fines is expected during periods of enhanced bottom-current flow. Jacobs et al. (1974) reported strong diurnal signals and average and maximum velocities of >17 and >40 cm/s, respectively, at 4 m above the seafloor in 527–1201 m water depth in the Ross Sea.

The primary objectives of Site U1523 were to reconstruct fluctuations in the ACC during the Neogene and Quaternary (Objective 3) and to recover a high-resolution record that can be correlated with inner and outer shelf records of ice sheet advance and retreat (e.g., Site U1522 and ANDRILL AND-1B; Naish et al., 2009). Drilling at Site U1523 therefore aimed to sample the upper sedimentary section above Unconformity RSU4 to achieve this objective. The record of deposition and winnowing beneath the ACC from Site U1523 will enable us to test the hypothesis that changes in the strength of this wind-driven ocean current regulated the southward transport of warm CDW onto the Ross Sea continental shelf during past ice sheet retreat events. Another objective was the reconstruction of ice-proximal oceanic temperatures and surface water properties during periods of pelagic/hemipelagic sedimentation. This reconstruction will constrain the magnitude of polar amplification during past warm periods of the Neogene and Quaternary (Objective 2). An additional objective was to identify processes that govern sediment transfer between the outermost continental shelf and the upper continental slope/rise.

Operations

After a 147 nmi transit from Site U1522 that averaged 11.5 kt, the vessel arrived at Site U1523 at 0158 h (UTC + 13 h) on 29 January 2018. This site is an alternate that was occupied after coring at Site U1522 demonstrated that core recovery would likely be poor in the targeted upper interval of the original proposed primary Site EBOCS-04B. We planned to core two holes at Site U1523: one cored with the APC system to refusal, followed by an APC/XCB hole to 450 m DSF. Instead, we ultimately cored five holes because difficult coring conditions required additional holes to achieve the objectives (Table T2). Prior to starting coring, we conducted a seafloor camera survey to ensure we could avoid large rocks. The survey included tagging the seafloor at four potential hole locations.

Hole U1523A was cored with a combination of the APC and HLAPC systems to 46.3 m DSF, where we were unable to land the HLAPC core barrel. The hole was terminated, and we pulled the drill string above the seafloor to try to clean out the bottom-hole assembly (BHA). After we were unable to reestablish circulation through the drill string, we had to pull the pipe back to the surface to clean the debris (rocks and sand/gravel) from the BHA. The debris was curated as a ghost core. The APC/XCB BHA was reassembled and run back to the seafloor, and Hole U1523B was cored to a total depth of 164.4 m DSF. Toward the end of coring operations in Hole U1523B, hole cleaning became a problem, and off-bottom torque steadily increased despite efforts to clean the hole. In addition, rotary coring with the XCB system yielded very poor recovery, so we terminated operations in Hole U1523B with the intention of using the HLAPC system in Hole U1523C to target specific stratigraphic gaps not recovered in Holes U1523A and U1523B. After pulling clear of the seafloor from Hole U1523B, it became apparent that our ability to circulate through the bit jets was compromised. After attempting to clear the bit jets, we started Hole U1523C and drilled without coring to 43.3 m DSF. At that depth, we completely lost circulation through the drill string and were forced to terminate operations and pull the drill string back to the rig floor.

We then decided to use the RCB system to core and log to at least 300 m DSF. Hole U1523D was drilled without coring from the seafloor to 135.0 m DSF. RCB coring then penetrated from 135.0 m DSF to a total depth of 307.8 m DSF. We opted not to deepen the hole farther because of very poor recovery (0.9 m; <1%). At the end of coring operations, the hole was displaced with heavy mud (10.5 lb/gal) and logged with two tool strings: a modified triple combo and the FMS. The DSI was run on the triple combo instead of with the FMS, and the HLDS was run without the source for borehole diameter measurement with the caliper. After logging was completed, we used the APC and HLAPC systems to spot core in Hole U1523E to cover stratigraphic gaps from Holes U1523A and U1523B. Hole U1523E was successfully spot cored to 130.8 m DSF. After coring was completed, the drill string was recovered, and the rig floor was secured at 0547 h on 3 February, ending Hole U1523E and Site U1523. A total of 147.5 h (6.15 days) were spent at Site U1523.

We collected a total of 64 cores at Site U1523. The APC coring system was deployed five times, recovering 41.57 m of sediment (91%). The HLAPC coring system was used 33 times, collecting 87.99 m (59%). The XCB coring system collected 3.16 m of core (5%) over eight cores. The RCB system was deployed 18 times over 172.8 m, recovering 0.9 m (0.5%) (Table T2).

Principal results

The upper ~155 m of sediment recovered at Site U1523 is divided into three lithostratigraphic units (I–III) dated to the late Miocene–Pleistocene (Figure F17). Deeper than ~155 m CSF-A, poor recovery in Hole U1523D precluded definition of lithostratigraphic units. Several intervals shallower than 155 m CSF-A are characterized by poor recovery, fall-in, and washed gravel, which compromises our ability to identify lithologic variations and some contacts between units but may indicate the presence of unRecovered sand- and/or gravel-rich beds. Where recovered, the contacts between units are mostly sharp. The major facies at Site U1523 are massive diamict, mud, diatomite to diatom-rich mudstone, diatom-bearing mudstone, and sand. The assemblage of facies reflects open-water to ice-proximal depositional environments on the outer Ross Sea continental shelf since the late Miocene.

Lithostratigraphic Unit I consists of ~35 m of Pleistocene massive to laminated bioturbated greenish gray to grayish brown diatom-bearing mud interbedded at the decimeter scale with foraminifer-bearing/rich sand with dispersed clasts and clast-rich sandy to muddy diamict. Large rock clasts of diverse lithologies, mud clasts, and pyrite staining occur throughout, and a few shell fragments and lignite were observed in some intervals. The base of Unit I is defined by a decrease in foraminifer abundance and an increase in diatom abundance. Unit II is an ~60 m thick sequence of Pliocene to Pleistocene massive to laminated greenish gray diatom-bearing mud and olive brown to olive gray diatom-rich mud interbedded at the decimeter to meter scale with massive gray to greenish gray muddy sand, sand, and diamict. Bioturbation is common throughout Unit II and is defined by the presence of both diatom-rich mud/diatom ooze and glauconite, which is most abundant in sand beds. Pyrite staining, large rock clasts, and mud clasts were observed throughout, and shell fragments, bryozoans, and worm tubes were observed in some intervals. The base of Unit II is defined by the deepest diatom-rich sandy mud. Unit III includes ~50 m of upper Miocene massive to laminated pale green, grayish green, and dark gray diatom-bearing mud interbedded at the decimeter scale with greenish gray mud with dispersed clasts, sandy mud, and diamict. Unit III is similar to Unit II but is distinguished by a decrease in diatoms and an increase in terrigenous components relative to Unit II.

Core catcher samples from Holes U1523A, U1523B, U1523D, and U1523E were examined for siliceous (diatoms, radiolarians, silicoflagellates, ebridians, and chrysophycean cysts), calcareous (foraminifers), and organic (dinoflagellate cysts and other aquatic palynomorphs, pollen, and spores) microfossils. Diatom remains were encountered in all samples, and radiolarians are generally rare, but several intervals record higher abundance and better preservation that provide important biostratigraphic control, especially for the upper Miocene (Figure F17). A distinctive modern open-ocean radiolarian assemblage is present in the mudline sample of this site, contrasting with the coastal assemblage present in the mudline sample from Site U1522. Organic and calcareous microfossils occur sporadically throughout the entire recovered sequence. Dinocysts are often rare, except in the upper Pliocene and upper Miocene intervals. Foraminifers are most abundant in the upper Pleistocene. A unique monospecific assemblage of agglutinated benthic foraminifers was observed in the upper Miocene of Holes U1523B and U1523E, and foraminifer assemblages could be correlated between different holes.

Diatoms, radiolarians, and dinocysts provide a sequence of biostratigraphic datums that allow for correlation across holes and development of a composite age model. Three broad stratigraphic intervals separated by disconformities correspond generally to lithostratigraphic units and represent deposition of the following intervals (Figure F17):

- An upper Pleistocene interval composed largely of mixed and reworked sediments (corresponding to lithostratigraphic Unit I),
- An upper Pliocene to lower Pleistocene interval (Unit II) with sediment accumulation rates approaching 23 cm/ky of diatom-rich mud and diatom ooze, and
- An upper middle Miocene to upper Miocene interval (Unit III).

Paleomagnetic analyses of Holes U1523A, U1523B, and U1523E focused on constructing a magnetostratigraphy using ChRM directions. The NRM of archive-half core sections was measured before and after progressive AF demagnetization in 5 mT steps to 20 mT. NRM intensities prior to demagnetization are mostly $\sim 10^{-1}$ A/m and agree well with WRMSL, SHMSL, and Kappabridge magnetic susceptibility values. This agreement suggests that all of these parameters are approximately equally influenced by magnetic concentration, which seems to be relatively constant throughout all three lithostratigraphic units. NRM inclinations are predominantly positive prior to demagnetization but group in clusters of normal and reversed polarity after AF demagnetization. Discrete samples were used to test the fidelity of the archive-half NRM measurements in a 20 mT peak AF demagnetization sequence. At least three components are present with variable coercivities: a viscous remanent magnetization, a drilling overprint, and a third component with higher coercivity that most likely carries the ChRM.

The normal and reversed polarity zones identified in both archive halves and discrete samples are correlated to the GPTS using constraints from biostratigraphic datums. These tie points allow us to tentatively identify the tops of Subchron C2An.1n and Chron C4An. AMS measurements on discrete samples demonstrate that the magnetic fabric is often oblate. However, k_{\min} inclinations $<60^\circ$ also occur and coincide with intervals of coarser grain sizes, suggesting a change in compaction in these intervals relative to fine-grained intervals.

Physical property measurements were conducted on cores from Holes U1523A, U1523B, and U1523E. In general, whole-round core bulk density, magnetic susceptibility, and *P*-wave velocity measurements are in good agreement with discrete MAD samples and point measurements of magnetic susceptibility and *P*-wave velocity on the section halves (Figure F17). Downhole changes in physical properties are in good overall agreement with the defined lithostratigraphic units based on sedimentologic characteristics, and changes in physical properties can provide insight into lithologic variations in each unit. Magnetic susceptibility is highly variable in lithostratigraphic Unit I and corresponds to alternating sandy and muddy layers with abundant clasts and muddy diamict. Bulk density increases downhole and is anticorrelated with porosity, which decreases downhole in Unit I, suggesting compaction. Deeper than Unit I, bulk density and porosity show significant variation that likely reflects diatom content. For instance, low bulk density, magnetic susceptibility, and NGR in the middle of Unit II (~ 60 – 70 m CSF-A) correspond to diatom-rich mud intervals. Relatively high and stable NGR measurements in Unit III indicate relatively high clay mineral content in the massive bioturbated to laminated diatom-bearing mud and sandy mud.

Samples for headspace gas, interstitial water chemistry, and bulk sediment geochemistry were analyzed at Site U1523. Concentrations of methane and ethane are close to and below the detection limit, respectively. In addition to low-resolution interstitial water sampling (~ 1 sample per core or every other half-length core) throughout Holes U1523A, U1523B, and U1523E, a high-resolution profile of interstitial water chemistry was obtained for the upper 8 m in Hole U1523B. Low-resolution downhole trends suggest manganese and sulfate reduction in the suboxic to anoxic transition zone (~ 130 m CSF-A) (Figure F17). Rapid increases in silica and manganese concentrations in the upper ~ 2 m probably reflect shallow diagenesis of silica. Bulk sediment TOC and CaCO_3 are generally low (<0.6 and <2.5 wt%, respectively). TOC is generally slightly lower in the diatom-bearing mud and diamict of Unit III. Higher carbonate (up to ~ 15 wt%) was observed in foraminifer-bearing sandy mud in lithostratigraphic Units I and II. TOC/TN ratios do not display a discernible trend and suggest mixed input of marine and terrestrially derived organic matter. pXRF data indicate lower and more invariant Ba/Al ratios compared with Sites U1521 and U1522. In contrast, significant downhole variations can be observed in ratios of refractory elements such as Th/Ti, which alongside ratios like Fe/Ti, may serve as a provenance proxy at this site (Figure F17).

Downhole logging in Hole U1523D consisted of two tool strings: a modified triple combo with the sonic tool and without the source in the density tool and the FMS. The triple combo measured borehole diameter, NGR, resistivity, sonic velocity, and magnetic susceptibility. The triple combo tool string reached 292 m WSF, ~ 15 m above the total borehole depth, and the FMS tool string reached 288 m WSF. Downhole logging data will be key for interpreting lithologic variation deeper than 155 m CSF-A in Hole U1523D, where overall core recovery was very poor (0.5%), and in poorly recovered intervals in the upper parts of the site. Although the caliper data identified a number of minor washouts, borehole conditions were reasonable, and the log data show good correspondence with the core data over the ~ 80 m of overlap. Interestingly, although the trends and relative changes in magnitude of the NGR log data are similar to those from the cores, the core data are higher than those measured in situ. On the other hand, core-based *P*-wave velocity data are consistently lower than those from the downhole sonic log. The resistivity data show clear alternations of high and low resistivity throughout the borehole that may correspond to alternating layers of fine and coarse sediments. These alterations are also apparent in the FMS resistivity images, together with localized high-resistivity spots that are interpreted to be clasts in diamictite.

Site U1524

Background and objectives

Site U1524 (proposed Site RSCR-10A) is located on the continental rise at $74^\circ 13.05' S$, $173^\circ 37.98' W$ at 2394 m water depth on the southeastern levee of the Hillary Canyon (Figure F18). The levee at this site has a relief of ~ 500 m and is located ~ 120 km north of the Ross Sea continental shelf edge. The head of the Hillary Canyon system is located at the mouths of Pennell Basin and Glomar Challenger Basin. The Hillary Canyon is one of the largest conduits for newly formed Ross Sea Bottom Water (RSBW; a type of AABW), which is focused in this channel by dense water formed on the Ross Sea continental shelf cascading through the troughs and down the continental slope and rise. The site also lies beneath the modern-day westward-flowing ASC (Figure F5). The targeted sediments are interpreted from seismic profiles to be channel-overspill and drift

deposits characterized by stratified, parallel seismic reflectors with high to medium amplitude (Figure F19).

The primary objectives of Site U1524 were to obtain a near-continuous post-Unconformity RSU3 (upper Miocene to Pleistocene) and pre-Unconformity RSU3 (middle to upper Miocene) sediment sequence to provide a high-resolution chronology and an ice-distal record of glacial–interglacial cycles. The continental rise location of Site U1524 should allow a more complete assessment of oceanic response to AIS variability. The record of deposition from Site U1524 was anticipated to be primarily influenced by RSBW flowing down the Hillary Canyon, but also by an alongslope component caused by the westerly flowing ASC. Consequently, this site will enable assessment of the oceanographic influence on ice sheet variability and bottom water production (Objective 2). The direct record of AABW flow down the Hillary Canyon obtained at Site U1524 could potentially be extrapolated to high-fidelity paleoceanographic records farther afield in the abyssal Pacific Ocean to better constrain the Antarctic influences on the global oceanic deep circulation. The Hillary Canyon is also a main route for glacial sediments being eroded and transported by ice streams from the innermost continental shelf to its edge, and provenance studies of the terrigenous sediment may allow for identification of changing ice sheet drainage pathways through the Neogene and Quaternary. Because Site U1524 is near the crest of the levee of the Hillary Canyon, it will also provide a high-resolution record for documenting the deep-sea response to ice sheet change on the continental shelf, which is recorded in the Ross Sea inner (ANDRILL Site AND-1B; Naish et al., 2009) and outer (IODP Site U1522) continental shelf. IBRD could be sourced by icebergs calving from the Ross Sea, as well as transported from the east through the ASC, providing a proxy for dynamic ice discharge from the Pacific coastline sector of the WAIS. Pelagic sediments deposited during periods of high productivity or a lull in turbidity current overspill deposition will provide a record of surface water properties, including sea ice cover, SST, stratification, and salinity. These proxy records will enable us to assess the magnitude of polar amplification during past warm climates (Objective 2), as well as the role of oceanic forcing of ice sheet retreat or advance at these times (Objective 3). In addition, continuous deposition was anticipated at this site through much of the Neogene and Quaternary to allow for assessment of the orbital response of the WAIS and adjacent oceanic/biological system over a range of past climatic conditions (Objective 4).

Operations

After a 52 nmi transit from Site U1523 that averaged 11.1 kt, the vessel arrived at Site U1524 at 1027 h (UTC + 13 h) on 4 February 2018. This site is an alternate site for primary proposed Site RSCR-02B. We decided to occupy the alternate site because the highest priority target is shallower, the seismic facies show less evidence for transported sediment, and the sea ice edge was farther away. The original plan called for three holes, one cored to refusal with the APC system followed by an APC/XCB hole to 350 m DSF. The third hole was to be cored to 1000 m DSF with the RCB system and then logged with three tool strings. We ultimately cored three holes (Table T2). Hole U1524A was cored with the APC/XCB system to 299.5 m CSF-A. Hole U1524B consists of a single mudline core collected for high-resolution interstitial water and microbiology sampling. Hole U1524C is an RCB hole cored to 441.9 m DSF.

Hole U1524A was cored to APC refusal at 270.3 m DSF, after which we deployed the HLAPC system; however, the first core advanced only 0.4 m to 270.7 m DSF, indicating HLAPC refusal.

Downhole formation temperatures were taken on Cores 6H (51.5 m DSF), 9H (80.0 m DSF), 12H (108.5 m DSF), and 15H (137 m DSF) using the Advanced Piston Corer Temperature tool (APCT-3). Following HLAPC refusal, we deployed the XCB system and cored to 299.5 m DSF, but each XCB core returned with a shattered liner and highly disturbed sediment. At that point, we terminated coring and pulled out of the hole because of approaching sea ice. After pulling out of the hole, enough time remained to collect a single mudline core (Hole U1524B) for high-resolution interstitial water and microbiological studies. After terminating coring in Hole U1524B, we retrieved the drill string and departed Site U1524 at 2030 h on 6 February. With sea ice estimated to remain over Site U1524 for at least 2 days, we opted to occupy Site U1525 (proposed Site RSCR-03A), located only 47 nmi away but in a position south of the sea ice edge. After ice monitoring determined that the sea ice was moving away from Site U1524, we ended operations at Site U1525 at 0535 h on 9 February to return to Site U1524. After arriving back at Site U1524 at 1006 h, we prepared for RCB coring operations in Hole U1524C. While deploying the drill string, we lowered the subsea camera to retrieve the beacon, which had failed to release when abandoning the site. After retrieving the beacon, Hole U1524C was drilled without coring to 260.5 m DSF and then RCB cored to 441.9 m DSF, where we were forced to terminate operations because of a mechanical breakdown of the port stern tube shaft and arrangement that ended Expedition 374 science operations. The rig floor was secured for transit at 1835 h on 11 February, ending Site U1524. Total time spent at Site U1524 was 117.25 h (4.9 days).

We collected a total of 54 cores at Site U1524. The APC system was deployed 31 times, collecting 284.17 m of core (102%). The HLAPC system was deployed once, recovering 0.43 m of core (108%). The XCB system collected 5.51 m over three cores (19%). The RCB system was used 19 times, collecting 19.2 m of core (11%) (Table T2).

Principal results

Site U1524 includes three holes, the deepest cored to 441.9 m CSF-A. The upper Miocene to Pleistocene sediment recovered is divided into three lithostratigraphic units (I–III). Unit I is divided into three subunits (IA, IB, and IC) (Figure F20). Contacts between units and subunits are mostly gradational and are distinguished by gradual changes in biogenic content. The major facies at Site U1524 are diatom-bearing mud, diatom-rich mud, diatom ooze, sandy mud, and muddy diamict. The assemblage of facies reflects pelagic sedimentation with ice rafting and winnowing/redeposition by downslope, alongslope, and turbidity currents. The sediment recovered at Site U1524 reveals reworking by these current systems superimposed on variations in terrigenous and marine sediment supply since the late Miocene on the upper continental rise of the Ross Sea.

Lithostratigraphic Unit I consists of ~200 m of upper Pliocene to Pleistocene unconsolidated massive to laminated diatom-bearing/rich mud interbedded with muddy diatom ooze. A gradual downhole increase in diatom content characterizes this unit and was used to distinguish three subunits based on increasing percentage of biogenic material. Subunit IA consists of ~78 m of massive to laminated light yellowish brown to brown diatom-bearing/rich mud interbedded at the decimeter to meter scale with greenish gray diatom-bearing/rich mud to sandy mud with dispersed clasts. Sand laminae and lenses are increasingly abundant toward the base of the unit. A 20 cm thick volcanic ash layer is present in Subunit IA. The base of this subunit is marked by a transition from olive gray diatom-rich mud to greenish gray diatom-rich mud with sandy mud

interbeds. Subunit IB (~78 m thick) consists of meter-scale interbeds of olive gray and greenish gray diatom-rich mud/sandy mud to muddy diatom ooze with dispersed clasts. The abundance of millimeter-scale silty to sandy laminations increases downhole in this subunit. The base of Subunit IB is defined by an increase in thickness and frequency of sandy mud beds with clasts. Subunit IC consists of ~45 m of interbedded olive gray diatom-rich mud and muddy diatom ooze that is similar to Subunit IB but features an increase in the biogenic component with thinner greenish gray beds and thicker beds of sandy mud with dispersed clasts. Pyrite staining is present throughout this subunit. The boundary between Units I and II is marked by a sharp contact between diatom-rich mud and muddy diatom ooze. Unit II consists of ~117 m of massive to laminated olive gray muddy diatom ooze interbedded with bioturbated to laminated greenish gray diatom ooze and diatom-rich sandy mud. The olive gray muddy diatom ooze beds include pyrite staining and sand/silt laminations, and the greenish gray diatom ooze beds contain more intense bioturbation. The contact between Units II and III is defined by the first downhole occurrence of massive diamict. Unit III (120 m thick) consists of massive to laminated diatom-rich dark greenish gray mud interbedded with greenish gray massive diatom-rich sand and sandy mud with dispersed clasts, muddy diamict, and muddy diatom ooze. The lower contacts of sandy mud beds are usually gradational and bioturbated.

A total of 47 core catcher samples from Holes U1524A and U1524C were analyzed for siliceous (diatoms, radiolarians, silicoflagellates, ebridians, and chrysophycean cysts), calcareous (foraminifers), and organic (dinoflagellate cysts and other aquatic palynomorphs, pollen, and spores) microfossils. The mudline and core catcher samples from Core 374-U1524B-1H were also examined. The occurrence and abundance of the different microfossil groups varies greatly throughout the Site U1524 sediment column. Rich assemblages of diatoms, silicoflagellates, and ebridians occur throughout, whereas radiolarians are generally rare but common to abundant in several samples, particularly in the lower Pliocene and Miocene intervals where they provide valuable biostratigraphic control (Figure F20). Foraminifers and palynomorphs are generally sparse.

Although all investigated microfossil groups supply valuable information, radiolarians and diatoms provide well-constrained age-diagnostic taxa used to develop an age-depth model for the site (Figure F20). Reworking and mixing of diatom assemblages of multiple ages limited the biostratigraphic utility of diatoms from the seafloor to ~80 m CSF-A. The underlying stratigraphic sequence can be assigned to several biostratigraphic zones that are sometimes bounded by unconformities that also correspond to the lithostratigraphic unit boundaries. The ~80–120 m CSF-A interval is dated to the early Pleistocene. Deeper than 120 m CSF-A is an ~160 m thick Pliocene interval rich in diatoms. A disconformity representing >1.0 My is interpreted between ~273 and 283 m CSF-A. An ~30 m thick interval of lower Pliocene between ~283 and 310 m CSF-A overlies another disconformity interpreted between ~310 and 320 m CSF-A. Sediment deeper than this hiatus is dated to >8.5 Ma (late Miocene), and the deepest sample from the site (~437 m CSF-A) is dated to <10 Ma.

Paleomagnetic investigations primarily focused on generating a magnetostratigraphy to assist with establishing a chronostratigraphy. NRM measurements were generally conducted prior to and after AF demagnetization with peak fields of 10 and 20 mT. Initial NRM intensities oscillate around $\sim 10^{-1}$ to 10^{-3} A/m and decrease after demagnetization to $\sim 10^{-2}$ to 10^{-5} A/m. These oscillations agree

well with variations in magnetic susceptibility, suggesting that magnetic particle concentration has a comparable effect on these parameters and potentially decreases downhole. After removal of the drilling-induced, downward-directed overprint, inclinations cluster in generally steep upward and downward directions. These clusters represent normal and reversed polarity zones, respectively, that can be tied to the GPTS using independent biostratigraphic datums. We identified all normal and reversed (sub)chrons between Chron C1n (Brunhes; 0–0.781 Ma) and the top of Subchron C2An.2r (3.207 Ma). Magnetic fabric experiments were also conducted to check for subtle disturbances that may yield unreliable directions, as well as for differential compaction in the different lithostratigraphic units. Generally, most samples have an undisturbed oblate fabric common in sedimentary settings, but the degree of anisotropy is variable between lithostratigraphic units and may relate to factors such as differences in sedimentation rate.

Physical properties measurements were conducted on whole-round cores from Holes U1524A and U1524C, together with additional measurements on split-core sections and discrete samples. In general, data from whole-round measurements show trends similar to those from split-core measurements. A small deviation between whole-round measurements of GRA bulk density and *P*-wave velocity compared with discrete measurements deeper than ~100 m CSF-A in Hole U1524A is likely due to core expansion generated by degassing during the equilibration of the cores to room temperature. Downhole changes in physical properties are in good overall agreement with the defined lithostratigraphic units based on sedimentologic characteristics, and changes in physical properties in each unit can provide insight into lithologic changes in each unit.

Overall, there is a good correlation between magnetic susceptibility, NGR, and bulk density measurements (Figure F20). These parameters are inversely correlated with the sediment color *b** parameter and appear to relate to diatom content, with a general increase downhole over tens of meters, together with variability caused by interbedded lithologies. Taken together, these results suggest that sedimentary deposition is governed by variations in biogenic and terrigenous inputs. Apparent cyclicity is observed in these parameters. Overall, these parameters suggest a higher terrigenous content in lithostratigraphic Subunit IA, decreasing terrigenous content and increasing biogenic content throughout Subunits IB and IC, and maximum biogenic content in Unit II, which is predominantly diatom ooze. Lithostratigraphic Unit III also has higher terrigenous content corresponding to interbedded diatom-rich mud. Downhole formation temperature measurements with the advanced piston corer temperature tool (APCT-3) indicate a geothermal gradient of 58°C/km, which when combined with thermal conductivity measured on sediment cores from Site U1524, indicates a heat flow of 53.7 mW/m².

Samples for headspace gas, interstitial water chemistry, and bulk sediment geochemistry were analyzed at Site U1524. Concentrations of methane and ethane are close to or below the detection limit in the uppermost ~100 m CSF-A but increase to higher concentrations at greater depths (to 42,000 ppmv at 180 m CSF-A for methane). Interstitial water sampling was conducted at low resolution (~1 sample per core in the upper 100 m and approximately every third core downhole from that depth, depending on core recovery) in Holes U1524A and U1524C. A high-resolution interstitial water profile was also obtained for the upper 7.56 m CSF-A in Hole U1524B. Low- and high-resolution downhole trends show clear manganese and sulfate reduction in the suboxic to anoxic transition zone in the upper ~90 m CSF-A (Figure F20). A rapid in-

crease in silica concentration in the upper 2 m CSF-A probably reflects shallow diagenesis of silica. Elevated barium concentration deeper than ~90 m CSF-A may indicate barite dissolution in an environment where interstitial water is undersaturated with respect to barite. Bulk sediment TOC and CaCO_3 contents are generally low throughout the site but reveal distinct variability in lithostratigraphic Unit I. Higher percentages of carbonate content were observed in Subunits IB and IC and in a carbonate-cemented mudstone in Unit III. TN content in the bulk sediments is very low, and TOC/TN ratios display similar trends to total organic carbon.

Site U1525

Background and objectives

Site U1525 (proposed Site RSCR-03A) is located on the continental slope at $75^{\circ}0.06'\text{S}$, $173^{\circ}55.20'\text{W}$ at 1776 m water depth on the southeastern levee of the Hillary Canyon in a depositional setting similar to that of Site U1524 (~87 km northeast) (Figure F21). Site U1525 is closer to the continental shelf edge, which lies ~60 km south of the site, and the mouths of the Pennell and the Glomar Challenger Basins. The levee shows asymmetric flanks: a steep northeastern erosional flank with a relief of ~500 m and a less steep southwestern flank with a relief of only 30 m. The northwest flank sharply truncates parallel high-amplitude reflectors, outcropping at the seafloor, and chaotic seismic facies suggest that slope failure features affect the mid- to lower units of the seismic profile (Figure F22).

The Hillary Canyon is one of the largest conduits for newly formed RSBW, which is focused in this channel by cascading dense water formed on the Ross Sea continental shelf passing down the continental rise. The site also lies beneath the modern-day westward flowing ASC (Figure F5), which is thought to be stronger here than at the deeper water Site U1524 (Whitworth et al. 1995; Orsi and Wiederwohl, 2009). Seismic profiles indicate that the targeted sediments at Site U1525 are dominated by channel-overspill and drift deposits characterized by stratified, parallel seismic reflectors with high to medium amplitude (Figure F22). These strata in the upper ~50 m of the site are likely glacial debris flows interlayered with interglacial hemipelagic units of Pleistocene age that formed a prograding shelf-margin trough mouth fan at the mouth of the Glomar Challenger Basin since the late Miocene (Unconformity RSU3).

The continental slope location of Site U1525 should allow for a more complete assessment of oceanic forcing of (and response to) AIS variability. The record of deposition from Site U1525 was anticipated to be primarily influenced by RSBW flowing down the Hillary Canyon, but this signal is modified by an alongslope component associated with the westerly flowing ASC. Consequently, this site will enable assessment of ocean forcing for ice sheet variability and drivers of bottom water production (Objective 2). The direct record of RSBW flow down Hillary Canyon obtained at Site U1525 could potentially be extrapolated to high-fidelity paleoceanographic records farther afield in the abyssal Pacific Ocean to better constrain the Antarctic influences on the global oceanic deep circulation. Hillary Canyon is also a main route for glacial sediments being eroded and transported by ice streams from the innermost continental shelf to its edge. Provenance studies of the terrigenous sediment may allow identification of changing ice sheet drainage pathways through the Neogene and Quaternary.

IBRD could be sourced by icebergs from the Ross Sea, as well as those transported from the east by the ASC, providing a proxy for dynamic ice discharge from the Pacific Ocean coastline sector of the WAIS. Pelagic deposits are from periods of high productivity or a

lull in turbidity current–overspill deposition and will provide proxy records of surface water properties, including sea ice cover, SST, stratification, and salinity. These proxy records will enable an assessment of the magnitude of polar amplification during past warm climates (Objective 2), as well as the role of oceanic forcing of ice sheet fluctuations during those times (Objective 3). In addition, continuous deposition was anticipated through much of the late Neogene and Quaternary at this site, which would allow assessment of the orbital response of the WAIS and adjacent oceanic/biological systems over a range of past climatic conditions (Objective 4). The late Quaternary record in the uppermost 50 m of glacial strata can also shed light on recent ice sheet advances.

Operations

After a 50 nmi transit from Site U1524 averaging 8.9 kt, the vessel arrived at Site U1525 at 0200 h (UTC + 13 h) on 7 February 2018. This alternate site was added to the schedule when we were forced to temporarily leave Site U1524 because of encroaching sea ice. The operational plan for Site U1525 consisted of APC/XCB coring in a single hole until ice moved away from Site U1524. Hole U1525A was cored to a total depth of 213.2 m DSF using a combination of APC, HLAPC, and XCB coring (Table T2). The XCB system was deployed in the upper part of the hole (43.0–55.7 m DSF) to core past an indurated interval. We then switched back to piston coring and continued to core using both the APC and HLAPC systems to 131.2 m DSF. We continued coring with the XCB system to 213.2 m DSF and terminated the hole at that depth after receiving confirmation that the sea ice was expected to clear from Site U1524 by the next day. The rig floor was secured for transit at 0535 h on 9 February to return to Site U1524. A total of 51.25 h (2.1 days) was spent in Hole U1525.

We collected 33 cores at Site U1525. The APC system was deployed 8 times, collecting 63.23 m of core (103%). The HLAPC system was deployed 14 times, recovering 52.64 m of core (92%). The XCB system was used 11 times and collected 42.83 m (45%).

Principal results

Site U1525 cored a single hole to 208.28 m CSF-A. The 158.70 m of Pleistocene sediment recovered is divided into three lithostratigraphic units (I–III). Unit II is divided into Subunits IIA and IIB (Figure F23). A few intervals (typically <15 m in length) are characterized by poor recovery, compromising our ability to identify lithologic variations. The major facies at Site U1525 are massive to stratified diamict, sand, mud, diatom-bearing mud, and diatom-rich mud to diatom ooze. The assemblage of facies reflects an interplay between distal down-slope, alongslope (e.g., winnowing), hemipelagic, and pelagic processes in a relatively ice distal glaciomarine setting. Both thin laminations (millimeter to centimeter scale) and thick beds (meter scale) are recognized in all units and may be linked to glacial dynamics and ocean circulation variations during the Pleistocene.

Lithostratigraphic Unit I consists of ~51 m of unconsolidated massive bioturbated gray diatom-bearing/rich mud to sandy mud with dispersed clasts interbedded on a meter scale with gray to light yellowish brown clast-poor to clast-rich muddy diamict. Unit I bedding contacts are sharp to gradational. The muddy diamict is overcompacted in some intervals and contains randomly distributed clasts of igneous and metamorphic composition. The base of Unit I is in an interval of poor recovery; however, it is defined by a sharp contact between the overlying diamict and diatom-rich mud. Unit II consists of ~68 m of massive to laminated greenish gray diatom-

bearing/rich mud and diatom ooze with dispersed clasts interbedded at the decimeter to meter scale with sandy mud and diamict. Unit II is divided into two subunits based on diatom abundance and the structure and texture of laminations. Subunit IIA contains well-defined millimeter-scale fine sand, silt, and biosiliceous laminations with sharp lower boundaries and internal normal grading. Clasts, soft-sediment deformation features, and microfaulting can be observed in the laminated sequences. Subunit IIA also contains intervals of bioturbated foraminifer-bearing sand with sharp upper and lower contacts in the massive diatom-bearing/rich mud beds. The boundary between Subunits IIA and IIB is distinguished by the onset of very thinly laminated silt and mud with better preservation and higher percentages of intact diatom frustules. Subunit IIB contains fine-grained sand and silt laminae in coarser grained sandy mud and diamict beds. Clasts, pyrite staining, and sand pods, lenses, and stringers can be observed throughout the subunit. The base of Unit II is defined by a sharp contact between the laminated mud of Unit II and the underlying clast-rich sandy diamict. Unit III consists of ~90 m of massive to laminated greenish gray diatom-rich mud to muddy diatom ooze with dispersed to common clasts interbedded with massive bioturbated greenish gray diatom-rich sandy mud with dispersed clasts and diamict. Clasts, pyrite staining, and coarse sand pods/lenses and stringers occur throughout.

Core catcher samples from Site U1525 were analyzed for siliceous (diatoms, radiolarians, silicoflagellates, and ebridians), calcareous (foraminifers and nannofossils), and organic (dinoflagellate cysts and other aquatic palynomorphs, pollen, and spores) microfossils. Samples in the upper ~107 m CSF-A of the section are mostly devoid of microfossils, contain only trace numbers, or include a “residual” assemblage of resistant forms that have likely been engaged in multiple phases of transport and reworking by ice and/or bottom currents (Figure F23). Diatom taxa found in this interval are eroded and were transported from discrete source beds of Miocene to early Pliocene age. One age-diagnostic radiolarian event found in this interval indicates an age >0.65 Ma at ~30 m CSF-A. Several discrete intervals of foraminifer-bearing/rich sand are present near the base of this interval, and a sparse, moderately well-preserved Neogene assemblage of calcareous nannofossils was found in one of these beds.

Deeper than ~107 m CSF-A, siliceous microfossils are more abundant and well preserved, and several age diagnostic radiolarians and diatoms were encountered (Figure F23). Although a small background presence of reworked diatoms continues in this interval, the sequence can confidently be assigned an early Pleistocene age. Planktonic and benthic foraminifers are also most abundant and diverse in this lower Pleistocene section, and the presence of the temperate planktonic species *Globoconella inflata* at ~89 m CSF-A and *Globigerina bulloides* and *Globigerina falconensis* at ~125 m CSF-A indicates the presence of warmer-than-present water. Dinocysts are sparse in this interval, and only one sample from the lower Pleistocene (~155 m CSF-A) contains abundant specimens, comprising species so far only known from upper Quaternary sediments of the Atlantic sector of the Southern Ocean, south of the Polar Front.

We developed an age model for Site U1525 using a combination of radiolarian and diatom biostratigraphic events. A hiatus is detected by biostratigraphic (diatom) marker species between ~111 and 117 m CSF-A that constrains the age of sediments deeper than this interval to >2.35 Ma and shallower sediments to <1.9 Ma. The lowermost ~100 m CSF-A of the Site U1525 sequence represents an expanded lower Pleistocene section (Figure F23) with a sustained

high sediment accumulation rate of >60 cm/ky. Above the disconformity, significant amounts of reworked microfossils in the upper ~107 m CSF-A preclude definitive age assignment for the interval.

Paleomagnetic investigations were primarily focused on determining the ChRM to construct a magnetostratigraphy. The initial NRM was measured at 5 cm intervals on most archive-half core sections, followed by NRM measurements after AF demagnetization of 10 and 20 mT to remove a potential drilling overprint. NRM intensity of cores shallower than ~100 m CSF-A decreases up to an order of magnitude after 10 mT, whereas NRM intensity of cores deeper than ~100 m CSF-A decreases by 30%–50% after demagnetization. Initial NRM inclination is generally steep and downward directed, but AF demagnetization removes this overprint to reveal clusters of steep upward- and downward-directed inclinations. We interpret these clusters to be normal and reversed polarity zones. To test the fidelity of these polarity zones, we also subjected a selected group of oriented discrete samples to a 20-step demagnetization protocol and used PCA to determine the ChRM direction. The discrete and archive-half measurements agree well, so we can correlate the normal and reversed polarity zones to the GPTS aided by the independent biostratigraphic age control. We identify the Jaramillo (0.988–1.072 Ma) and Cobb Mountain (1.173–1.185 Ma) Subchrons and the Olduvai Chron (1.778–1.945 Ma). We correlate a zone of reversed polarity below the hiatus to Subchron C2r.2r (2.148–2.581 Ma) based on diatom constraints.

Physical property measurements were conducted on all cores from Hole U1525A. In general, the whole-round core GRA bulk density, magnetic susceptibility, and *P*-wave velocity measurements are in good agreement with discrete MAD samples and point measurements of magnetic susceptibility and *P*-wave velocity on the section halves over the upper 131 m CSF-A, which were primarily cored with the APC and HLAPC systems (Figure F23). The switch to XCB coring deeper than 131 m CSF-A had an effect on whole-round measurements, especially magnetic susceptibility, NGR, and GRA bulk density, because the diameter of XCB cores does not completely fill the core liner. The *P*-wave logger was turned off deeper than 131 m CSF-A.

In lithostratigraphic Unit I, magnetic susceptibility, NGR, bulk density, *P*-wave velocity, and shear strength increase downhole and porosity decreases (Figure F23). These changes reflect both compaction and slight changes in lithology in the diatom-bearing sandy mud interbedded with clast-poor muddy diamict. Peaks in magnetic susceptibility, NGR, bulk density, *P*-wave velocity, and shear strength and a decrease in porosity occur in a short interval in Unit I (~15–18 m CSF-A), reflecting increased clasts, clay, and compaction in this clast-rich diamict unit interpreted to be a debris flow. In Unit II, decimeter-scale cyclicity is visible in magnetic susceptibility and NGR and is likely related to downhole changes in lithology. Shear strength in Unit II also demonstrates downhole cyclicity that may be related to lithologic changes or compaction. Generally lower magnetic susceptibility, NGR, density, and *P*-wave velocity in Unit III reflect increased diatom content.

Samples for headspace gas, interstitial water chemistry, and bulk sediment geochemistry were analyzed at Site U1525. Headspace gas (methane and ethane) concentration is low in the upper 124 m CSF-A and increases to 6640 and 7 ppmv, respectively, at 194 m CSF-A. Interstitial water analyses of the mudline and 12 whole-round samples indicate biogeochemical zonation with sulfate reduction in the uppermost 100 m CSF-A. Downhole variations in silica concentration broadly correspond with lithologic changes (Figure F23), whereas calcium concentration decreases from seawater-like values

in the uppermost 32 m CSF-A to a minimum value around the boundary between lithostratigraphic Subunit IIB and Unit III. Lithium concentration increases by a factor of three along a linear trend deeper than ~60 m CSF-A. TOC and carbonate contents are low (<1% and 5%, respectively) throughout the site. The highest and most variable carbonate content and TOC/TN ratios occur in the uppermost ~35 m CSF-A in lithostratigraphic Unit I.

Expedition synthesis and preliminary scientific assessment

Operational considerations relating to the science objectives

The overarching goal of Expedition 374 was to drill a transect from the outer Ross Sea continental shelf to the continental rise (Figure F24) to identify oceanic forcings and feedbacks relating to past ice sheet variability from the Neogene to Quaternary. Unfortunately, this ambition was not fully realized because a mechanical failure with the vessel resulted in termination of all drilling operations and a loss of 16 onsite operational days (from a total of 41). The loss of 39% of our operational time restricted our ability to achieve all objectives as originally envisioned. Although aspects of all objectives can be met in part, this unforeseen change in the operations plan severely compromised the plan to recover continuous records from the deep-water sites covering contemporaneous periods collected on the continental shelf. We also note that drilling operations in the Antarctic are inherently more challenging than other regions due to weather, ice, and lithologic considerations that have traditionally resulted in poor recovery on the Antarctic continental shelf. Expedition 374 was highly successful in this context. The discussion below provides a synthesis of these successes and highlights the importance of a flexible operations plan and large numbers of alternate sites to adapt to these Antarctic-specific considerations. We also document some of the challenges that remain despite our very targeted approach to drilling in this environment.

In general, the operations plan successfully mitigated most risks associated with weather, ice, and lithology. Recovery rates using the RCB coring method at the continental shelf sites were higher than expected, particularly in the lithified Miocene strata at Site U1521 with 63% total recovery, which is the highest recovery rate for ship-based drilling on the Antarctic continental shelf. Total recovery at Site U1522 on the outer continental shelf was 40% but proved more difficult in the unlithified Plio–Pleistocene sediments shallower than 400 m CSF-A (21% recovery). However, recovery was far more successful in the upper Miocene lithified diamictite intervals deeper than 400 m CSF-A (64% recovery), which were the primary targets of this site. Our original operations plan included coring at proposed Site EBOCS-04B after completing operations at Site U1522. Seismic correlations indicated that the targeted section at proposed Site EBOCS-04B is almost identical to the unlithified Plio–Pleistocene lithologies we encountered in the upper 400 m CSF-A at Site U1522. Given our experience of poor recovery in these lithologies at Site U1522, we had low confidence in our ability to obtain a recovery rate at proposed Site EBOCS-04B suitable to meet our objectives. Consequently, we modified the operations plan to core a different depositional setting at Site U1523, which targeted a Miocene to Pleistocene sediment drift on the outermost continental shelf. This depositional setting had never been sampled by deep drilling in the Antarctic, although shallow piston and gravity cores indicate that the upper sediment at the site location consists of un-

consolidated diatomaceous mud and sand with clasts. This site provided its own challenges, with soft diatom-rich and mud-rich lithologies interbedded with unconsolidated gravels and indurated strata. Consequently, we adopted a novel approach of targeted half-length piston coring, whereby the gravel-rich and indurated lithologies that were impossible to recover with any type of coring method were identified in the first two holes (U1523A and U1523B). After examination of drilling parameters (e.g., penetration rate and weight on bit), core catcher material, and assessment of downhole logs from Hole U1523D, a final hole (U1523E) was advanced without coring through these difficult lithologies, and HLAPC cores were successfully collected in the underlying softer lithologies. This resulted in high recovery (73%) of the targeted ~95 m thick Plio–Pleistocene interval. XCB coring in Miocene strata below this depth was less successful, but sporadic intervals of high recovery will provide an important archive of this rarely sampled time period in Antarctica. An attempt was made to RCB core at Site U1523 but, as anticipated for these lithologies, recovery was very poor (0.5%), and this hole was primarily intended to serve as a “clean” hole for downhole logging purposes to complete the missing stratigraphy of the APC/HLAPC- and XCB-cored intervals. Thus, despite the extremely poor recovery in Hole U1523D, this RCB hole proved highly valuable because hole conditions were suitable to obtain downhole logs.

Recovery rates with the APC coring methods were expected to be very high on the continental rise sites, and this proved to be the case, with Site U1524 obtaining 100% recovery in the 270 m thick interval that was APC/HLAPC cored. Recovery was poor in the XCB cored interval, and many XCB cores returned with shattered core liners (14 out of 22; 64%). We speculated that this unexpected result was due to the very cold surface sea waters (-1.5° to -2°C) used as drilling fluid. This issue should be investigated for future expeditions that drill in extreme cold-water regions. At Site U1524, XCB coring was terminated due to poor recovery, and this decision coincided with a weather event that pushed sea ice toward the site. We mitigated for sea ice risk in our plan by identifying a large number of alternate sites. The shipboard ice observer indicated that the sea ice would pass completely over Site U1524 in ~3 days. Considering the short time window for operations elsewhere before we could return to Site U1524 to complete our primary objectives, we collected a single APC core in Hole U1524B for high-resolution microbiological and interstitial water sampling. We then temporarily abandoned Site U1524 due to the encroaching sea ice and decided to piston core a nearby (47 nmi) upper continental rise site (U1525). This site required minimal transit time and provided a complementary record that overlaps with the upper part of Site U1524 but in a more proximal setting to the continental shelf, thus providing a hybrid record of the depositional processes observed at Sites U1523 and U1524 (e.g., ASC vigor and AABW formation, respectively). After being informed that the sea ice would drift off Site U1524 by the next day, we terminated coring at 213.2 m CSF-A because the XCB coring at Site U1525 also proved problematic, with multiple shattered core liners. We returned to Site U1524 to core with the RCB system to a target depth of 1000 m CSF-A, but the site was terminated at 442 m DSF due to the mechanical failure and termination of all drilling operations. Consequently, Site U1524 was terminated before our stratigraphic target could fully be met, and we were unable to obtain the deeper sediment that was a primary objective of that site. This deeper sediment would have contained a middle Miocene continental rise record of paleoenvironments from the same time period as the high-quality continental shelf record from Site

U1521. Termination of operations also precluded us from coring a final hole to APC refusal to recover a complete stratigraphy in the upper part of the sequence. Despite these setbacks, many aspects of the continental shelf-to-rise transect can be achieved for the Plio-Pleistocene interval through comparison with records from Sites U1522–U1525 and the ANDRILL program.

The mechanical failure also meant we could not recover a record from proposed Site RSCR-19A, which was a late addition alternate site that was upgraded to a primary site during the early phase of the expedition because we recognized it was the most suitable site at which to obtain a high-fidelity and continuous record of pelagic/hemipelagic sedimentation in the Ross Sea. Despite the unforeseen mechanical issue compromising much of the science plan, the material recovered during Expedition 374 will still provide unprecedented insights into the coupled nature of past marine-based ice sheets in West Antarctica and the adjacent water masses directly offshore. Our operational plan and risk mitigation strategy were successful, and recovery of upper Miocene and older strata on the Ross Sea continental shelf was successful using rotary coring methods, whereas APC coring methods also demonstrated that high-quality, continuous drill core records can be obtained from the Antarctic continental slope and rise.

Preliminary scientific assessment

Our drilling plan identified a series of sites where a source-to-sink sedimentary system could be mapped through the extensive network of seismic surveys that exist in the Ross Sea and targeted a continental shelf-to-rise transect approach (Figure F24) that would allow for a detailed assessment of oceanic/ice sheet interactions back to at least the middle Miocene (Figure F3). Critically, we located the drill sites on the outer Ross Sea continental shelf because models indicate that this sector of the Antarctic is the most sensitive to oceanic heat flux during deglacial events and, conversely, is one of the last areas of the continental shelf to become glaciated during past glacial advance events (Figure F4). Thus, the records from the sites provide an end-member scenario for identifying the climatic thresholds required to achieve a fully glaciated state in Antarctica, as well as identifying oceanic triggers for glacial retreat during past warming events. Sites U1521 and U1522 were drilled on the outer Ross Sea continental shelf (Figure F2) and were explicitly designed to directly identify the timing of past grounding and retreat events of marine-based ice sheets in the Ross Sea. Site U1521 targeted a middle Miocene record to identify the processes that lead to the expansion of large ice streams emanating from the EAIS across the western Ross Sea continental shelf and to recover a semi-continuous record of the MMCO in an ice-proximal location.

We cored a 650 m thick sequence of interbedded diamictite, mudstone, and diatomite strata at Site U1521 (Figure F11) with the aim of sampling above and below seismic Unconformity RSU4. The depositional reconstructions obtained from these lithologies will provide unprecedented insight into environmental change at the Antarctic margin during the middle Miocene. Site U1522 targeted a Pleistocene to upper Miocene sequence from the outer shelf (Figure F14) with the primary objective to penetrate and date Unconformity RSU3, which is interpreted to represent the first major continental shelf-wide expansion and coalescing of marine-based ice streams from both East and West Antarctica. Recovery at Site U1522 was in line with expectations, and the primary objective of

dating Unconformity RSU3 was achieved. The lithology at Site U1522 is dominated by diamictite, and lithologic variations are subtler than at Site U1521. Lithologic variation was anticipated to be higher at this site based on the interpretation of the seismic profiles, but thin diatom-rich mudstone and diatomite beds were recovered in some intervals that will provide snapshot records of a deglaciated outer shelf environment in the late Miocene. Finer grained (diatomite and mud) and unconsolidated diamict and gravel-rich beds were possibly washed away in the coring process at both Sites U1521 and U1522. However, downhole logging operations were successful at both sites, allowing for a fuller assessment of lithologic cyclicity. Outer continental shelf Site U1523 is a sediment drift located beneath the westward flowing ASC (Figure F15) and will provide a reconstruction of the changing vigor of this current through time. This reconstruction will enable testing of the hypothesis that changes in ASC vigor regulates heat flux onto the continental shelf, making the ASC a key control on ice sheet mass balance. At this site, we recovered a sequence of diatom ooze, foraminifer-rich sand, gravel, and diamict that will also provide a record of changing surface and intermediate water properties (e.g., SST, salinity, and nutrient availability) and productivity at this location near the continental shelf break.

At Site U1524, we cored a sedimentary sequence on the continental rise on the levee of the Hillary Canyon (Figure F18), one of the largest conduits of AABW delivery from the Antarctic continental shelf into the abyssal ocean. We were mostly successful in achieving our objectives at this site; it recovered a high-quality Plio-Pleistocene record (Figure F20) of turbidite activity relating to transport of cascading water masses (e.g., AABW) down the Hillary Canyon, providing a reconstruction of this critical component of the global oceanic overturning circulation. These overspill turbidite deposits are interbedded with periods of pelagic deposition that will enable proxy reconstructions of surface and bottom water properties. However, Site U1524 was intended to provide a record extending to the middle Miocene to overlap with the continental record obtained at Site U1521. This objective was not achieved as originally planned due to the mechanical failure that ended operations. Correlation of the Plio-Pleistocene AABW record collected at Site U1524 can be made to the ice sheet variability record at Site U1522, but recovery was poor in the Plio-Pleistocene interval of Site U1522, which makes such correlations challenging. However, previous drilling at ANDRILL Site AND-1B recovered an exceptional record of continental shelf ice sheet variance through this time (Naish et al., 2009), and correlation to that site will allow for an unprecedented link between continental shelf processes and changing AABW flux into the deep ocean through this time period. In addition, links to changing surface water properties and ASC vigor can be made through correlations to Site U1523.

Operations at Site U1525 also cored a continental slope levee system near the flank of the Hillary Canyon (Figure F21), but the upper ~50 m was buried by the margin of a large trough-mouth fan deposit west of the site. The site is closer to the continental shelf break and consequently is more influenced by the ASC than Site U1524. The lithofacies suggest an increased influence of traction currents relating to this current together with a higher IBRD content (Figure F23). Thus, this site may provide an important and unique hybrid record of AABW formation, ASC current vigor, and iceberg discharge relating to dynamic ice sheet processes on the

continental shelf. This core overlaps in time with the records obtained at Sites U1523 and U1524 and ANDRILL Site AND-1B.

Science objectives achieved during Expedition 374

The discussion above provides an overview of the difficulties of achieving all of the expedition objectives due to the mechanical failure of the vessel and early return to port. Critically, we lost the ability to develop stratigraphic ties between the continental shelf and the deep ocean during the Miocene time period. This was a fundamental component of our science plan, which sought a continental shelf-to-rise transect to understand ocean–ice sheet interactions during the warmer-than-present Neogene, with a particular focus on the MMCO (~17–15 Ma). The successes relating to the science objectives, noting this caveat and that key aspects of most objectives were not achieved as originally intended, are discussed below.

Evaluate the contribution of West Antarctica to far-field ice volume and sea level estimates

Seismic Unconformities RSU4 and RSU3 were penetrated at Sites U1521 and U1522, respectively, during Expedition 374, and ages will be refined during postcruise analysis. The ages of these unconformities were previously very poorly constrained, and improved estimates of these ages (Figure F6) will constrain the timing of the first expansion of the marine-based ice sheets sourced from the EAIS into the western and central Ross Sea (Unconformity RSU4), as well as the first marine-based WAIS advances to the continental shelf edge (Unconformity RSU3). Models indicate that grounded ice sheets at these locations imply a maximum ice sheet extent on the Antarctic continent as a whole (Golledge et al 2013; Pollard and DeConto 2009). Therefore, integration with the ice sheet retreat events from the ANDRILL records (Sites AND-1B and AND-2A) will allow for assessment of the WAIS contribution to Neogene sea level estimates. Lithofacies analyses at continental shelf Sites U1521 and U1522 combined with seismic stratigraphic correlations will identify deposition during periods of grounded-ice, glaciomarine, and open-marine conditions. Sediment provenance studies at Sites U1521 and U1522 will enable understanding of the changes in the source region of sediments and identify whether glacial transport and deposition is sourced from local ice caps or large-scale ice sheet expansion (e.g., East versus West Antarctic source).

Reconstruct ice-proximal atmospheric and oceanic temperatures to identify past polar amplification and assess its forcings/feedbacks

All of the records obtained during Expedition 374 are relevant to addressing this objective, with most sites containing lithofacies suitable for proxy-based reconstruction of past climatic and oceanographic conditions at the Antarctic margin during warmer-than-present climates. Diatom-rich mud and diatom ooze (diatomite) are present in discrete intervals at all sites, and initial microfossil analyses demonstrate the possibility for high-resolution diatom, radiolarian, and palynological studies (Figures F25, F26) to reconstruct past variations in SSTs, surface water stratification (related to meltwater input and sea ice formation), and biological productivity. Calcareous foraminifers generally occur sporadically but are more abundant in some Pleistocene interglacial sequences at Sites U1523 and U1525 (Figures F17, F23). Biogenic carbonate is more common in middle Miocene sequences, and a diatom-rich mud and diatomite

interval at Site U1521 (Figure F11) contains abundant articulated bivalves, providing opportunities for stable isotope, trace element, and clumped isotope analyses and the application of additional proxies for past temperature reconstructions. Biomarker proxies of past SST change (e.g., TEX_{86}) will be investigated at all sites. Pollen-based reconstructions, alongside terrestrial biomarker proxies (e.g., MBT/CBT), will allow us to determine the extent of atmospheric polar amplification during these time periods and to track the resulting terrestrial runoff during the warmer climates of the Pliocene and Miocene.

Assess the role of oceanic forcing on WAIS stability/instability

ANDRILL Sites AND-1B and AND-2A provided compelling evidence of a smaller-than-present WAIS during the MMCO, the warm Pliocene, and early Pleistocene climates, likely as a consequence of wind-driven upwelling of warm CDW onto the continental shelf (Naish et al., 2009; Pollard and DeConto, 2009; Levy et al., 2016). Expedition 374 aimed to test this hypothesis by obtaining new records of ice sheet extent from outer continental shelf Sites U1521 and U1522 to complement and expand on the ANDRILL record, as well as provide a record of changing ocean current vigor and water masses near the continental shelf break (e.g., Site U1523) and the uppermost continental rise (e.g., Sites U1524 and U1525). At the sites most proximal to the continental shelf break (Sites U1523 and U1525), paleocurrent strength associated with changes in the westerly flowing ASC will be reconstructed by examining the sedimentologic (e.g., facies analysis and grain size) characteristics and magnetic fabrics.

Micropaleontological, geochemical, and sedimentologic studies from these drill cores will provide reconstructions of changing regional surface conditions that are relevant to water mass exchange between the Southern Ocean and the Ross Sea continental shelf/WAIS (e.g., sea ice, surface stratification, SSTs, polynya mixing, glacial meltwater discharge, nutrient uptake, and supercooling of dense water by ice shelves). Downslope currents resulting from the transfer of RSBW into the abyssal ocean (e.g., AABW formation) can also be assessed (and distinguished from ASC flow) by integrated facies analysis, geochemistry, and micropaleontology at Sites U1523–U1525. Foraminifer-rich/bearing beds occur in several intervals at both Sites U1523 and U1525 and hold promise for stable isotope and trace element analysis to reconstruct past water mass and temperature variations at these sites.

Identify the sensitivity of WAIS to Earth's orbital configuration under a variety of climate boundary conditions

Fundamental questions remain about the orbital pacing of AIS variability. In particular, records obtained from Expedition 374 should shed light on whether orbitally paced AIS variations respond to local insolation forcing or were regulated by interhemispheric teleconnections associated with low-latitude or high-northern latitude insolation forcings. Sedimentologic analyses (complemented by downhole logs) will enable development of a direct record of orbital-scale ice sheet advance and retreat events across the continental shelf at Sites U1521 and U1522. The turbidite levee deposits at continental rise and slope Sites U1524 and U1525 are believed to be the consequence of water masses cascading down the Hillary Canyon (Figure F5). As such, these deposits are anticipated to provide a record of changes in AABW production and delivery of sediment to

the continental shelf via ice sheet advance through time. These can then be directly related to changing ice sheet and sea ice extent on the Ross Sea continental shelf and tied to far-field records. Superimposed on this AABW signal will be an orbital-scale IBRD record, together with ASC vigor, that will link these changes in AABW to shifting ice dynamics along the Pacific Ocean margin of the WAIS.

Reconstruct eastern Ross Sea bathymetry to examine relationships between seafloor geometry, ice sheet stability/instability, and global climate

The modern-day bathymetry of the Ross Sea is characterized by an overdeepened continental shelf that makes the WAIS vulnerable to marine ice sheet instability. With this bathymetric configuration, once an ice sheet retreat event is triggered by a climatic warming, the grounding line retreats into increasingly deeper water, resulting in increased flux of ice discharging into the ocean (and melting) (Weertman, 1974; Thomas and Bentley, 1978). This increased flux leads to a runaway retreat process, even if there is no further climate forcing. Consequently, the transition from a terrestrial- or shallow marine-based West Antarctica with a seaward-dipping shallow continental shelf to that of the modern overdeepened (i.e., landward dipping) continental shelf has a first-order control on the sensitivity of the AIS to external climate and oceanic boundary conditions (Wilson et al., 2013; Gasson et al., 2016). The timing of Ross Sea shelf overdeepening is poorly constrained, and the location of Expedition 374 sites was selected to help improve the age constraints on the key unconformities relating to this event. The sites should also provide important reconstructions of the depositional environment (e.g., water depth) relevant to the paleobathymetry at the time of formation of seismic Unconformities RSU4, RSU3, and RSU2 (Figure F6) at Sites U1521 and U1522. These three unconformities document fundamental shifts in the eastern Ross Sea relating to erosion by advancing ice streams across a relatively shallow continental shelf from East Antarctica (Unconformity RSU4), West Antarctica (Unconformity RSU3), and the transition toward an overdeepened continental shelf by Unconformity RSU2 time. All three of these unconformities were penetrated on the continental shelf during Expedition 374, greatly reducing the uncertainties regarding their ages.

Additional expedition highlights and contributions

Numerous campaigns have been conducted to drill the Antarctic margin over the past five decades. Despite these efforts, the region still remains understudied with respect to the deep biosphere and the hydrological system. To address this shortcoming, dedicated mudline APC cores were collected at Sites U1523 and U1524 for high-resolution microbiological and interstitial water sampling. Microbiology sampling allows the first characterization of the vertical distribution of microbial flora in the deep biosphere of the Ross Sea. Additional metagenomics analyses of high-resolution subsamples provide information on the biodiversity of bacteria, methanogens, and fungi. Furthermore, biogeochemical and molecular studies enable us to explore the metabolism and activities of deep-biosphere communities. Interstitial water and sediment profiles can elucidate biogeochemical cycling of elements and isotopes. Being able to do so at high resolution in the uppermost part of the sediment column is unprecedented on the Ross Sea shelf and slope and

provides unique insights into early diagenetic processes and redox profiles.

Operations

Port call

Expedition 374 began with the first line ashore at Berth 2 in Lyttelton, New Zealand, at 0706 h (all times are local ship time; UTC + 13 h) on 4 January 2018. After clearing immigration and customs, the *JOIDES Resolution* Science Operator (JRSO) technical staff, Co-Chief Scientists, and Expedition Project Manager boarded the vessel. The Expedition 372 science party moved off the vessel, and after a 5 h crossover, the Expedition 372 JRSO technical staff departed the vessel. After conducting a press conference, holding VIP and media tours, and loading IODP and Siem airfreight and some critical ocean freight, the vessel shifted from Berth 2 to Berth 7 to begin the remainder of port call operations. The following day, the Expedition 374 science party came on board, and the Siem Offshore crew change was completed. Local university faculty, staff, and students were given tours of the vessel. Most of the Schlumberger logging-while-drilling (LWD) tools were off-loaded, and bulk loading operations began. We also received 41 short tons of barite and 135 short tons of sepiolite. On the third day of port call, the aft core line was removed in preparation for installing new coring line. Frozen food and dry stores were loaded, and the remaining Schlumberger LWD tools were off-loaded. After completing loading operations on 6 January, the vessel was shifted from Berth 7 to the Oil Berth for fueling. The last mooring line was released at 1735 h, and the first line ashore at the Oil Berth was secured at 1750 h, ending the very short passage.

After loading 640 metric tons of fuel oil, fuel operations were secured. At 0812 h on 7 January, the last line was released for the move back to Berth 7. The first line was secured at 0827 h, ending the brief transit. Loading operations resumed, and during the day, fresh fruit and vegetables were loaded, the FMS tool was repaired and tested, and Polar Code training for the science party and technicians was completed. On 8 January, the final day of our 4.4 day port call, the vessel was inspected and issued a Polar Code certificate, all remaining trash was discharged, the last remaining items of freight were loaded or discharged, and immigration cleared the vessel for departure. After the vessel was secured for the sea passage to Antarctica, the harbor pilot came on board at 1552 h, and two port tugs arrived to assist with departure. The mooring lines were released and pulled back on board, with the last line released at 1624 h. The vessel proceeded to the pilot station, and the pilot departed the vessel at 1648 h after a 2 nmi transit. The vessel began its sea passage at 1648 h on 8 January.

Transit to Site U1521

The R/V *JOIDES Resolution* met the RVIB *Nathaniel B. Palmer* at 1930 h on 14 January 2018. The *Nathaniel B. Palmer* acted as an escort through the sea ice into the Ross Sea polynya. At 1220 h on 15 January, the *JOIDES Resolution* cleared the southern edge of the sea ice and the *Nathaniel B. Palmer* was released from escort duty at 1300 h. The vessel arrived at Site U1521 at 0954 h on 16 January after a 2014 nmi transit from Lyttelton that averaged 10.8 kt. The vessel switched to dynamic positioning at 0938 h, and the thrusters were lowered and secured. At 0957 h, the drill floor was cleared for

operations, beginning Hole U1521A. At 1019 h, an acoustic beacon was deployed.

Site U1521

Site U1521 consisted of Hole U1521A, which was cored to 650.1 m DSF using the RCB coring system. Hole U1521A was logged with the triple combo, FMS-sonic, and VSI tool strings. Operations at Site U1521 concluded at 2245 h on 21 January. A total of 132.75 h (5.5 days) were spent at Site U1521. A total of 71 cores were re-cored for the site. RCB coring in Hole U1521A penetrated to 650.1 m DSF, recovering 411.50 m of core (63%) (Table T2).

Hole U1521A

Initial operations consisted of picking up and assembling the RCB BHA and then deploying the drill string to 143.81 m drilling depth below rig floor (DRF). During deployment, the drill pipe was drifted (checked to ensure that the interior was clear) and strapped (measured). The nonmagnetic core barrels were spaced out after assembling the outer core barrel. The top drive was picked up and spaced out, and a wiper pig was inserted into the drill string. The wiper pig was pumped through the drill string with 2 times the annular volume of the drill string to clean any loose rust or debris from the inside of the drill string. The calculated precision depth recorder (PDR) depth for the site was 573.4 m DRF. The core barrels were dressed with liners, and a core barrel was deployed.

The drill string was spaced out to spud and lowered slowly to tag the seafloor. Hole U1521A was started at 1845 h on 16 January 2018. The mudline core recovered 4.28 m of sediment, and the seafloor tag was measured at 573.0 m DRF (562.2 meters below sea level [mbsl]). RCB coring continued through Core 374-U1521A-37R (352.5 m DSF). Because of reduced recovery over the previous cores, we proceeded to cut half cores (4.8 m advance instead of 9.6 m advance) from Core 38R through 43R (352.5–381.3 m DSF) to improve core recovery. Coring with full 9.6 m advances continued from Core 44R through 71R (381.3–650.1 m DSF), at which point coring was terminated when the science objectives were met. High-viscosity mud sweeps (30 bbl) were pumped every two to four cores from Core 13R through 68R (113.0–611.7 m DSF).

To prepare for downhole logging after terminating coring in Hole U1521A, the hole was cleaned with a 40 bbl high-viscosity mud sweep. The rotary shifting tool (RST) was run in the hole on the coring line, releasing the RCB C-4 coring bit at 1505 h on 20 January. The RST was then run to reposition the bit shifting sleeve back to the circulating position in the mechanical bit release (MBR). After shifting the sleeve in the MBR, the RST was pulled back to the surface, and the sinker bars were removed from the drill string. The hole was displaced with 217 bbl of 10.5 lb/gal mud from 650.1 m DSF to the seafloor. The top drive was set back, and the drill string was pulled back to logging depth (54.4 m DSF). After positioning the end of the pipe with knobs through the guide horn, the circulating head was attached, and the hole was top-displaced to the seafloor with 20 bbl of 10.5 lb/gal mud. The rig floor was then rigged up for logging.

A triple combo tool string was assembled with the MSS, High-Resolution Laterolog Array (HRLA; to measure resistivity), HLDS (with source), Hostile Environment Natural Gamma Ray Sonde (HNGS), and the Enhanced Digital Telemetry Cartridge (EDTC). The tools were assembled and tested and then lowered into the hole at 2325 h on 20 January. The active heave compensator was switched on when the tools reached the open hole. A downlog was performed from just above the seafloor to the total hole depth of

648 m WSF. The hole was then logged up for a 126.5 m calibration pass. The triple combo tool string was lowered back to bottom (648 m WSF), and the hole was logged up. Before reaching the end of the drill pipe at 54.4 m DSF, the drill pipe was raised to 38.2 m DSF to provide additional log coverage of the upper part of the borehole before the caliper was closed and the tool string entered the pipe. The tools were pulled from the hole and were back at the surface at 0330 h on 21 January. By 0430 h, the triple combo tool string was rigged down.

The FMS-sonic tool string was assembled with the FMS, DS1, HNGS, and EDTC. The FMS-sonic tool string was deployed at 0620 h. The tool string was lowered into the drill pipe, and a downlog with the FMS calipers closed began at 54.4 m WSF. NGR was logged from above the seafloor to depth-match to the seafloor from the first logging run with the triple combo tool string. The tool string reached the bottom of the hole at 648 m WSF. The hole was logged up from 648 to 103 m WSF with the FMS calipers open. The calipers were then closed, and the tool string was lowered back to 648 m WSF. A second uplog was performed, and as the tool string approached the end of the drill string, it was again raised to ~38 m DSF to gain log coverage over the upper part of the borehole. The FMS calipers were closed just prior to entering the drill pipe. The FMS-sonic tool string was rigged down by 1245 h.

The VSI tool string for a VSP experiment consisted of the VSI and EDTC. The VSI tool string was assembled, tested, and deployed at 1330 h. While lowering the tool string in the hole, the protected species watch was initiated, and the seismic source (two 250 inch³ Sercel G guns in parallel cluster) was lowered into the water and fired with increasing intensity per the guidelines for a “soft start.” The VSI tool string was lowered to 648 m WSF for the first station test. The caliper was opened, and 17 stations were analyzed with good results. At 1755 h, the last station was completed, and the seismic source was secured. The logging tool string was at the rig floor at 1835 h, and by 1930 h all Schlumberger logging equipment was rigged down.

The drilling crew then began to secure the drilling equipment for transit. After laying out the knobs, the drill string was pulled back to the rig floor, clearing the seafloor at 2020 h. The acoustic beacon was released during the pipe trip and recovered on deck at 2105 h. The rest of the pipe was pulled to the rig floor, three drill collar stands were racked back in the derrick, and the outer core barrel was disassembled and inspected. The rig floor was secured for transit at 2245 h on 21 January, ending Hole U1521A and Site U1521. A total of 132.75 h (5.5 days) were spent at Site U1521.

Transit to Site U1522

The 88 nmi transit to Site U1522 was completed in 8.2 h averaging 10.7 kt. The vessel arrived at Site U1522 at 0629 h on 22 January 2018. The thrusters were lowered and secured at 0654 h, clearing the drill floor for operations. We deployed the acoustic positioning beacon at 0720 h.

Site U1522

The original operations plan for Site U1522 consisted of a single RCB hole to 545 m DSF; however, after requesting and receiving approval from the EPSP and Texas A&M Safety Panel, we ultimately cored Hole U1522A to 701.8 m DSF (Cores 374-U1522A-1R through 76R). At the end of coring operations, the hole was logged with three tool strings: a modified triple combo, the VSI, and the FMS. Operations at Site U1522 concluded at 1311 h on 28 January 2018. A total of 149.25 h (6.2 days) were spent at Site U1522. RCB

coring in Hole U1522A penetrated to 701.8 m DSF and recovered 279.57 m of core (40%) (Table T2).

Hole U1522A

The RCB BHA was assembled and lowered toward the seafloor to 143.82 m DRF before the top drive was picked up and spaced out and a RCB core barrel was deployed. The calculated PDR depth for the site was 567.5 m DRF; however, the final seafloor depth was measured at 568.5 m DRF (557.6 mbsl) based on the seafloor tag depth obtained while starting the hole. Hole U1522A was started at 1115 h on 22 January 2018, and the mudline core (374-U1522A-1R) recovered 2.89 m of sediment. RCB coring continued through Core 35R (337.6 m DSF). We then switched to cutting half-length cores (4.8 m advance instead of 9.6 m advance) in an attempt to improve core recovery. After poor recovery in Core 36R (9%), this strategy worked for Cores 37R and 38R (70% recovery). However, these cores were followed by almost no recovery in Cores 39R through 41R. We then switched back to full 9.6 m advances for Core 42R with negligible core recovery until Core 45R. Coring continued to a total depth of 701.8 m DSF (Core 76R), where science objectives were met.

While coring, 30 bbl of high-viscosity mud were pumped every two to four cores between 145.2 and 501.3 m DSF. Because of deteriorating hole conditions, 90 bbl of high-viscosity mud were pumped at 520.5 m DSF. Below 549.3 m DSF, mud was circulated on each core to try to improve hole cleaning and reduce the off-bottom torque. After terminating coring in Hole U1522A, the hole was cleaned with two 50 bbl high-viscosity mud sweeps followed by a third high-viscosity sweep in an effort to improve hole conditions for downhole logging. The RST was lowered into the hole on the coring line to release the RCB bit at 0645 h on 27 January. Several slugs of heavy mud were pumped to offset the high pressure in the annulus. The RST was then run again to reposition the bit shifting sleeve back to the circulating position in the MBR. After shifting the sleeve, the RST was pulled back to the surface, and the sinker bars were removed from the drill string. The end of the drill string was raised to 583.9 m DSF with the top drive installed because of the poor hole conditions. After a decrease in torque, the hole was displaced with 190 bbl of 10.5 lb/gal mud from 583.9 m DSF to the seafloor. The top drive was set back, and the end of the drill string was pulled up to a logging depth of 91.3 m DSF while monitoring for drag. After positioning the end of pipe, the circulating head was attached, and the hole was top-displaced to the seafloor with 20 bbl of 10.5 lb/gal mud. The rig floor was then prepared for downhole logging.

A modified triple combo tool string was assembled with the MSS, HRLA, DSI, HLDS (without source), HNGS, and EDTC. The tools were tested and lowered into the drill string at 1630 h on 27 January. The average heave was estimated to be 0.3 m just prior to logging. The wireline active heave compensator was turned on once the tools reached open hole. A downlog was performed from just above seafloor to 650.3 m WSF (~50 m above the bottom of the hole). The hole was then logged up with a 143 m calibration pass, run back to bottom (650.3 m WSF), and logged up to the end of the drill pipe at 91.3 m DSF. Before reaching the end of pipe at 91.3 m DSF, the drill string was raised 15 m to 76.3 m DSF to increase log coverage of the borehole. The caliper was closed prior to the tool string being pulled into the end of the drill pipe. The tool string was back on the rig floor at 2035 h on 27 January, and by 2200 h the triple combo tool string was disassembled.

The VSI tool string was assembled with the VSI and EDTC. After the VSI tool string was tested, it was run into the pipe at 2245 h and lowered to 194.5 m WSF, where it was unable to pass a narrow area in the borehole. We retrieved the VSI tool string to the rig floor at 0025 h on 28 January and added a HNGS to the tool string to increase the weight. The VSI tool string was lowered into the drill string at 0055 h and again encountered the bridge at 203.5 m WSF; however, after working the tool string with the added weight up and down for 30 min, the tool string passed the bridge and reached 297.5 m WSF before encountering another bridge that could not be passed. Protected species observation began while lowering the tool string in the hole. The seismic source was then deployed, and a soft start was initiated. Eight stations were selected and tested, each yielding good results. Several shutdowns occurred during the logging run when marine mammals (whales and seals) entered the exclusion zone during the VSP experiment. At 0600 h on 28 January, the last station was completed and the seismic source secured. The VSI tool string returned to the rig floor at 0630 h and was secured by 0700 h.

The third logging tool string used in Hole U1522A was the FMS, which contained the FMS, HNGS, and EDTC. The FMS tool string was lowered into the hole at 0730 h. NGR was logged from just above the seafloor while lowering the tool to depth-match the seafloor to the triple combo tool string run. The FMS tool string reached 193.5 m WSF, and the first upward pass collected data with the FMS calipers open from 193.5 to 101.5 m WSF. The tool string was lowered back to 193.5 m WSF, and a second upward pass was collected. The end of the pipe was raised to 86.5 m DSF as the FMS tool approached to increase log coverage of the borehole. After completing the uplog, the calipers were closed, and the tool string was returned to the rig floor. All logging equipment was disassembled by 1030 h on 28 January.

We then retrieved the drill string back to the rig floor. The acoustic beacon was released while raising the drill string and was recovered to the deck at 1213 h. Three drill collar stands were racked in the derrick, and the outer core barrel was disassembled and inspected. The rig floor was secured for transit at 1311 h on 28 January, ending Hole U1522A and Site U1522.

Transit to Site U1523

The 148 nmi transit to Site U1523 was completed in 12.9 h at an average speed of 11.5 kt. The vessel arrived at Site U1523 at 0158 h on 29 January 2018. The thrusters were lowered and secured at 0218 h, clearing the drill floor for operations. The acoustic positioning beacon was deployed at 1000 h after completing a seafloor survey.

Site U1523

Site U1523 is an alternate site that was occupied after coring at Site U1522 demonstrated that core recovery would likely be poor in the targeted upper interval of the original proposed primary Site EBOCS-04B. We cored five holes at Site U1523 because difficult coring conditions required additional holes to achieve the objectives. Prior to coring, we conducted a seafloor camera survey to ensure we could avoid large rocks on the seafloor. The survey included tagging the seafloor at four potential hole locations. Hole U1523A was cored with a combination of the APC and HLAPC coring systems to 46.3 m DSF. Hole U1523B was cored using the APC, HLAPC, and XCB systems to a final depth of 164.4 m DSF. Hole U1523C was intended to use the HLAPC to target specific stratigraphic gaps not recovered in Holes U1523A and U1523B; however, Hole U1523C was drilled without coring to 43.3 m DSF, where we

had to abandon it due to loss of circulation. Hole U1523D was drilled without coring from the seafloor to 135.0 m DSF, and then RCB coring penetrated to a final depth of 307.8 m DSF. Hole U1523D was then logged with two tool strings: a modified triple combo and the FMS. Hole U1523E was spot cored to 130.8 m DSF using the APC and HLAPC systems to cover stratigraphic gaps from Holes U1523A and U1523B. A total of 147.5 h (6.15 days) were spent at Site U1523.

We collected a total of 64 cores at Site U1523. The APC system was deployed 5 times, recovering 41.57 m of sediment (91%). The HLAPC system was used 33 times, collecting 87.99 m (59%). The XCB system collected 3.16 m of core (5%) over 8 cores. The RCB system was deployed 18 times over 172.8 m, recovering 0.9 m (0.5%) (Table T2).

Hole U1523A

Operations for Hole U1523A began with assembling an APC/XCB BHA and then lowering the drill string toward the seafloor. Because of uncertain seafloor conditions, we decided to survey the seafloor prior to starting the first hole. After the drill string reached 599.1 m DRF, we pulled the upper guide horn to deploy the subsea camera for the seafloor survey to look for large rocks in the vicinity of the potential hole locations. While lowering the subsea camera, we also continued to lower the drill string. Because this site is in deeper water than the two previous sites (PDR depth of 837 m DRF), some additional drill pipe had to be drifted and strapped as it was deployed. We picked up the top drive and prepared a nonmagnetic APC core barrel before conducting the seafloor survey, which included tagging the seafloor at four potential hole positions. All tag depths were 839 m DRF (828 mbsl). An acoustic positioning beacon was deployed at 1000 h after completing the survey. The vessel was moved back to the first tag location, and we left the subsea camera down to observe the core barrel being shot into the seafloor to start Hole U1523A.

After installing the sinker bars and orientation tool, the first APC core barrel was lowered into the drill string with the drill bit at 838.0 m DRF (1 m above the seafloor tag depth). Hole U1523A was started at 1050 h on 22 January 2018. The mudline core recovered 8.51 m of sediment. We continued to core with the APC system with nonmagnetic core barrels and orientation through Core 374-U1523A-3H (0–25.2 m DSF). Because Core 3H was a partial stroke, we switched to the HLAPC system and continued coring through Core 7F (46.3 m DSF). While drilling out the cored interval, backflow of sand/gravel/stones into the BHA blocked the drill string. Because we were unable to land a core barrel or circulate, we abandoned Hole U1523A. We pulled the drill string out of the hole and attempted to clear the BHA while it was above the seafloor. We then dropped an XCB core barrel with a deplugs; this attempt to clear the BHA also failed. After the XCB core barrel was retrieved, the drill string was pulled up to the rig floor, and the BHA was disassembled and cleaned of debris. The lockable float valve was damaged either by debris or the XCB core barrel. The bit cleared the rotary table at 0450 h, ending Hole U1523A. Total time spent in Hole U1523A was 26.5 h (1.1 days).

The APC system was deployed three times, recovering 23.22 m of core over 27.5 m of coring (84%). The HLAPC system was deployed four times, collecting 10.29 m of core over 18.8 m of coring (55%). Total core recovered for the hole was 33.51 m (72%).

Hole U1523B

After clearing out the BHA, the outer core barrel was reassembled, and the drill string was lowered toward the seafloor. The vessel was positioned 20 m east of Hole U1523A. After picking up the top drive, the drill bit was positioned at 838 m DRF (1 m above the seafloor) to start Hole U1523B. A nonmagnetic APC core barrel was deployed, and Hole U1523B was started at 1100 h on 30 January 2018. Core 374-U1523B-1H recovered 8.49 m of sediment. We then dropped an XCB center bit and advanced the hole without coring to 46.7 m DSF. A hard layer was observed at 45.9 m DSF. After recovering the XCB center bit, we deployed a HLAPC core barrel. Coring continued from Core 3F through Core 13F (46.7–93.8 m DSF). We pumped 20 or 30 bbl mud sweeps every few cores to maintain good hole conditions. Core 13F was a partial stroke, so we switched to the XCB coring system. Cores 14X through 16X penetrated from 93.8 to 103.3 m DSF with almost no recovery. Because Core 16X only advanced 0.1 m, we dropped a center bit and drilled ahead without coring for 5.0 m to try to advance past a very hard layer. We then resumed XCB coring and cut Cores 18X and 19X (108.3–127.5 m DSF), again with minimal recovery (3%). Because drilling parameters suggested we had successfully passed the hard layers, we switched back to the HLAPC coring system for Cores 20F and 21F (127.5–135.6 m DSF). We had to drill over Core 21F to release it from the formation because of excessive overpull, so we switched back to the XCB system. We cut Cores 22X through 24X (135.6–164.4 m DSF) with minimal recovery (9%). We terminated coring at 164.4 m DSF in Hole U1523B because of unstable hole conditions causing excessive torque. In addition, core liners used with the XCB system shattered at a high rate (63%), causing significant core disturbance. We pumped a 30 bbl mud sweep and pulled the drill string clear of the seafloor, ending Hole U1523B at 2120 h on 31 January. Total time spent in Hole U1523B was 37.0 h (1.5 days).

A single APC core recovered 8.49 m over an 8.5 m advance (100%). The HLAPC system was deployed 13 times, recovering 33.48 m over 55.2 m of coring (61%). The XCB was deployed eight times, collecting 3.16 m over 57.5 m of coring (5%). Total recovery for Hole U1523B was 45.13 m (37%).

Hole U1523C

After clearing the seafloor, the vessel was repositioned 20 m south of Hole U1523B. Hole U1523C was planned to selectively core intervals of poor recovery with the HLAPC while avoiding hard layers encountered in previous holes. We dropped a center bit in preparation to start Hole U1523C and noticed high pump pressures that indicated clogged jets in the drill bit. After attempting to clear the jets, we started Hole U1523C at 1915 h on 31 January 2018 and drilled ahead without coring to 43.3 m DSF, where we lost circulation through the drill string, forcing us to abandon Hole U1523C. The bit cleared the seafloor at 2120 h and was retrieved back to the rig floor at 0130 h on 1 February, ending Hole U1523C. Total time spent in Hole U1523C was 7.75 h (0.3 days).

Hole U1523D

We then decided to switch to the RCB coring system to core and log a deeper hole, with the intention of coring a final APC/HLAPC hole if time permitted after logging. The RCB BHA was assembled and lowered toward the seafloor. After picking up the top drive, we prepared a core barrel with a center bit. Hole U1523D was started at 0725 h on 1 February 2018. The hole was advanced to 135.0 m DSF without coring. We pumped a 30 bbl high-viscosity mud sweep and retrieved the center bit. RCB coring continued from Core 374-

U1523D-2R through 19R (135.0–307.8 m DSF) with very poor recovery (0.90 m; 0.5%). We pumped 30 bbl high-viscosity mud sweeps every two to three cores to clear cuttings. We terminated coring after reaching our minimum target depth of ~300 m DSF and prepared the hole for downhole logging by circulating two 50 bbl high-viscosity mud sweeps to improve hole conditions. The RST was lowered on the coring line to release the RCB bit in the bottom of the hole at 0800 h on 2 February. After running the RST a second time to shift the sleeve in the MBR back to the circulating position, we displaced the hole with 94 bbl of 10.5 lb/gal mud from 307.8 m DSF to the seafloor. We then pulled the drill string to 258.5 m DSF, set back the top drive, and continued to pull the drill string up to a logging depth of 82.3 m DSF. After displacing the upper part of the hole with 20 bbl of 10.5 lb/gal mud, the drill floor was prepared for downhole logging operations at 1130 h on 2 February.

The first logging run consisted of a modified triple combo tool string assembled with the MSS, DSI, HRLA, HLDS (without source), HNGS, and EDTC. The triple combo tool string was lowered into the drill string at 1320 h on 2 February. The average heave was estimated to be 0.3 m just prior to logging. The active heave compensator was switched on when the tools reached open hole. A downlog was performed from just above seafloor to 292 m WSF, with the tool string reaching to within 15 m of the bottom of the hole. The hole was then logged up with a 136 m calibration pass. The tool string was lowered back to the bottom (288 m WSF) and then logged up. When the tool string neared the end of the pipe, it was raised to 67 m DSF to provide additional log coverage of the borehole. The tools were back at the surface at 1630 h on 2 February, and the triple combo tool string was disassembled by 1745 h.

The second logging run was with the FMS tool string, which was assembled with the FMS, HNGS, and EDTC. The FMS tool string was lowered into the hole at 1820 h. NGR was logged from above the seafloor as the tool string was lowered to depth-match results to the first logging run. The FMS tool string reached a total depth of 289.6 m WSF. Two upward passes were logged with the FMS tool string. During the second uplog, the end of the pipe was raised to 67 m DSF to provide additional coverage of the borehole. The FMS tool string was returned to the rig floor at 2130 h, and all logging equipment was disassembled by 2245 h on 2 February. We then began to raise the drill string back toward the rig floor, clearing the seafloor at 2315 h on 2 February. After placing three stands of drill collars in the derrick, the outer core barrel was disassembled and inspected. The end of the drill string cleared the rotary table at 0240 h on 3 February, ending Hole U1523D. Total time spent in Hole U1523D was 49.25 h (2.1 days), with 0.90 m of core recovered over 172.8 m of RCB coring (0.5%).

Hole U1523E

We switched back to the APC/XCB coring system to target poorly recovered intervals from Holes U1523A and U1523B. The drill string was lowered toward the seafloor, and the bit was set at 830 m DRF for the first core. Hole U1523E was started at 0810 h on 3 February 2018, and Core 374-U1523E-1H recovered a full barrel (9.86 m). We drilled ahead 9.5 m without coring and then switched to the HLAPC coring system and proceeded with spot coring. Over the upper ~90 m, spot coring consisted of collecting one to three HLAPC cores followed by a 2.8–12.3 m drill-ahead interval. Depths were chosen to avoid gravel encountered in Holes U1523A and U1523B. Deeper than ~90 m, the coring plan included dropping a center bit to drill through hard layers encountered between 93 and 95, 104 and 108, and 116 and 117 m DSF, with HLAPC cores col-

lected in between. This technique proved particularly successful for the interval deeper than 100 m DSF, allowing us to fill in substantial gaps in the stratigraphy. The last core (25F) in Hole U1523E arrived on deck at 2350 h on 3 February. After pumping a 30 bbl mud sweep, we left the top drive installed while pulling the drill string out of the hole because of unstable hole conditions causing excessive torque and overpull. After clearing the seafloor at 0150 h on 4 February, the top drive was set back and the drill string was retrieved to the vessel. The acoustic beacon was released and recovered at 0450 h, and the rig floor was secured at 0547 h, ending operations in Hole U1523E and Site U1523.

A single APC core collected 9.86 m of core over 9.5 m of coring (104%). The HLAPC was deployed 16 times, recovering 44.22 m of core over 75.2 m of coring (59%). Total recovery for Hole U1523E was 54.08 m (64%).

Transit to Site U1524

The 52 nmi transit to Site U1524 was completed in 4.7 h at an average speed of 11.1 kt. The vessel arrived at Site U1524 at 1027 h on 4 February 2018. The thrusters were lowered and secured at 1044 h, clearing the drill floor for operations. The acoustic positioning beacon was deployed at 1100 h.

Site U1524

Site U1524 is an alternate for proposed primary Site RSCR-02B. We decided to occupy the alternate site because the highest priority target is shallower, the seismic facies show less evidence for transported sediment, and the sea ice edge was farther away. We cored three holes at Site U1524. Hole U1524A was cored with the APC/XCB system to 299.5 m DSF. Hole U1524B consisted of a single mudline core collected for high-resolution sampling. After briefly abandoning the site because of encroaching sea ice, we returned and cored Hole U1524C with the RCB system to 441.9 m DSF. Total time spent at Site U1524 was 117.25 h (4.9 days).

We collected a total of 54 cores at Site U1524. The APC system was deployed 31 times, collecting 284.17 m of core (102%). The HLAPC system was deployed once, recovering 0.43 m of core (108%). The XCB system collected 5.51 m over three cores (19%). The RCB system was used 19 times, collecting 19.2 m of core (11%) (Table T2).

Hole U1524A

Operations in Hole U1524A began by picking up an APC/XCB BHA and lowering it toward the seafloor. Because this site is in deeper water than the previous sites, some of the drill pipe was drifted and strapped while being deployed. After positioning the drill string with the bit at 2400 m DRF based on the PDR depth for the site, we installed the Icefield MI-5 core orientation tool with the sinker bars. We then deployed a nonmagnetic APC core barrel and started Hole U1524A at 2025 h on 4 February 2018. Core 374-U1524A-1H recovered 4.02 m of core, indicating a seafloor depth of 2394 mbsl.

Oriented APC coring continued through Core 30H (270.3 m DSF). Downhole formation temperatures were taken on Cores 6H (51.5 m DSF), 9H (80.0 m DSF), 12H (108.5 m DSF), and 15H (137 m DSF) using the APCT-3. After Core 30H recorded a partial stroke, indicating piston core refusal, we removed the Icefield MI-5 core orientation tool and switched to the HLAPC system to collect Core 31F. This core also recorded a partial stroke and recovered only 0.4 m of sediment. We then switched to the XCB coring system and cut Cores 32X through 34X to 299.5 m DSF; all XCB core liners

were shattered upon recovery, resulting in highly disturbed sediment. We suspect that the XCB liners were shattering at a high rate due to extremely cold seawater (-1.5° to -2.0°C) coupled with the small gap between the core liner and core barrel that allows for vibration. After collecting Core 34X, we had to terminate coring and pull out of the hole because of approaching sea ice. After pulling the bit up to 249.5 m DSF, we set back the top drive and continued to pull out of the hole, clearing the seafloor at 0950 h on 6 February and ending Hole U1524A. We attempted to retrieve the acoustic positioning beacon while pulling out of the hole, but the beacon would not release. Total time spent in Hole U1524A was 47.0 h (2.0 days).

Overall recovery in Hole U1524A was 282.35 m (94%). The APC coring system was deployed 30 times, recovering 276.41 m of core over 270.3 m of coring (102%). The HLAPC coring system was deployed once, recovering 0.43 m of core over a 0.4 m advance (108%). The XCB coring system was deployed three times, recovering 5.51 m of core over 28.8 m of coring (19%).

Hole U1524B

With ~ 1.5 h of time left before the arrival of sea ice, we decided to collect a single mudline core for high-resolution interstitial water and microbiological studies. We moved the vessel 20 m east of Hole U1524A and started Hole U1524B at 1155 h on 6 February 2018. Core 374-U1524B-1H collected 7.76 m of sediment, establishing a seafloor depth of 2394 m. We terminated Hole U1524B as the sea ice continued to approach and began to retrieve the drill string back to the ship. The dynamic positioning system was engaged at 1215 h to move away from the ice. The drill collar stands were secured in the derrick, and the BHA components were disassembled and inspected. After the bit cleared the rig floor, the remaining rig floor equipment was secured at 2030 h on 6 February, ending Hole U1524B. A total of 10.75 h (0.4 days) was spent in Hole U1524B.

A single APC core collected 7.76 m of core over a 7.7 m advance (101%).

Transit to Site U1525

After abandoning Site U1524 because of encroaching sea ice, we departed for Site U1525 at 2030 h on 6 February 2018. We decided to go to this alternate site because it was close to Site U1524 (47 nmi) but outside the sea ice edge and the Ross Sea Unconformity RSU3 (primary objective at Site U1524) is at a shallower depth. The 50 nmi transit to Site U1525 was completed in 5.6 h at an average speed of 8.9 kt. A small deviation in course was required to navigate around sea ice. The vessel arrived at Site U1525 at 0200 h on 7 February. The thrusters were lowered and secured at 0215 h, clearing the drill floor for operations. We did not deploy an acoustic positioning beacon at this site.

Site U1525

Site U1525 was added to the schedule when we were forced to temporarily leave Site U1524 because of encroaching sea ice. The operational plan for Site U1525 consisted of APC/XCB coring in a single hole until ice moved away from Site U1524. Hole U1525A was cored to a total depth of 213.2 m DSF using a combination of APC, HLAPC, and XCB coring. A total of 51.25 h (2.1 days) was spent at Site U1525.

We collected 33 cores at Site U1525. The APC system was deployed eight times, collecting 63.23 m of core (103%). The HLAPC system was deployed 14 times, recovering 52.64 m of core (92%). The XCB system was used 11 times and collected 42.83 m (45%). (Table T2).

Hole U1525A

Operations for Hole U1525A began by preparing the APC/XCB BHA and then lowering the drill string toward the seafloor. The calculated PDR depth for the site was 1790.8 m DRF. We picked up the top drive and lowered the drill bit to tag the seafloor. Because the tag indicated the seafloor was soft, we prepared a nonmagnetic APC core barrel and positioned the drill bit at 1786 m DRF. Hole U1525A was started at 1000 h on 7 February 2018. Core 374-U1525A-1H recovered 8.62 m of sediment, establishing a seafloor depth of 1776 mbsl. We continued to APC core with nonmagnetic core barrels through Core 4H (28.9 m DSF), which was a partial stroke. We switched to the HLAPC coring system to collect Cores 5F through 8F (28.9–43.0 m DSF). Because Core 8F was a partial stroke with no recovery, we switched to the XCB system to cut Cores 9X and 10X (43.0–55.7 m DSF) to get through an indurated zone. We then switched back to the HLAPC system for Cores 11F through 15F (55.7–79.2 m DSF). With continued successful piston coring, we switched back to full-length APC core barrels and collected Cores 16H through 19H, which penetrated to 111.8 m DSF. Because Core 19H recorded a partial stroke, we advanced 4.1 m based on recovery and switched back to the HLAPC coring system, collecting Cores 20F through 24F (111.8–131.2 m DSF). Core 24F also recorded a partial stroke, indicating HLAPC refusal, so we switched to the XCB coring system. The remainder of the hole was cored with the XCB system, cutting Cores 25X through 33X to a total depth of 213.2 m DSF. We experienced multiple shattered core liners (6 out of 11; 55%) using the XCB system, which we suspect resulted from a combination of very cold seawater (-1.7°C) circulating through the drill string and the small space between the core liner and the core barrel, which allows vibration of the core liner. Because ice conditions at Site U1524 were forecast to improve over the next 24 h, we opted to terminate coring after Core 33X. We pulled the drill string out of the hole, clearing the seafloor at 2150 h on 8 February. After conducting routine rig maintenance (slip and cut 115 ft of drill line), the remainder of the drill string was retrieved, and the rig floor was secured at 0535 h on 9 February, ending operations at Site U1525.

Total recovery in Hole U1525A was 158.70 m over 213.2 m of coring (74%). The APC coring system was deployed eight times, collecting 63.23 m of core over 61.5 m of coring (103%). The HLAPC was deployed 14 times, collecting 52.64 m of core over 57.0 m of coring (92%). The XCB was deployed 11 times, recovering 42.83 m of core over 94.7 m of coring (45%).

Return to Site U1524

The transit back to Site U1524 covered 47 nmi in 4.4 h at an average speed of 10.7 kt. We arrived at Site U1524 at 1006 h on 9 February 2018, and the vessel was positioned over the acoustic positioning beacon that we had left there.

Hole U1524C

We prepared a RCB BHA and lowered the drill string toward the seafloor. After the drill bit reached 1766 m DRF, we deployed the subsea camera to recover the seafloor acoustic positioning beacon because it had failed to release when we previously abandoned the site because of approaching sea ice. We lowered the drill string to near the seafloor, maneuvered the vessel to the beacon, and captured it with a grapple hanging from the camera frame. We recovered the subsea camera to the ship, with the beacon arriving on deck at 1915 h on 9 February 2018. After securing the subsea camera, we continued to prepare for drilling operations. We dropped a

RCB core barrel with center bit and started Hole U1524C at 2110 h on 9 February. The hole was advanced by drilling without coring to 260.5 m DSF. A 30 bbl high-viscosity mud sweep was pumped at the end of the drilled interval, and the RCB core barrel with the center bit was retrieved. We started RCB coring and cut Cores 374-U1524C-2R through 20R (260.5–441.9 m DSF). At 0915 h on 11 February, coring operations for the remainder of the expedition were terminated because of a mechanical breakdown of the port stern tube and shaft arrangement. After recovering the last core, 50 bbl of high-viscosity mud was circulated to improve hole conditions for the trip out of the hole. The drill string was pulled out of the hole, with the bit clearing the seafloor at 1150 h and arriving on the rig floor at 1820 h on 11 February. The rig floor was secured for transit at 1835 h, ending Hole U1524C and Expedition 374 science operations. The time spent in Hole U1524C was 56.50 h (2.4 days).

The RCB coring system was deployed 19 times, collecting 19.20 m of core over 181.4 m of coring (11%) (Table T2).

Transit to Lyttelton

After abandoning operations at Site U1524, we headed north toward Lyttelton while attempting to resolve the mechanical problem. When it became clear that the problem could not be fixed without returning to port, we set a course for a waypoint 12 nmi from the Lyttelton pilot station. The 1876 nmi transit was completed in 173.0 h (7.2 days) at an average speed of 10.8 kt. We arrived at the waypoint at 0148 h on 19 February 2018. The thrusters were lowered, and we switched to dynamic positioning control at 0230 h. Our original plan was to take on supplies to fix the mechanical problem at sea; however, with the approach of Cyclone Gita we asked and received confirmation that we could move to a berth in Lyttelton for shelter. We raised the thrusters and proceeded to the pilot station. The pilot boarded the vessel at 1342 h on 19 February, and the 30 nmi transit to Lyttelton ended with the first line ashore at Berth 2 West at 1512 h on 19 February.

Tie-up in Lyttelton

Upon arrival in Lyttelton, we loaded supplies to repair the vessel. Repairs were completed on 22 February 2018. A pilot boarded the vessel at 0754 h on 22 February, and we shifted to Berth 7 East, with the first line secure at 0902 h. After completing the expedition science reports and conducting our final science meeting, Expedition 374 scientists were free to disembark the vessel after 1200 h on 22 February. While tied up in Lyttelton, we began to load supplies for upcoming Expedition 375 and offload core and samples from Expedition 374. While at Berth 7 East, we loaded two refrigerated containers of catering supplies and three flats of drill pipe on 23 February. We also off-loaded an empty core liner box. At 0558 h on 25 February, the harbor pilot arrived to shift the vessel to the Oil Berth. Bunkering began at 0735 h, and 1100 metric tons of marine gas oil were loaded by 2350 h on 25 February. A harbor pilot boarded the vessel at 1624 h on 26 February and shifted the vessel to Berth 2 West with the aid of two harbor tugs. We remained tied up at this berth until 1500 h on 7 March. During this time, we loaded 10% inch casing, 4½ inch casing, and pup joints to the riser hold. We also loaded seven flats of equipment for Expedition 375, including four flats of CORK equipment, two 40 ft containers of equipment (one for IODP and one for Siem Offshore), and some of the IODP airfreight. The Expedition 374 cores were off-loaded to a refrigerated container on 1 March, and 10 coolers of Expedition 374 samples packed in dry ice were off-loaded for shipment on 2 March. A 20 ft container was also loaded with equipment for return to Col-

lege Station, TX. Fresh food for Expedition 375 was loaded on 6 March. We met with the Expedition 375 Expedition Project Manager to finalize logistics for critical equipment to be transferred to the ship, which occurred on 7 March.

Because of a scheduled strike at the port of Lyttelton, we opted to shift the vessel to Timaru, New Zealand, for the end of Expedition 374 to avoid the possibility of getting stuck in port because of a labor shutdown. Prior to departing on 7 March, we gave a ship tour to local government and business officials. The pilot boarded the vessel at 1456 h, and the last line was released at 1518 h. The pilot departed the vessel at 1536 h, and we began our sea voyage to port in Timaru.

Transit to Timaru

The 138 nmi transit to Timaru was completed in 17.5 h at an average speed of 7.6 kt. The pilot boarded the vessel at 0746 h. Expedition 374 officially ended with the first line ashore at Berth 2 North at 0848 h on 8 March 2018.

References

- Ainley, D.G., and Jacobs, S.S., 1981. Sea-bird affinities for ocean and ice boundaries in the Antarctic. *Deep Sea Research, Part A: Oceanographic Research Papers*, 28(10):1173–1185.
[https://doi.org/10.1016/0198-0149\(81\)90054-6](https://doi.org/10.1016/0198-0149(81)90054-6)
- Alonso, B., Anderson, J.B., Diaz, J.I., and Bartek, L.R., 1992. Pliocene–Pleistocene seismic stratigraphy of the Ross Sea: evidence for multiple ice sheet grounding episodes. In Elliot, D.H. (Ed.), *Antarctic Research Series* (Volume 57): *Contributions to Antarctic Research III*: Washington DC (American Geophysical Union), 93–103.
<https://doi.org/10.1029/AR057p0093>
- Anderson, J.B., 1999. *Antarctic Marine Geology*: Cambridge, United Kingdom (Cambridge University Press).
<https://doi.org/10.1017/CBO9780511759376>
- Anderson, J.B., and Bartek, L.R., 1992. Cenozoic glacial history of the Ross Sea revealed by intermediate resolution seismic reflection data combined with drill site information. In Kennett, J.P., and Warnke, D. (Eds.), *Antarctic Research Series* (Volume 56): *The Antarctic Paleoenvironment: A Perspective on Global Change: Part One*: Washington, DC (American Geophysical Union), 231–263. <https://doi.org/10.1029/AR056p0231>
- Arndt, J.E., Schenke, H.W., Jakobsson, M., Nitsche, F.O., Buys, G., Goleby, B., Rebasco, M., et al., 2013. The International Bathymetric Chart of the Southern Ocean (IBCSO) Version 1.0—a new bathymetric compilation covering circum-Antarctic waters. *Geophysical Research Letters*, 40(12):3111–3117. <https://doi.org/10.1002/grl.50413>
- Barrett, P.J., 1975. Textural characteristics of Cenozoic preglacial and glacial sediments at site 270, Ross Sea, Antarctica. In Hayes, D.E., Frakes, L.A., et al., *Initial Reports of the Deep Sea Drilling Project*, 28. Washington, DC (U.S. Government Printing Office), 757–767.
<https://doi.org/10.2973/dsdp.proc.28.122.1975>
- Barrett, P.J., 1981. History of the Ross Sea region during the deposition of the Beacon Supergroup 400–180 million years ago. *Journal of the Royal Society of New Zealand*, 11(4):447–458.
<https://doi.org/10.1080/03036758.1981.10423334>
- Barrett, P.J., 1989. Antarctic Cenozoic history from the CIROS-1 drillhole, McMurdo Sound. *DRIS Bulletin*, 245.
- Barrett, P.J., 2007. Cenozoic climate and sea level history from glaciomarine strata off the Victoria Land coast, Cape Roberts Project, Antarctica. In Hambrey, M.J., Christoffersen, P., Glasser, N.F., and Hubbard, B. (Eds.), *Glacial Sedimentary Processes and Products*. Special Publication of the International Association of Sedimentologists, 39:259–288.
- Bart, P.J., 2003. Were West Antarctic Ice Sheet grounding events in the Ross Sea a consequence of East Antarctic Ice Sheet expansion during the middle Miocene? *Earth and Planetary Science Letters*, 216(1–2):93–107.
[https://doi.org/10.1016/S0012-821X\(03\)00509-0](https://doi.org/10.1016/S0012-821X(03)00509-0)

- Bart, P.J., De Batist, M., and Jokat, W., 1999. Interglacial collapse of Crary Trough-mouth fan, Weddell Sea, Antarctica: implications for Antarctic glacial history. *Journal of Sedimentary Research*, 69(6):1276–1289. <https://doi.org/10.2110/jsr.69.1276>
- Bart, P.J., and De Santis, L., 2012. Glacial intensification during the Neogene: a review of seismic stratigraphic evidence from the Ross Sea, Antarctica, continental shelf. *Oceanography*, 25(3):166–183. <https://doi.org/10.5670/oceanog.2012.92>
- Bart, P.J., and Iwai, M., 2012. The overdeepening hypothesis: how erosional modification of the marine-scape during the early Pliocene altered glacial dynamics on the Antarctic Peninsula's Pacific margin. *Palaeogeography, Palaeoclimatology, Palaeoecology*, 335–336:42–51. <https://doi.org/10.1016/j.palaeo.2011.06.010>
- Bart, P.J., Sjunneskog, C., and Chow, J.M., 2011. Piston-core based biostratigraphic constraints on Pleistocene oscillations of the West Antarctic Ice Sheet in western Ross Sea between North Basin and AND-1B drill site. *Marine Geology*, 289(1–4):86–99. <https://doi.org/10.1016/j.margeo.2011.09.005>
- Behrendt, J.C., LeMasurier, W.E., Cooper, A.K., Tessensohn, F., Tréhu, A., and Damaske, D., 1991. Geophysical studies of the West Antarctic rift system. *Tectonics*, 10(6):1257–1273. <https://doi.org/10.1029/91TC00868>
- Bianchi, G.G., Hall, I.R., McCave, I.N., and Joseph, L., 1999. Measurement of the sortable silt current speed proxy using the Sedigraph 5100 and Coulter Multisizer II: precision and accuracy. *Sedimentology*, 46(6):1001–1014. <https://doi.org/10.1046/j.1365-3091.1999.00256.x>
- Böhm, G., Ocakoğlu, N., Picotti, S., and De Santis, L., 2009. West Antarctic Ice Sheet evolution: new insights from a seismic tomographic 3D depth model in the Eastern Ross Sea (Antarctica). *Marine Geology*, 266(1–4):109–128. <https://doi.org/10.1016/j.margeo.2009.07.016>
- Brancolini, G., Busetti, M., Marchetti, M., De Santis, L., Zanolla, C., Cooper, A.K., Cochrane, G.R., Zayatz, I., Belyaev, V., Knyazev, M., Vinnikovskaya, O., Davey, F.J., and Hinz, K., 1995. Seismic stratigraphic atlas of the Ross Sea, Antarctica. In Cooper, A.K., Barker, P.F., and Brancolini, G. (Eds.), *Antarctic Research Series (Volume 68): Geology and Seismic Stratigraphy of the Antarctic Margin*: Washington, DC (American Geophysical Union).
- Caburlotto, A., Lucchi, R.G., De Santis, L., Macrì, P., and Tolotti, R., 2010. Sedimentary processes on the Wilkes Land continental rise reflect changes in glacial dynamic and bottom water flow. *International Journal of Earth Sciences*, 99(4):909–926. <https://doi.org/10.1007/s00531-009-0422-8>
- Chow, J.M., and Bart, P.J., 2003. West Antarctic Ice Sheet grounding events on the Ross Sea outer continental shelf during the middle Miocene. *Palaeogeography, Palaeoclimatology, Palaeoecology*, 198(1–2):169–186. [https://doi.org/10.1016/S0031-0182\(03\)00400-0](https://doi.org/10.1016/S0031-0182(03)00400-0)
- Cody, R., Levy, R., Crampton, J., Naish, T., Wilson, G., and Harwood, D., 2012. Selection and stability of quantitative stratigraphic age models: Plio-Pleistocene glaciomarine sediments in the ANDRILL 1B drillcore, McMurdo Ice Shelf. *Global and Planetary Change*, 96–97:143–156. <https://doi.org/10.1016/j.gloplacha.2012.05.017>
- Cody, R.D., Levy, R.H., Harwood, D.M., and Sadler, P.M., 2008. Thinking outside the zone: high-resolution quantitative diatom biochronology for the Antarctic Neogene. *Palaeogeography, Palaeoclimatology, Palaeoecology*, 260(1–2):92–121. <http://dx.doi.org/10.1016/j.palaeo.2007.08.020>
- Cook, C.P., van de Flierdt, T., Williams, T., Hemming, S.R., Iwai, M., Kobayashi, M., Jimenez-Espejo, F.J., et al., 2013. Dynamic behaviour of the East Antarctic Ice Sheet during Pliocene warmth. *Nature Geoscience*, 6(9):765–769. <https://doi.org/10.1038/ngeo1889>
- Cooper, A.K., Barker, P.F., and Brancolini, G. (Eds.), 1997. *Antarctic Research Series (Volume 68): Geology and Seismic Stratigraphy of the Antarctic Margin*: Washington, DC (American Geophysical Union). <https://agu-pubs.onlinelibrary.wiley.com/doi/book/10.1029/AR068>
- Cooper, A.K., Barrett, P.J., Hinz, K., Traube, V., Leitchenkov, G., and Stagg, H.M.J., 1991. Cenozoic prograding sequences of the Antarctic continental margin: a record of glacio-eustatic and tectonic events. *Marine Geology*, 102(1–4):175–213. [https://doi.org/10.1016/0025-3227\(91\)90008-R](https://doi.org/10.1016/0025-3227(91)90008-R)
- Cooper, A.K., and O'Brien, P.E., 2004. Leg 188 synthesis: transitions in the glacial history of the Prydz Bay region, East Antarctica, from ODP drilling. In Cooper, A.K., O'Brien, P.E., and Richter, C. (Eds.), *Proceedings of the Ocean Drilling Program, Scientific Results*, 188: College Station, TX (Ocean Drilling Program), 1–42. <https://doi.org/10.2973/odp.proc.sr.188.001.2004>
- Cramer, B.S., Toggweiler, J.R., Wright, J.D., Katz, M.E., and Miller, K.G., 2009. Ocean overturning since the Late Cretaceous: inferences from a new benthic foraminiferal isotope compilation. *Paleoceanography*, 24(4). <https://doi.org/10.1029/2008PA001683>
- Crampton, J.S., Cody, R.D., Levy, R., Harwood, D., McKay, R., and Naish, T.R., 2016. Southern Ocean phytoplankton turnover in response to stepwise Antarctic cooling over the past 15 million years. *Proceedings of the National Academy of Sciences*, 113(25):6868–6873. <https://doi.org/10.1073/pnas.1600318113>
- Dahl-Jensen, D., Albert, M.R., Aldahan, A., et al., 2013. Eemian interglacial reconstructed from a Greenland folded ice core. *Nature*, 493(7433):489–494. <https://doi.org/10.1038/nature11789>
- De Santis, L., Anderson, J.B., Brancolini, G., and Zayatz, I., 1995. Seismic record of late Oligocene through Miocene glaciation on the Central and Eastern Continental Shelf of the Ross Sea. In Cooper, A.K., Barker, P.F., and Brancolini, G. (Eds.), *Antarctic Research Series (Volume 68): Geology and Seismic Stratigraphy of the Antarctic Margin*: Washington, DC (American Geophysical Union), 235–260. <https://doi.org/10.1029/AR068p0235>
- De Santis, L., Prato, S., Brancolini, G., Lovo, M., and Torelli, L., 1999. The eastern Ross Sea continental shelf during the Cenozoic: implications for the West Antarctic ice sheet development. *Global and Planetary Change*, 23(1–4):173–196. [https://doi.org/10.1016/S0921-8181\(99\)00056-9](https://doi.org/10.1016/S0921-8181(99)00056-9)
- Decesari, R.C., Sorlien, C.C., Luyendyk, B.P., Wilson, D.S., Bartek, L., Diebold, J., and Hopkins, S.E., 2007. Regional seismic stratigraphic correlations of the Ross Sea: implications for the tectonic history of the West Antarctic rift system. In Cooper, A.K., Raymond, C.R., et al. (Eds.), *Antarctica: A Keystone in a Changing World—Online Proceedings of the 10th ISAES*. USGS Open File Report 2007-1047, Short Research Paper 052. <https://doi.org/10.3133/of2007-1047.srp052>
- DeConto, R.M., and Pollard, D., 2016. Contribution of Antarctica to past and future sea-level rise. *Nature*, 531(7596):591–597. <https://doi.org/10.1038/nature17145>
- Elderfield, H., Ferretti, P., Greaves, M., Crowhurst, S., McCave, I.N., Hodell, D., and Piotrowski, A.M., 2012. Evolution of ocean temperature and ice volume through the mid-Pleistocene Climate Transition. *Science*, 337(6095):704–709. <https://doi.org/10.1126/science.1221294>
- Expedition 318 Scientists, 2011. Expedition 318 summary. In Escutia, C., Brinkhuis, H., Klaus, A., and the Expedition 318 Scientists, *Proceedings of the Integrated Ocean Drilling Program, 318: Tokyo (Integrated Ocean Drilling Program Management International, Inc.)*. <https://doi.org/10.2204/iodp.proc.318.101.2011>
- Feakins, S.J., Warny, S., and Lee, J.-E., 2012. Hydrologic cycling over Antarctica during the middle Miocene warming. *Nature Geoscience*, 5(8):557–560. <https://doi.org/10.1038/ngeo1498>
- Fielding, C.R., Browne, G.H., Field, B., Florindo, F., Harwood, D.M., Krissel, L.A., Levy, R.H., Panter, K.S., Passchier, S., and Pekar, S.F., 2011. Sequence stratigraphy of the ANDRILL AND-2A drillcore, Antarctica: a long-term, ice-proximal record of early to mid-Miocene climate, sea-level and glacial dynamism. *Palaeogeography, Palaeoclimatology, Palaeoecology*, 305(1–4):337–351. <https://doi.org/10.1016/j.palaeo.2011.03.026>
- Fielding, C.R., Naish, T.R., Woolfe, K.J., and Lavelle, M.A., 2000. Facies analysis and sequence stratigraphy of CRP-2/2A, Victoria Land Basin, Antarctica. *Terra Antartica*, 7(3):323–338. <https://epic.awi.de/27384/1/Fie2000b.pdf>
- Florindo, F., Bohaty, S.M., Erwin, P.S., Richter, C., Roberts, A.P., Whalen, P.A., and Whitehead, J.M., 2003. Magnetobiostratigraphic chronology and palaeoenvironmental history of Cenozoic sequences from ODP sites 1165 and 1166, Prydz Bay, Antarctica. In Florindo, F., Cooper, A.K., and

- O'Brien, P.E. (Eds.), *Antarctic Cenozoic Palaeoenvironments: Geologic Record and Models*. Palaeogeography, Palaeoclimatology, Palaeoecology, 198 (1–2):69–100. [https://doi.org/10.1016/S0031-0182\(03\)00395-X](https://doi.org/10.1016/S0031-0182(03)00395-X)
- Florindo, F., Wilson, G.S., Roberts, A.P., Sagnotti, L., and Verosub, K.L., 2005. Magnetostratigraphic chronology of a late Eocene to early Miocene glaci-marine succession from Victoria Land Basin, Ross Sea, Antarctica. *Global and Planetary Change*, 45(1–3):207–236. <http://dx.doi.org/10.1016/j.gloplacha.2004.09.009>
- Flower, B.P., and Kennett, J.P., 1994. The middle Miocene climatic transition: East Antarctic ice sheet development, deep ocean circulation and global carbon cycling. *Palaeogeography, Palaeoclimatology, Palaeoecology*, 108(3–4):537–555. [https://doi.org/10.1016/0031-0182\(94\)90251-8](https://doi.org/10.1016/0031-0182(94)90251-8)
- Ford, A.B., and Barrett, P.J., 1975. Basement rocks of the south-central Ross Sea, Site 270, DSDP Leg 28. In Hayes, D.E., Frakes, L.A., et al., *Initial Reports of the Deep Sea Drilling Project*, 28. Washington DC (U.S. Government Printing Office), 861–868. <https://doi.org/10.2973/dsdp.proc.28.131.1975>
- Foster, G.L., and Rohling, E.J., 2013. Relationship between sea level and climate forcing by CO₂ on geological timescales. *Proceedings of the National Academy of Sciences*, 110(4):1209–1214. <https://doi.org/10.1073/pnas.1216073110>
- Foster, G.L., Lear, C.H., and Rae, J.W.B., 2012. The evolution of pCO₂, ice volume and climate during the middle Miocene. *Earth and Planetary Science Letters*, 341–344:243–254. <https://doi.org/http://dx.doi.org/10.1016/j.epsl.2012.06.007>
- Galeotti, S., DeConto, R., Naish, T., Stocchi, P., Florindo, F., Pagani, M., Barrett, P., Bohaty, S.M., Lanci, L., Pollard, D., Sandroni, S., Talarico, F.M., and Zachos, J.C., 2016. Antarctic Ice Sheet variability across the Eocene–Oligocene boundary climate transition. *Science*, 352(6281):76–80. <https://doi.org/10.1126/science.aab0669>
- Gasson, E., DeConto, R.M., Pollard, D., and Levy, R.H., 2016. Dynamic Antarctic Ice Sheet during the early to mid-Miocene. *Proceedings of the National Academy of Sciences of the United States of America*, 113(13):3459–3464. <https://doi.org/10.1073/pnas.1516130113>
- Golledge, N.R., Fogwill, C.J., Mackintosh, A.N., and Buckley, K.M., 2012. Dynamics of the Last Glacial Maximum Antarctic Ice Sheet and its response to ocean forcing. *Proceedings of the National Academy of Sciences of the United States of America*, 109(40):16052–16056. <https://doi.org/10.1073/pnas.1205385109>
- Golledge, N.R., Levy, R.H., McKay, R.M., Fogwill, C.J., White, D.A., Graham, A.C.C., Smith, J.A., et al., 2013. Glaciology and geological signature of the Last Glacial Maximum Antarctic Ice Sheet. *Quaternary Science Reviews*, 78:225–247. <https://doi.org/10.1016/j.quascirev.2013.08.011>
- Grützner, J., Rebasco, M.A., Cooper, A.K., Forsberg, C.F., Kryc, K.A., and Wefer, G., 2003. Evidence for orbitally controlled size variations of the East Antarctic Ice Sheet during the late Miocene. *Geology*, 31(9):777–780. <https://doi.org/10.1130/G19574.1>
- Hall, I.R., McCave, I.N., Shackleton, N.J., Weedon, G.P., and Harris, S.E., 2001. Intensified deep Pacific inflow and ventilation in Pleistocene glacial times. *Nature*, 412(6849):809–812. <https://doi.org/10.1038/35090552>
- Harland, R., and Pudsey, C.J., 2002. Protoperidiniacean dinoflagellate cyst taxa from the upper Miocene of ODP Leg 178, Antarctic Peninsula. *Review of Palaeobotany and Palynology*, 120(3–4):263–284. [https://doi.org/10.1016/S0034-6667\(02\)00080-5](https://doi.org/10.1016/S0034-6667(02)00080-5)
- Hepp, D.A., Mörz, T., and Grützner, J., 2006. Pliocene glacial cyclicity in a deep-sea sediment drift (Antarctic Peninsula Pacific Margin). *Palaeogeography, Palaeoclimatology, Palaeoecology*, 231(1–2):181–198. <https://doi.org/10.1016/j.palaeo.2005.07.030>
- Hinz, K., and Block, M., 1984. Results of geophysical investigations in the Weddell Sea and in the Ross Sea, Antarctica. *Proceedings of the 11th World Petroleum Congress*, 11(2):79–91.
- Hodell, D.A., and Venz-Curtis, K.A., 2006. Late Neogene history of deepwater ventilation in the Southern Ocean. *Geochemistry, Geophysics, Geosystems*, 7(9). <https://doi.org/10.1029/2005GC001211>
- Holbourn, A., Kuhnt, W., Schulz, M., Flores, J.-A., and Andersen, N., 2007. Orbitally-paced climate evolution during the middle Miocene “Monte-rey” carbon-isotope excursion. *Earth and Planetary Science Letters*, 261(3–4):534–550. <http://dx.doi.org/10.1016/j.epsl.2007.07.026>
- Houben, A.J.P., Bijl, P.K., Pross, J., Bohaty, S.M., Passchier, S., Stickley, C.E., Röhl, U., et al., 2013. Reorganization of Southern Ocean plankton ecosystem at the onset of Antarctic glaciation. *Science*, 340(6130):341–344. <https://doi.org/10.1126/science.1223646>
- Huck, C.E., van de Flierdt, T., Bohaty, S.M., and Hammond, S.J., 2017. Antarctic climate, Southern Ocean circulation patterns, and deep water formation during the Eocene. *Paleoceanography*, 32(7):674–691. <https://doi.org/10.1002/2017PA003135>
- Huybers, P., 2006. Early Pleistocene glacial cycles and the integrated summer insolation forcing. *Science*, 313(5786):508–511. <https://doi.org/10.1126/science.1125249>
- Jacobs, S.S., Bauer, E.B., Bruchhausen, P.M., Gordon, A.L., Root, T.F., and Rosselot, F.L., 1974. *Eltanin Reports: Cruises 47–50, 1971*, 52–55, 1972: *Hydrographic Stations, Bottom Photographs, Current Measurements, Nephelometer Profiles*: Palisades, NY (Lamont-Doherty Geological Observatory, Columbia University), CU 2–74.
- Jacobs, S.S., Giulivi, C.F., and Mele, P.A., 2002. Freshening of the Ross Sea during the late 20th Century. *Science*, 297(5580):386–389. <https://doi.org/10.1126/science.1069574>
- Jacobs, S.S., Jenkins, A., Giulivi, C.F., and Dutrieux, P., 2011. Stronger ocean circulation and increased melting under Pine Island Glacier ice shelf. *Nature Geoscience*, 4(8):519–523. <https://doi.org/10.1038/ngeo1188>
- John, C.M., Karner, G.D., Browning, E., Leckie, R.M., Mateo, Z., Carson, B., and Lowery, C., 2011. Timing and magnitude of Miocene eustasy derived from the mixed siliciclastic-carbonate stratigraphic record of the northeastern Australian margin. *Earth and Planetary Science Letters*, 304(3–4):455–467. <https://doi.org/10.1016/j.epsl.2011.02.013>
- Joseph, L.H., Rea, D.K., and van der Pluijm, B.A., 2004. Neogene history of the Deep Western Boundary Current at Rekohu sediment drift, Southwest Pacific (ODP Site 1124). In McCave, I.N., Carter, L., Carter, R.M., and Hayward, B.W. (Eds.), *Cenozoic Oceanographic Evolution of the Southwest Pacific Gateway*, ODP Leg 181. Marine Geology, 205(1–4):185–206. [https://doi.org/10.1016/S0025-3227\(04\)00023-4](https://doi.org/10.1016/S0025-3227(04)00023-4)
- Joughin, I., Alley, R.B., and Holland, D.M., 2012. Ice-sheet response to oceanic forcing. *Science*, 338(6111):1172–1176. <https://doi.org/10.1126/science.1226481>
- Karner, G.D., Studinger, M., and Bell, R.E., 2005. Gravity anomalies of sedimentary basins and their mechanical implications: application to the Ross Sea basins, West Antarctica. *Earth and Planetary Science Letters*, 235(3–4):577–596. <https://doi.org/10.1016/j.epsl.2005.04.016>
- Kennett, J.P., 1977. Cenozoic evolution of Antarctic glaciation, the circum-Antarctic Ocean, and their impact on global paleoceanography. *Journal of Geophysical Research: Oceans and Atmospheres*, 82(27):3843–3860. <https://doi.org/10.1029/JC082i027p03843>
- Kennett, J.P., and Barker, P.F., 1990. Latest Cretaceous to Cenozoic climate and oceanographic developments in the Weddell Sea, Antarctica: an ocean-drilling perspective. In Barker, P.F., Kennett, J.P., et al., *Proceedings of the Ocean Drilling Program, Scientific Results*, 113: College Station, TX (Ocean Drilling Program), 937–960. <https://doi.org/10.2973/odp.proc.sr.113.195.1990>
- Kim, S., De Santis, L., Hong, J.K., Cottlerle, D., Petronio, L., Colizza, E., Kim, Y.-G., et al., 2018. Seismic stratigraphy of the Central Basin in northwest Ross Sea slope and rise, Antarctica: clues to the late Cenozoic ice-sheet dynamics and bottom-current activity. *Marine Geology*, 395:363–379. <https://doi.org/10.1016/j.margeo.2017.10.013>
- Kominz, M.A., Browning, J.V., Miller, K.G., Sugarman, P.J., Misintseva, S., and Scotese, C.R., 2008. Late Cretaceous to Miocene sea-level estimates from the New Jersey and Delaware coastal plain coreholes: an error analysis. *Basin Research*, 20(2):211–226. <https://doi.org/10.1111/j.1365-2117.2008.00354.x>
- Kopp, R.E., Simons, F.J., Mitrovica, J.X., Maloof, A.C., and Oppenheimer, M., 2009. Probabilistic assessment of sea level during the last interglacial stage. *Nature*, 462(7275):863–867. <https://doi.org/10.1038/nature08686>

- Leckie, R.M., and Webb, P.-N., 1986. Late Paleogene and early Neogene foraminifers of Deep Sea Drilling Project Site 270, Ross Sea, Antarctica. In Kennett, J. P., von der Borch, C.C., et al., *Initial Reports of the Deep Sea Drilling Project*, 90: Washington, DC (U.S. Government Printing Office), 1093–1142. <https://doi.org/10.2973/dsdp.proc.90.124.1986>
- Levy, R., Harwood, D., Florindo, F., Sangiorgi, F., Tripati, R., von Eynatten, H., Gasson, E., et al., 2016. Antarctic Ice Sheet sensitivity to atmospheric CO₂ variations in the early to mid-Miocene. *Proceedings of the National Academy of Sciences of the United States of America*, 113(13):3453–3458. <https://doi.org/10.1073/pnas.1516030113>
- Lewis, A.R., Marchant, D.R., Ashworth, A.C., Hedenäs, L., Hemming, S.R., Johnson, J.V., Leng, M.J., et al., 2008. Mid-Miocene cooling and the extinction of tundra in continental Antarctica. *Proceedings of the National Academy of Sciences of the United States of America*, 105(31):10676–10680. <https://doi.org/10.1073/pnas.0802501105>
- Lewis, A.R., Marchant, D.R., Kowalewski, D.E., Baldwin, S.L., and Webb, L.E., 2006. The age and origin of the Labyrinth, western Dry Valleys, Antarctica: evidence for extensive middle Miocene subglacial floods and freshwater discharge to the Southern Ocean. *Geology*, 34(7):513–516. <https://doi.org/10.1130/G22145.1>
- Licht, K.J., Hennessy, A.J., and Welke, B.M., 2014. The U-Pb detrital zircon signature of West Antarctic ice stream tills in the Ross Embayment, with implications for Last Glacial Maximum ice flow reconstructions. *Antarctic Science*, 26(6):687–697. <https://doi.org/10.1017/S0954102014000315>
- Licht, K.J., Lederer, J.R., and Swope, R.J., 2005. Provenance of LGM glacial till (sand fraction) across the Ross Embayment, Antarctica. *Quaternary Science Reviews*, 24(12–13):1499–1520. <https://doi.org/10.1016/j.quascirev.2004.10.017>
- Lindeque, A., Gohl, K., Henrys, S., Wobbe, F., and Davy, B., 2016. Seismic stratigraphy along the Amundsen Sea to Ross Sea continental rise: a cross-regional record of pre-glacial to glacial processes of the West Antarctic margin. *Palaeogeography, Palaeoclimatology, Palaeoecology*, 443:183–202. <https://doi.org/10.1016/j.palaeo.2015.11.017>
- Lisiecki, L.E., and Raymo, M.E., 2005. A Pliocene–Pleistocene stack of 57 globally distributed benthic δ¹⁸O records. *Paleoceanography*, 20(1):PA1003. <https://doi.org/10.1029/2004PA001071>
- Luccia, R.G., and Rebesco, M., 2007. Glacial contourites on the Antarctic Peninsula margin: insight for palaeoenvironmental and palaeoclimatic conditions. *Geological Society Special Publication*, 276(1):111–127. <https://doi.org/10.1144/GSL.SP.2007.276.01.06>
- Luyendyk, B.P., Sorlien, C.C., Wilson, D.S., Bartek, L.R., and Siddoway, C.S., 2001. Structural and tectonic evolution of the Ross Sea rift in the Cape Colbeck region, Eastern Ross Sea, Antarctica. *Tectonics*, 20(6):933–958. <https://doi.org/10.1029/2000TC001260>
- Masson-Delmotte, V., Schulz, M., Abe-Ouchi, A., Beer, J., Ganopolski, A., González Rouco, J.F., Jansen, E., et al., 2013. Information from paleoclimate archives. In Stocker, T.F., Qin, D., Plattner, G.-K., Tignor, M., Allen, S.K., Boschung, J., Nauels, A., Xia, Y., Bex, V., and Midgley, P.M. (Eds.), *Climate Change 2013: The Physical Science Basis. Contribution of Working Group I to the Fifth Assessment Report of the Intergovernmental Panel on Climate Change*: Cambridge, United Kingdom (Cambridge University Press), 383–464. http://www.climatechange2013.org/images/report/WG1AR5_Chapter05_FINAL.pdf
- McKay, R., Browne, G., Carter, L., Cowan, E., Dunbar, G., Krissek, L., Naish, T., et al., 2009. The stratigraphic signature of the late Cenozoic Antarctic Ice Sheets in the Ross Embayment. *Geological Society of America Bulletin*, 121(11–12):1537–1561. <https://doi.org/10.1130/B26540.1>
- McKay, R., Naish, T., Carter, L., Riesselman, C., Dunbar, R., Sjunneskog, C., Winter, D., et al., 2012a. Antarctic and Southern Ocean influences on late Pliocene global cooling. *Proceedings of the National Academy of Sciences of the United States of America*, 109(17):6423–6428. <https://doi.org/10.1073/pnas.1112248109>
- McKay, R., Naish, T., Powell, R., Barrett, P., Scherer, R., Talarico, F., Kyle, P., et al., 2012b. Pleistocene variability of Antarctic ice sheet extent in the Ross Embayment. *Quaternary Science Reviews*, 34:93–112. <https://doi.org/10.1016/j.quascirev.2011.12.012>
- Meinshausen, M., Smith, S.J., Calvin, K., Daniel, J.S., Kainuma, M.L.T., Lamarque, J.-F., Matsumoto, K., et al., 2011. The RCP greenhouse gas concentrations and their extensions from 1765 to 2300. *Climatic Change*, 109:213–241. <https://doi.org/10.1007/s10584-011-0156-z>
- Mercer, J.H., 1978. West Antarctic Ice Sheet and CO₂ greenhouse effect: a threat of disaster. *Nature*, 271(5643):321–325. <https://doi.org/10.1038/271321a0>
- Miller, K.G., Kominz, M.A., Browning, J.V., Wright, J.D., Mountain, G.S., Katz, M.E., Sugarman, P.J., Cramer, B.S., Christie-Blick, N., and Pekar, S.F., 2005. The Phanerozoic record of global sea-level change. *Science*, 310(5752):1293–1298. <https://doi.org/10.1126/science.1116412>
- Miller, K.G., Mountain, G.S., Wright, J.D., and Browning, J.V., 2011. A 180-million-year record of sea level and ice volume variations from continental margin and deep-sea isotopic records. *Oceanography*, 24(2):40–53. <https://doi.org/10.5670/oceanog.2011.26>
- Miller, K.G., Mountain, G.S., Wright, J.D., and Browning, J.V., 2011. A 180-million-year record of sea level and ice volume variations from continental margin and deep-sea isotopic records. *Oceanography*, 24(2):40–53. <https://doi.org/10.5670/oceanog.2011.26>
- Miller, K.G., Wright, J.D., Browning, J.V., Kulpeck, A., Kominz, M., Naish, T.R., Cramer, B.S., Rosenthal, Y., Peltier, W.R., and Sosdian, S., 2012. High tide of the warm Pliocene: implications of global sea level for Antarctic deglaciation. *Geology*, 40(5):407–410. <https://doi.org/10.1130/G32869.1>
- Naish, T., Powell, R., Levy, R., Wilson, G., Scherer, R., Talarico, F., Krissek, L., et al., 2009. Obliquity-paced Pliocene West Antarctic ice sheet oscillations. *Nature*, 458(7236):322–328. <https://doi.org/10.1038/nature07867>
- Naish, T.R., and Wilson, G.S., 2009. Constraints on the amplitude of mid-Pliocene (3.6–2.4 Ma) eustatic sea-level fluctuations from the New Zealand shallow-marine sediment record. *Philosophical Transactions of the Royal Society, A: Mathematical, Physical & Engineering Sciences*, 367(1886):169–187. <https://doi.org/10.1098/rsta.2008.0223>
- Naish, T.R., Woolfe, K.J., Barrett, P.J., Wilson, G.S., Atkins, C., Bohaty, S.M., Bücker, C.J., et al., 2001. Orbitally induced oscillations in the East Antarctic Ice Sheet at the Oligocene/Miocene boundary. *Nature*, 413(6857):719–723. <https://doi.org/10.1038/35099534>
- Newkirk, D., and Martin, E.E., 2009. Circulation through the Central American Seaway during the Miocene carbonate crash. *Geology*, 37(1):87–90. <https://doi.org/10.1130/G25193A.1>
- Orsi, A.H., and Wiederwohl, C.L., 2009. A recount of Ross Sea waters. *Deep Sea Research, Part II: Topical Studies in Oceanography*, 56(13–14):778–795. <https://doi.org/10.1016/j.dsrr.2008.10.033>
- Padman, L., and Fricker, H.A., 2005. Tides on the Ross Ice Shelf observed with ICESat. *Geophysical Research Letters*, 32(14):L14503. <https://doi.org/10.1029/2005GL023214>
- Pagani, M., Zachos, J.C., Freeman, K.H., Tipple, B., and Bohaty, S., 2005. Marked decline in atmospheric carbon dioxide concentrations during the Paleogene. *Science*, 309(5734):600–603. <https://doi.org/10.1126/science.1110063>
- Pálike, H., Lyle, M.W., Nishi, H., Raffi, I., Ridgwell, A., Gamage, K., Klaus, A., et al., 2012. A Cenozoic record of the equatorial Pacific carbonate compensation depth. *Nature*, 488(7413):609–614. <https://doi.org/10.1038/nature11360>
- Passchier, S., Browne, G., Field, B., Fielding, C.R., Krissek, L.A., Panter, K., Pekar, S.F., and ANDRILL-SMS Science Team, 2011. Early and middle Miocene Antarctic glacial history from the sedimentary facies distribution in the AND-2A drill hole, Ross Sea, Antarctica. *Geological Society of America Bulletin*, 123(11–12):2352–2365. <https://doi.org/10.1130/B30334.1>
- Patterson, M.O., and Ishman, S.E., 2013. Neogene benthic foraminiferal assemblages and paleoenvironmental record for McMurdo Sound, Antarctica. *Geosphere*, 8(6):1331–1341. <https://doi.org/10.1130/GES00771.1>
- Patterson, M.O., McKay, R., Naish, T., Escutia, C., Jimenez-Espejo, F.J., Raymo, M.E., Meyers, S.R., Tauxe, L., Brinkhuis, H., and IODP Expedition 318 Scientists, 2014. Orbital forcing of the East Antarctic ice sheet during the Pliocene and early Pleistocene. *Nature Geoscience*, 7:841–847. <https://doi.org/10.1038/ngeo2273>

- Pollard, D., and DeConto, R.M., 2009. Modelling West Antarctic Ice Sheet growth and collapse through the past five million years. *Nature*, 458(7236):329–332. <https://doi.org/10.1038/nature07809>
- Powell, R.D., and Cooper, J.M., 2002. A glacial sequence stratigraphic model for temperate, glaciated continental shelves. In Dowdeswell, J.A., and Ó'Cofaigh, C. (Eds.), *Glacier-Influenced Sedimentation on High-Latitude Continental Margins*. Geological Society Special Publication, 203:215–244. <https://doi.org/10.1144/GSL.SP.2002.203.01.12>
- Prins, M.A., Bouwer, L.M., Beets, C.J., Troelstra, S.R., Weltje, G.J., Kruk, R.W., Kuijpers, A., and Vroon, P.Z., 2002. Ocean circulation and iceberg discharge in the glacial North Atlantic: inferences from unmixing of sediment size distributions. *Geology*, 30(6):555–558. [https://doi.org/10.1130/0091-7613\(2002\)030<0555:OCA-IDI>2.0.CO;2](https://doi.org/10.1130/0091-7613(2002)030<0555:OCA-IDI>2.0.CO;2)
- Pritchard, H.D., Ligtenberg, S.R.M., Fricker, H.A., Vaughan, D.G., van den Broeke, M.R., and Padman, L., 2012. Antarctic ice-sheet loss driven by basal melting of ice shelves. *Nature*, 484(7395):502–505. <https://doi.org/10.1038/nature10968>
- Parkey, S.G., and Johnson, G.C., 2010. Warming of global abyssal and deep Southern Ocean waters between the 1990s and 2000s: contributions to global heat and sea level rise budgets. *Journal of Climate*, 23(23):6336–6351. <https://doi.org/10.1175/2010JCLI3682.1>
- Raymo, M.E., Lisiecki, L.E., and Nisancioğlu, K.H., 2006. Plio–Pleistocene ice volume, Antarctic climate, and the global $\delta^{18}\text{O}$ record. *Science*, 313(5786):492–495. <https://doi.org/10.1126/science.1123296>
- Raymo, M.E., Mitrovica, J.X., O’Leary, M.J., DeConto, R.M., and Hearty, P.J., 2011. Departures from eustasy in Pliocene sea-level records. *Nature Geoscience*, 4(5):328–332. <https://doi.org/10.1038/ngeo1118>
- Rebesco, M., Camerlenghi, A., Geletti, R., and Canals, M., 2006. Margin architecture reveals the transition to the modern Antarctic Ice Sheet (AIS) ca. 3 Ma. *Geology*, 34(4):301–304. <https://doi.org/10.1130/G22000.1>
- Sangiorgi, F., Bijl, P.K., Passchier, S., Salzmann, U., Schouten, S., McKay, R., Cody, R.D., et al., 2018. Southern Ocean warming and Wilkes Land ice sheet retreat during the mid-Miocene. *Nature Communications*, 9(1):317. <https://doi.org/10.1038/s41467-017-02609-7>
- Scherer, H.D., and Martin, E.E., 2006. Timing and climatic consequences of the opening of Drake Passage. *Science*, 312(5772):428–430. <https://doi.org/10.1126/science.1120044>
- Scherer, R.P., Aldahan, A., Tulaczyk, S., Possnert, G., Engelhardt, H., and Kamb, B., 1998. Pleistocene collapse of the West Antarctic Ice Sheet. *Science*, 281(5373):82–85. <https://doi.org/10.1126/science.281.5373.82>
- Scherer, R.P., Bohaty, S.M., Dunbar, R.B., Esper, O., Flores, J.-A., Gersonde, R., Harwood, D.M., Roberts, A.P., and Taviani, M., 2008. Antarctic records of precession-paced insolation-driven warming during early Pleistocene marine isotope Stage 31. *Geophysical Research Letters*, 35(3):L03505. <https://doi.org/10.1029/2007GL032254>
- Shepherd, A., Ivins, E.R., Geruo, A., Barletta, V.R., Bentley, M.J., Bettadpur, S., Briggs, K.H., et al., 2012. A reconciled estimate of ice-sheet mass balance. *Science*, 338(6111):1183–1189. <https://doi.org/10.1126/science.1228102>
- Shevenell, A.E., Ingalls, A.E., Domack, E.W., and Kelly, C., 2011. Holocene Southern Ocean surface temperature variability west of the Antarctic Peninsula. *Nature*, 470(7333):250–254. <https://doi.org/10.1038/nature09751>
- Shevenell, A.E., Kennett, J.P., and Lea, D.W., 2004. Middle Miocene Southern Ocean cooling and Antarctic cryosphere expansion. *Science*, 305(5691):1766–1770. <http://dx.doi.org/10.1126/science.1100061>
- Shevenell, A.E., Kennett, J.P., and Lea, D.W., 2008. Middle Miocene ice sheet dynamics, deep-sea temperatures, and carbon cycling: a Southern Ocean perspective. *Geochemistry, Geophysics, Geosystems*, 9(2):Q02006. <https://doi.org/10.1029/2007GC001736>
- Shipboard Scientific Party, 1975a. Introduction. In Hayes, D.E., Frakes, L.A., et al., *Initial Reports of the Deep Sea Drilling Project*, 28: Washington, DC (U.S. Government Printing Office), 5–18. <https://doi.org/10.2973/dsdp.proc.28.101.1975>
- Shipboard Scientific Party, 1975b. Sites 270, 271, 272. In Hayes, D.E., Frakes, L.A., et al., *Initial Reports of the Deep Sea Drilling Project*, 28: Washington, DC (U.S. Government Printing Office), 211–334. <https://doi.org/10.2973/dsdp.proc.28.108.1975>
- Shipboard Scientific Party, 2001. Leg 189 summary. In Exon, N.F., Kennett, J.P., Malone, M.J., et al., *Proceedings of the Ocean Drilling Program, Initial Reports*, 189: College Station, TX (Ocean Drilling Program), 1–98. <https://doi.org/10.2973/odp.proc.ir.189.101.2001>
- Siddoway, C.S., Baldwin, S.L., Fitzgerald, P.G., Fanning, C.M., and Luyendyk, B.P., 2004. Ross Sea mylonites and the timing of intracontinental extension within the West Antarctic rift system. *Geology*, 32(1):57–60. <https://doi.org/10.1130/G20005.1>
- Sorlien, C.C., Luyendyk, B.P., Wilson, D.S., Decesari, R.C., Bartek, L.R., and Diebold, J.B., 2007. Oligocene development of the West Antarctic Ice Sheet recorded in eastern Ross Sea strata. *Geology*, 35(5):467–470. <https://doi.org/10.1130/G23387A.1>
- Talarico, F.M., McKay, R.M., Powell, R.D., Sandroni, S., and Naish, T., 2012. Late Cenozoic oscillations of Antarctic Ice Sheets revealed by provenance of basement clasts and grain detrital modes in ANDRILL core AND-1B. *Global and Planetary Change*, 96–97:23–40. <https://doi.org/10.1016/j.gloplacha.2009.12.002>
- Tauxe, L., Stickley, C.E., Sugisaki, S., Bijl, P.K., Bohaty, S.M., Brinkhuis, H., Escutia, C., et al., 2012. Chronostratigraphic framework for the IODP Expedition 318 cores from the Wilkes Land Margin: constraints for paleoceanographic reconstruction. *Paleoceanography*, 27(2):PA2214. <https://doi.org/10.1029/2012PA002308>
- Ten Brink, U.S., Schneider, C., and Johnson, A.H., 1995. Morphology and stratal geometry of the Antarctic continental shelf: insights from models. In Cooper, A.K., Barker, P.F., and Brancolini, G. (Eds.), *Antarctic Research Series (Volume 68): Geology and Seismic Stratigraphy of the Antarctic Margin*: Washington, DC (American Geophysical Union), 1–24. <https://doi.org/10.1029/AR068p0001>
- Theissen, K.M., Dunbar, R.B., Cooper, A.K., Mucciarone, D.A., and Hoffmann, D., 2003. The Pleistocene evolution of the East Antarctic Ice Sheet in the Prydz bay region: stable isotopic evidence from ODP Site 1167. *Global and Planetary Change*, 39(3–4):227–256. [https://doi.org/10.1016/S0921-8181\(03\)00118-8](https://doi.org/10.1016/S0921-8181(03)00118-8)
- Thomas, R.H., and Bentley, C.R., 1978. A model for Holocene retreat of the West Antarctic Ice Sheet. *Quaternary Research*, 10(02):150–170. [https://doi.org/10.1016/0033-5894\(78\)90098-4](https://doi.org/10.1016/0033-5894(78)90098-4)
- Tzedakis, P.C., Crucifix, M., Mitsui, T., and Wolff, E.W., 2017. A simple rule to determine which insolation cycles lead to interglacials. *Nature*, 542(7642):427–432. <https://doi.org/10.1038/nature21364>
- van de Flieerd, T., Frank, M., Halliday, A.N., Hein, J.R., Hattendorf, B., Günther, D., and Kubik, P.W., 2004. Deep and bottom water export from the Southern Ocean to the Pacific over the past 38 million years. *Paleoceanography*, 19(1):PA1020. <https://doi.org/10.1029/2003PA000923>
- Villa, G., Lupi, C., Cobianchi, M., Florindo, F., and Pekar, S.F., 2008. A Pleistocene warming event at 1 Ma in Prydz Bay, East Antarctica: evidence from ODP Site 1165. *Palaeogeography, Palaeoclimatology, Palaeoecology*, 260(1–2):230–244. <https://doi.org/10.1016/j.palaeo.2007.08.017>
- Vincent, E., and Berger, W.H., 1985. Carbon dioxide and polar cooling in the Miocene: the Monterey Hypothesis. In Sundquist, E.T., and Broecker, W.S. (Eds.), *The Carbon Cycle and Atmospheric CO₂: Natural Variations Archean to Present*. Geophysical Monograph, 32:455–468. <https://doi.org/10.1029/GM032p0455>
- Warny, S., Askin, R.A., Hannah, M.J., Mohr, B.A.R., Raine, J.I., Harwood, D.M., Florindo, F., and the SMS Science Team, 2009. Palynomorphs from a sediment core reveal a sudden remarkably warm Antarctica during the middle Miocene. *Geology*, 37(10):955–958. <https://doi.org/10.1130/G30139A.1>
- Weertman, J., 1974. Stability of the junction between an ice sheet and an ice shelf. *Journal of Glaciology*, 13(67):3–11. <https://doi.org/10.3189/S0022143000023327>
- Whitworth, T., III, Orsi, A.H., Kim, S.-J., Nowlin, W.D., Jr., and Locarnini, R.A., 1995. Water masses and mixing near the Antarctic slope front. In Jacobs, S.S., and Weiss, R.F. (Eds.), *Antarctic Research Series (Volume 75): Ocean, Ice, and Atmosphere: Interactions at the Antarctic Continental*

- Margin*: Washington, DC (American Geophysical Union), 1–27.
<https://onlinelibrary.wiley.com/doi/10.1029/AR075p0001/summary>
- Wilch, T.I., McIntosh, W.C., and Dunbar, N.W., 1999. Late Quaternary volcanic activity in Marie Byrd Land: potential $^{40}\text{Ar}/^{39}\text{Ar}$ -dated time horizons in West Antarctic ice and marine cores. *Geological Society of America Bulletin*, 111(10):1563–1580. [https://doi.org/10.1130/0016-7606\(1999\)111<1563:LQVAIM>2.3.CO;2](https://doi.org/10.1130/0016-7606(1999)111<1563:LQVAIM>2.3.CO;2)
- Williams, T., and Handwerger, D., 2005. A high-resolution record of early Miocene Antarctic glacial history from ODP Site 1165, Prydz Bay. *Paleoceanography*, 20(2):PA2017. <https://doi.org/10.1029/2004PA001067>
- Wilson, D.S., and Luyendyk, B.P., 2009. West Antarctic paleotopography estimated at the Eocene–Oligocene climate transition. *Geophysical Research Letters*, 36(16):L16302. <https://doi.org/10.1029/2009GL039297>
- Wilson, D.S., Pollard, D., DeConto, R.M., Jamieson, S.S.R., and Luyendyk, B.P., 2013. Initiation of the West Antarctic Ice Sheet and estimates of total Antarctic ice volume in the earliest Oligocene. *Geophysical Research Letters*, 40(16):4305–4309. <https://doi.org/10.1002/grl.50797>
- Wilson, G.S., Levy, R.H., Naish, T.R., Powell, R.D., Florindo, F., Ohneiser, C., Sagnotti, L., et al., 2012. Neogene tectonic and climatic evolution of the Western Ross Sea, Antarctica—chronology of events from the AND-1B drill hole. *Global and Planetary Change*, 96–97:189–203. <https://doi.org/10.1016/j.gloplacha.2012.05.019>
- Woodruff, F., and Savin, S.M., 1985. $\delta^{13}\text{C}$ values of Miocene Pacific benthic foraminifera: correlations with sea level and biological productivity. *Geology*, 13(2):119–122. [https://doi.org/10.1130/0091-7613\(1985\)13<119:CVOMPB>2.0.CO;2](https://doi.org/10.1130/0091-7613(1985)13<119:CVOMPB>2.0.CO;2)
- Wright, J.D., Miller, K.G., and Fairbanks, R.G., 1991. Evolution of modern deepwater circulation: evidence from the late Miocene Southern Ocean. *Paleoceanography*, 6(2):275–290. <https://doi.org/10.1029/90PA02498>
- You, Y., Huber, M., Müller, R.D., Poulsen, C.J., and Ribbe, J., 2009. Simulation of the Middle Miocene Climate Optimum. *Geophysical Research Letters*, 36(4):L04702. <https://doi.org/10.1029/2008GL036571>
- Zachos, J., Pagani, M., Sloan, L., Thomas, E., and Billups, K., 2001. Trends, rhythms, and aberrations in global climate 65 Ma to present. *Science*, 292(5517):686–693. <https://doi.org/10.1126/science.1059412>
- Zachos, J.C., Flower, B.P., and Paul, H., 1997. Orbitally paced climate oscillations across the Oligocene/Miocene boundary. *Nature*, 388(6642):567–570. <https://doi.org/10.1038/41528>

Table T1. Summary of Ross Sea stratigraphy prior to Expedition 374 drilling. Based on Brancolini et al. (1995) ANTOSTRAT project. Expedition 374 will provide new constraints for the ages of some of the main unconformities and seismic sequences.

Sequence	Sequence seismic character	Age	Bottom unconformity
RSS-8	Aggradational topset beds underlying locally backstepping grounding zone wedge	Pleistocene	RSU1 (0.7 Ma?)
RSS-7	Aggradational topset beds	Pliocene	RSU2 (4 Ma?)
RSS-6	Shelf topset beds and prograding trough mouth fan at the shelf edge	late Miocene	RSU3 (12 Ma?)
RSS-5	Alternating subsequences of grounding zone prograding wedges and subhorizontal strata packages	mid-Miocene	RSU4 (14–16 Ma?)
RSS-4	Grounding zone prograding wedges and subhorizontal strata packages	early Miocene	RSU4a (18.5 Ma?)
RSS-3	Alternating subsequences of grounding zone prograding wedges and subhorizontal strata packages	early Miocene	RSU5 (21 Ma?)
RSS-2	Alternating subsequences of grounding zone prograding wedges and subhorizontal strata packages	late Oligocene–early Miocene	RSU6 (29 Ma?)
RSS-1 (upper)	Subhorizontal strata filling basement basins	late Eocene–early Oligocene	RSU7
RSS-1 (lower)	Subhorizontal strata filling basement basins	?Late Cretaceous	Basement

Table T2. Hole summary, Expedition 374. DSF = drilling depth below seafloor, APC = advanced piston corer, HLAPC = half-length APC, XCB = extended core barrel, RCB = rotary core barrel.

Hole	Latitude	Longitude	Water depth (m)	Penetration DSF (m)	Cored interval (m)	Recovered length (m)	Recovery (%)	Drilled interval (m)	Drilled interval (N)	Total cores (N)	APC cores (N)	HLAPC cores (N)	XCB cores (N)	RCB cores (N)	Other cores (N)
U1521A	75°41.0351'S	179°40.3108'W	562.18	650.1	650.1	411.50	63.30	0.0	0	71	0	0	0	71	0
U1522A	76°33.2262'S	174°45.4652'W	557.60	701.8	701.8	279.57	39.84	0.0	0	76	0	0	0	76	0
U1523A	74°9.0172'S	176°47.7067'W	828.02	46.3	46.3	33.51	72.38	0.0	0	7	3	4	0	0	1
U1523B	74°9.0179'S	176°47.6660'W	827.99	164.4	121.2	45.13	37.24	43.2	2	22	1	13	8	0	0
U1523C	74°9.0288'S	176°47.6680'W	827.99	43.3	0.0	0.00	0.00	43.3	1	0	0	0	0	0	0
U1523D	74°9.0288'S	176°47.7087'W	827.97	307.8	172.8	0.90	0.52	135.0	1	18	0	0	0	18	0
U1523E	74°9.0290'S	176°47.7491'W	827.88	130.8	84.7	54.08	63.85	46.1	8	17	1	16	0	0	0
U1524A	74°13.0427'S	173°38.0185'W	2394.39	299.5	299.5	282.35	94.27	0.0	0	34	30	1	3	0	0
U1524B	74°13.0440'S	173°37.9834'W	2394.16	7.7	7.7	7.76	100.78	0.0	0	1	1	0	0	0	0
U1524C	74°13.0537'S	173°37.9338'W	2394.34	441.9	181.4	19.20	10.58	260.5	1	19	0	0	0	19	0
U1525A	75°0.0603'S	173°55.2028'W	1775.74	213.2	213.2	158.70	74.44	0.0	0	33	8	14	11	0	0
Totals:			3006.8	2478.7	1292.70			528.1	13	298	44	48	22	184	1

Hole	Latitude	Longitude	Date started (2018)	Time started UTC (h)	Date finished (2018)	Time finished UTC (h)	Time on hole (days)
U1521A	75°41.0351'S	179°40.3108'W	15 Jan	2057	21 Jan	0945	5.53
U1522A	76°33.2262'S	174°45.4652'W	21 Jan	1754	28 Jan	0011	6.26
U1523A	74°9.0172'S	176°47.7067'W	28 Jan	1318	29 Jan	1550	1.11
U1523B	74°9.0179'S	176°47.6660'W	29 Jan	1550	31 Jan	0440	1.53
U1523C	74°9.0288'S	176°47.6680'W	31 Jan	0440	31 Jan	1230	0.33
U1523D	74°9.0288'S	176°47.7087'W	31 Jan	1230	2 Feb	1340	2.05
U1523E	74°9.0290'S	176°47.7491'W	2 Feb	1340	3 Feb	1647	1.13
U1524A	74°13.0427'S	173°38.0185'W	3 Feb	2144	5 Feb	2050	1.96
U1524B	74°13.0440'S	173°37.9834'W	5 Feb	2050	6 Feb	0730	0.44
U1524C	74°13.0537'S	173°37.9338'W	8 Feb	2100	11 Feb	0535	2.36
U1525A	75°0.0603'S	173°55.2028'W	6 Feb	1315	8 Feb	1635	2.14

Figure F1. Data reconstructions. A. Compilation of atmospheric CO₂ proxies throughout the Cenozoic (left). Proxy methods (see legend) are from Masson-Delmotte et al. (2013). “Best and worst case” representative concentration pathways (RCPs) for historic and future atmospheric CO₂ emissions (right) are from Meinshausen et al. (2011). PD = present day. B. Composite deep-ocean benthic δ¹⁸O record for the last 65 My, which represents a combined signal of global ice volume and deep-ocean temperature after ~35 Ma (Zachos et al., 2001). C. Long-term trend in deep-sea temperature through the Cenozoic based on removal of the ice volume component of the benthic δ¹⁸O record using sequence stratigraphic records (black line with gray uncertainty band) and Mg/Ca estimates of deep-sea temperatures (Cramer et al., 2009) and scaled δ¹⁸O for the past 10 My (Miller et al., 2011). D. Reconstruction of sea level lowstands (black lines) with minimum uncertainty ranges (gray shading) and smoothed highstand trend (black dotted line) using sequence stratigraphy for the New Jersey margin. Sea levels >70 m imply a significant tectonic component to this record, particularly prior to the Oligocene (Kominz et al., 2008). Figure reproduced from McKay et al. (2016).

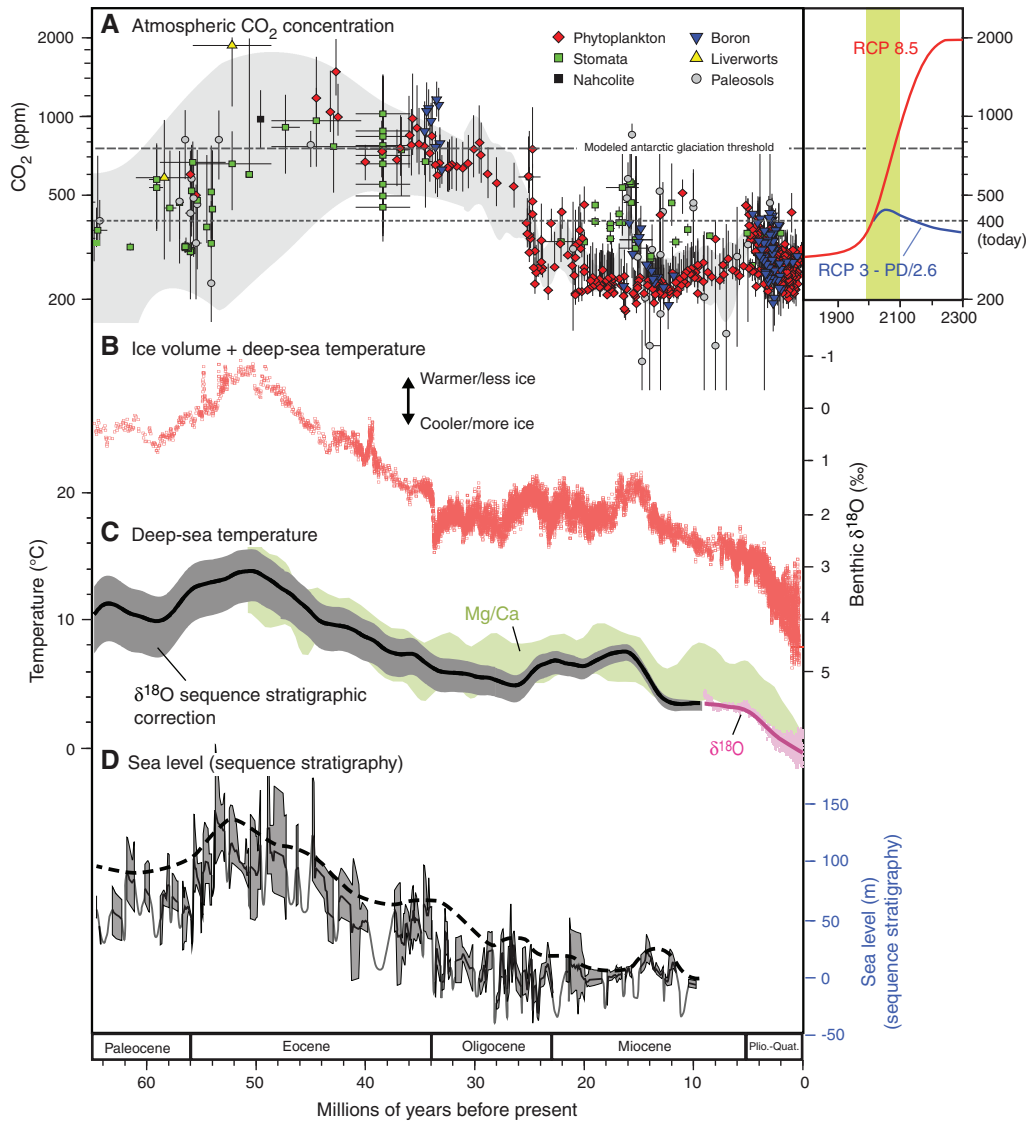


Figure F2. Bathymetric map with Expedition 374 sites and previous Deep Sea Drilling Project (DSDP) Leg 28, Antarctic Geological Drilling Project (AND), and Cape Roberts Project (CRP) sites. Ross Sea bathymetry is from the International Bathymetric Chart of the Southern Ocean (Arndt et al., 2013). Existing seismic network is from the Antarctic Seismic Data Library System and includes some single-channel seismic profiles.

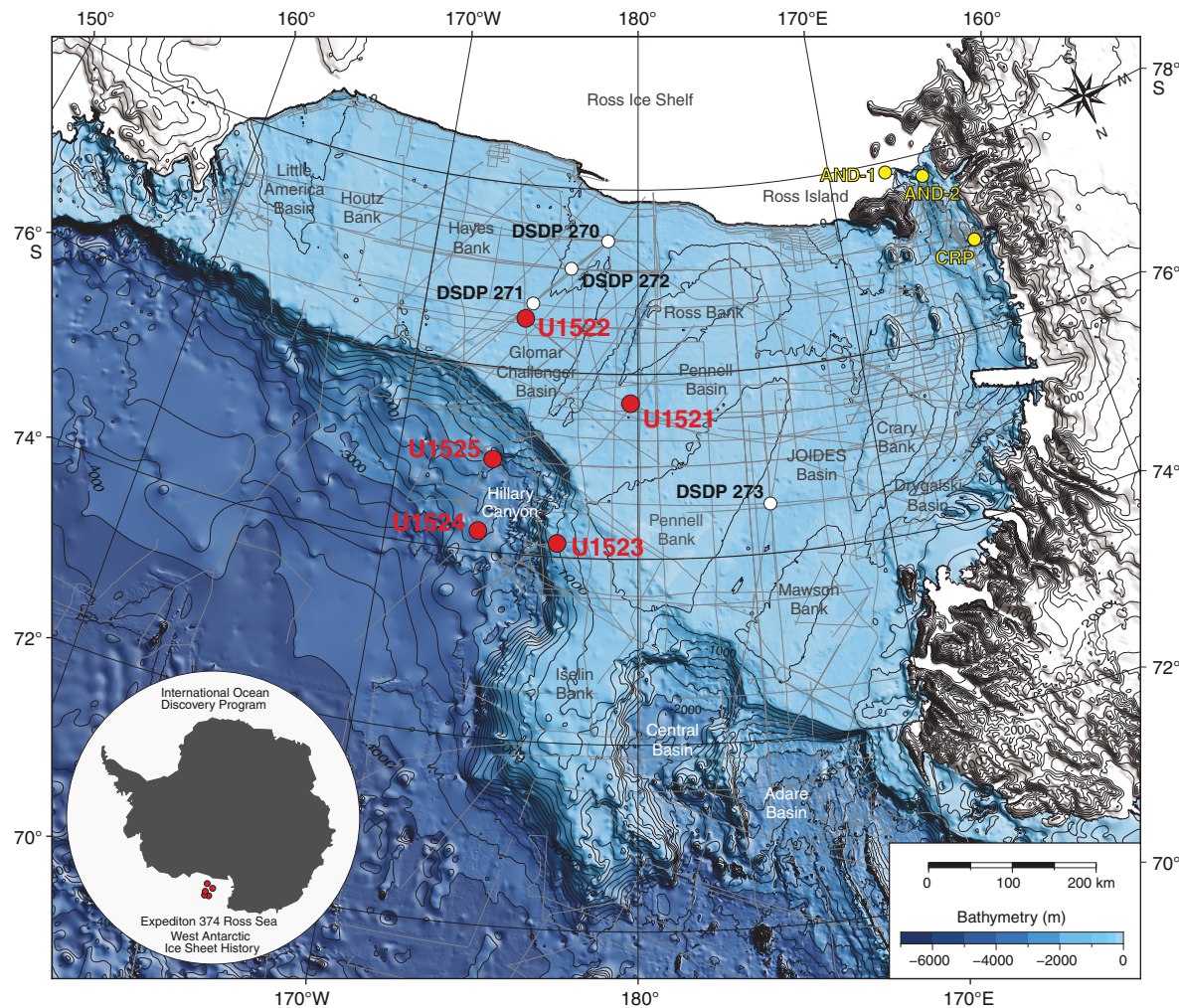


Figure F3. Ross Sea seismic stratigraphy and previous drilling (see Figure F7 for transect line). Expedition 374 sites form a continental shelf-to-rise transect designed to tie into inner shelf sites and to trace the Neogene and Quaternary evolution of the West Antarctic Ice Sheet and the forcings and feedbacks influencing past variability. ANDRILL/CRP = Antarctic Geological Drilling Project/Cape Roberts Project, DSDP = Deep Sea Drilling Project. RSU1–RSU4 and RSU6 = Ross Sea seismic unconformities.

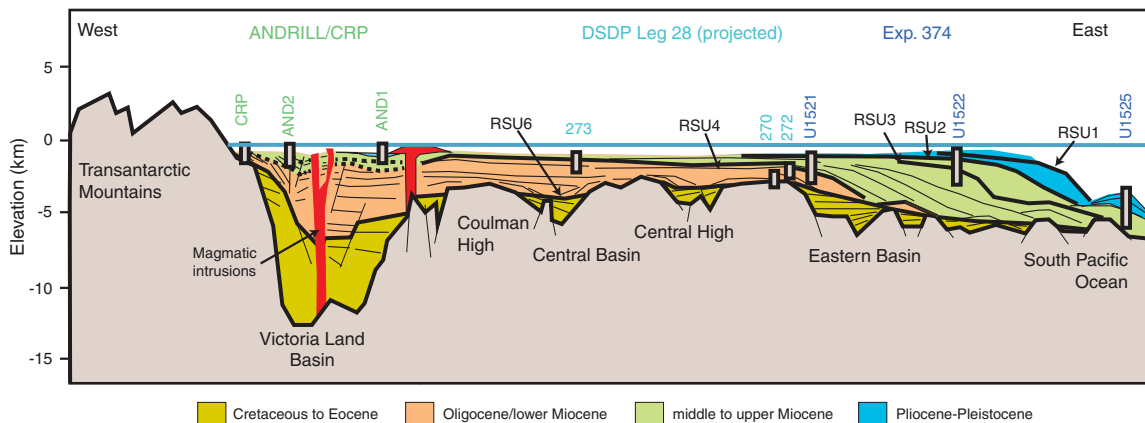


Figure F4. Expedition 374 sites are located in the most sensitive sector of the Antarctic for assessing ice sheet responses to (A) sea level and (B) ocean heat flux. AIS = Antarctic Ice Sheet, ANDRILL = Antarctic Geological Drilling Project. C–F. A more terrestrial West Antarctica in the Oligocene could support a larger ice sheet than present, despite a warmer climate (Wilson et al., 2013). Thus, the timing of Ross Sea overdeepening has important implications for sea level budgets and for understanding mass balance controls. E-O = Eocene–Oligocene, Elev = elevation. G. The integration of sedimentologic data with modeling was key to the success of ANDRILL (blue circle). Despite discontinuous sedimentation, targeting time intervals with short-duration magnetic reversals enabled orbital-scale West Antarctic Ice Sheet (WAIS) reconstructions. Models indicate that grounded ice sheets occur at Sites U1521 and U1522 (black circle) during periods of maximum Antarctic ice volume. These ice-proximal sites will enable the assessment of the Antarctic contributions to sea level lowstands, building significantly on the record of ANDRILL. Not all modeled glacial maxima are characterized by advance of ice to the continental shelf edge. LGM = Last Glacial Maximum.

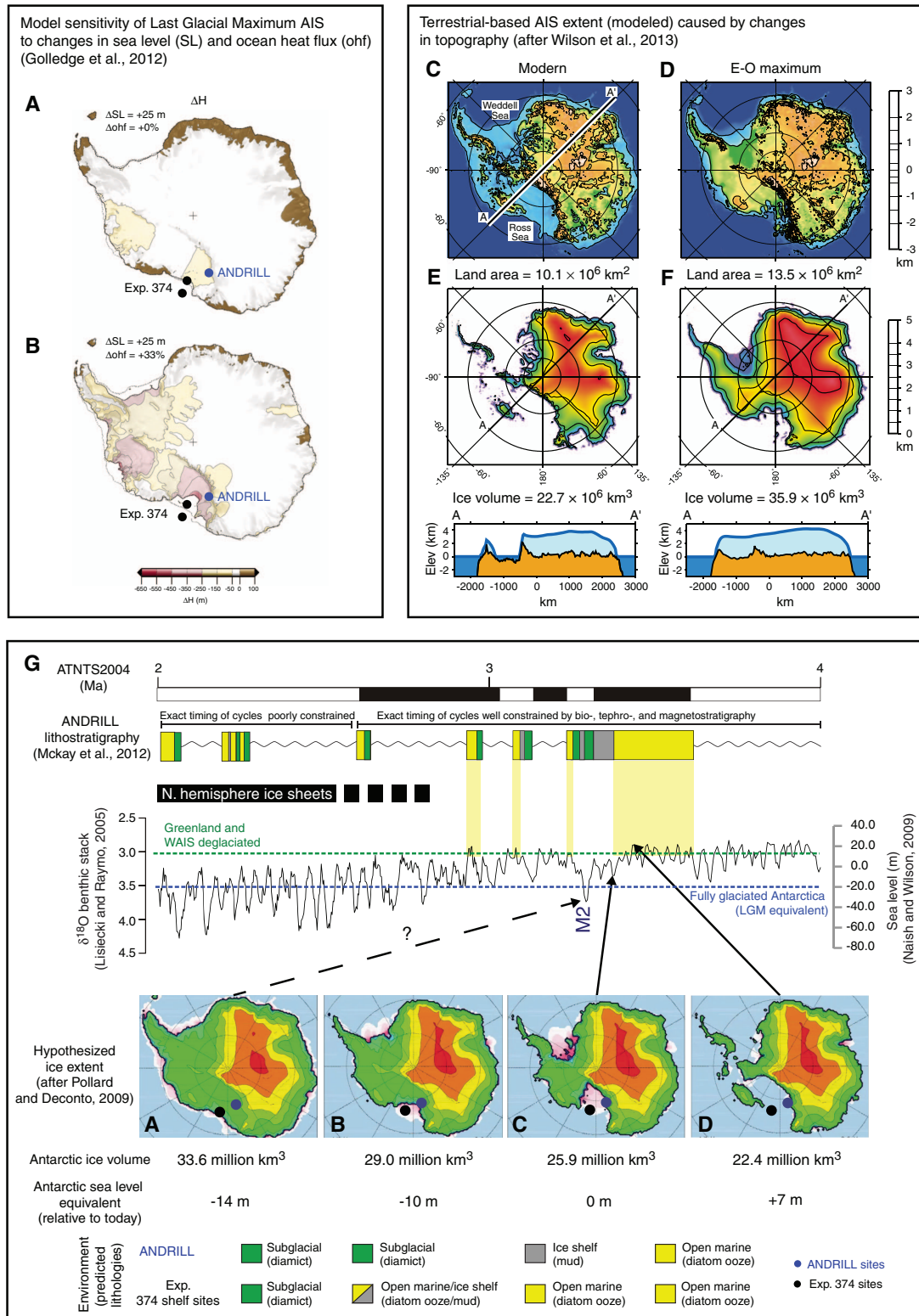


Figure F5. Ross Sea bathymetric map (from the International Bathymetric Chart of the Southern Ocean; Arndt et al., 2013). The Ross Sea Bottom Water (RSBW; blue arrow) derived from the ice shelf water (not shown) flows downslope in the Hillary Canyon, as well as along the central and western Ross Sea shelf slope, influencing deep waters (e.g., Antarctic Deep Water vs. Antarctic Bottom Water).

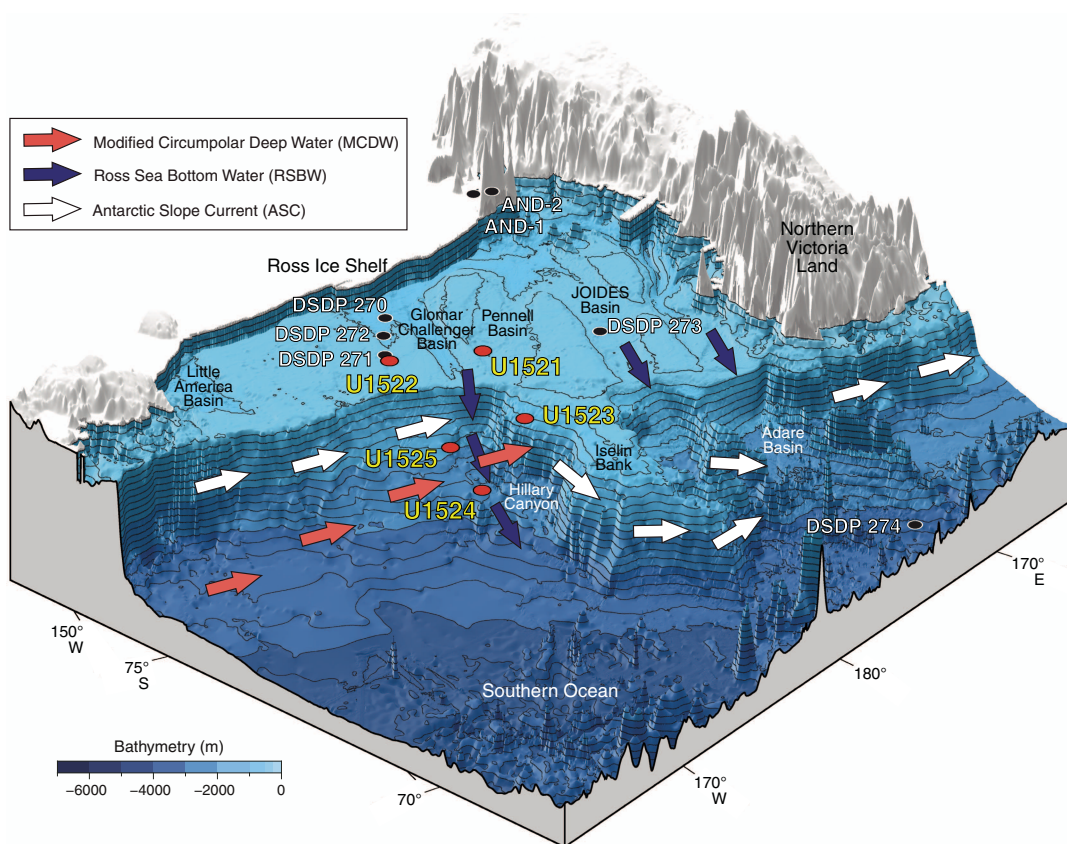


Figure F6. Chronostratigraphic summary of Ross Sea drilling. Seismic stratigraphy is constrained by drilling in Victoria Land Basin (SR-VLB) but not in the Central and Eastern Basins (EB-RSU). Postcruise research from the Expedition 374 sites will reduce uncertainties associated with Unconformities RSU2–RSU4 and assess the spatial coherency of these erosional features. Far-field climate ($\delta^{18}\text{O}$), CO_2 , carbon cycle ($\delta^{13}\text{C}$), Equatorial Pacific carbonate compensation depth (CCD), and sea level records discussed in the text are indicated (modified from Antarctic Geological Drilling Project [ANDRILL] Coulman High Drilling National Science Foundation proposal). DSDP = Deep Sea Drilling Project, TD = total depth, NJM = New Jersey margin, RSU = Ross Sea seismic unconformity.

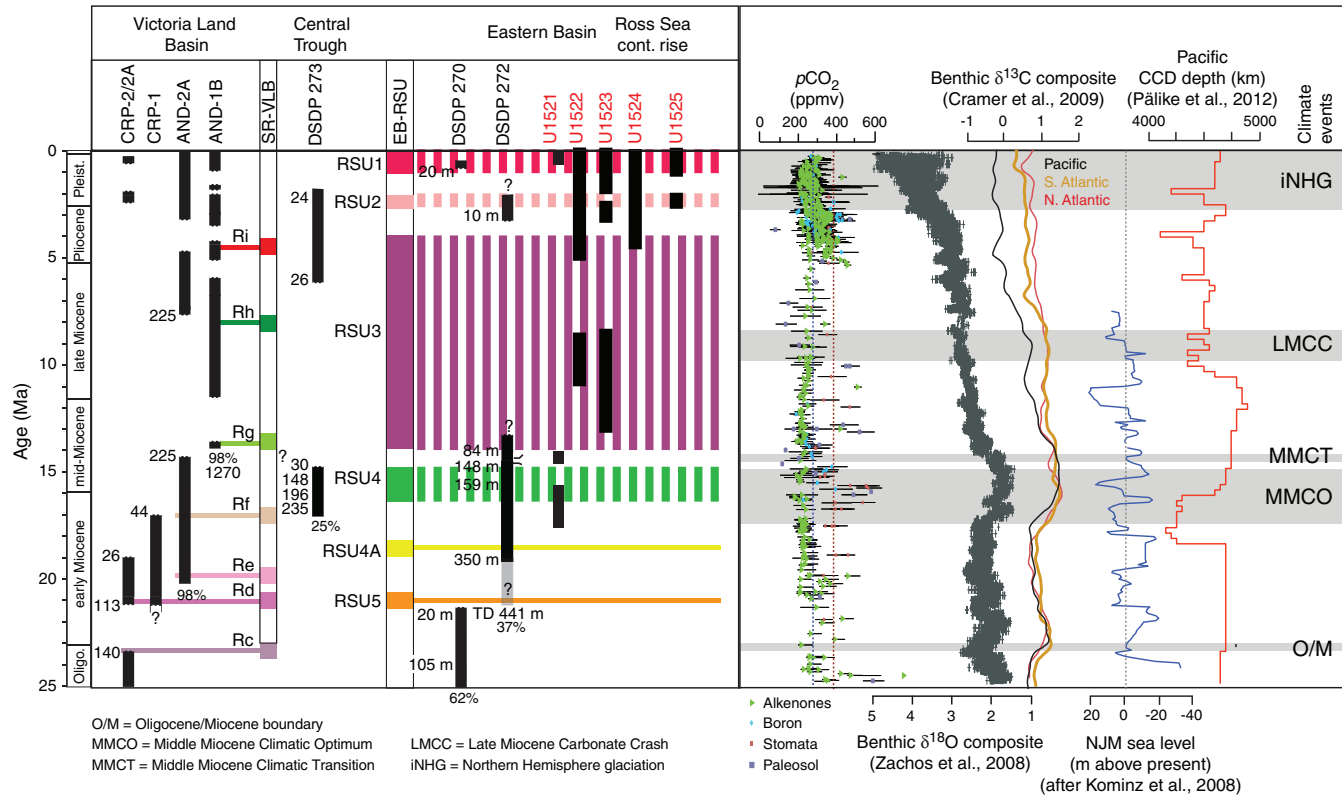


Figure F7. Depth maps (in two-way traveltimes [TWT]) for selected regional seismic ANTOSTRAT unconformities, with interpretations of ice sheet history (after Brancolini et al., 1995) and location of Expedition 374 sites. Maps of Ross Sea seismic Unconformities RSU4, RSU3, and RSU2 have now been extended into the continental slope and rise area (E. Olivo, unpubl. data; not shown) and into the western Ross Sea as part of the IPY Rossmap project. Gray shading in A shows the areas lying above sea level at the time of Unconformity RSU6 on the basis of Deep Sea Drilling Project (DSDP) Site 270 stratigraphy. Site U1521 is located at (A) the ocean margin of one of these areas, which subsided in the early Miocene and (B) was cut by a large glacial valley by the early to mid-Miocene. Site U1521 will provide environmental information about paleo-ice stream and ocean current interplay during the middle Miocene. Site U1522 is located at the edge of a large embayment of the continental shelf in the eastern Ross Sea, where West Antarctic Ice Sheet (WAIS) streams have carved glacial valleys since Unconformity RSU3. Sites U1522–U1525 will provide evidence for testing this hypothesis from subglacial ice proximal (Site U1522) and ice distal (Site U1523) to very ice distal (Sites U1525 and U1524) Miocene to Pleistocene records.

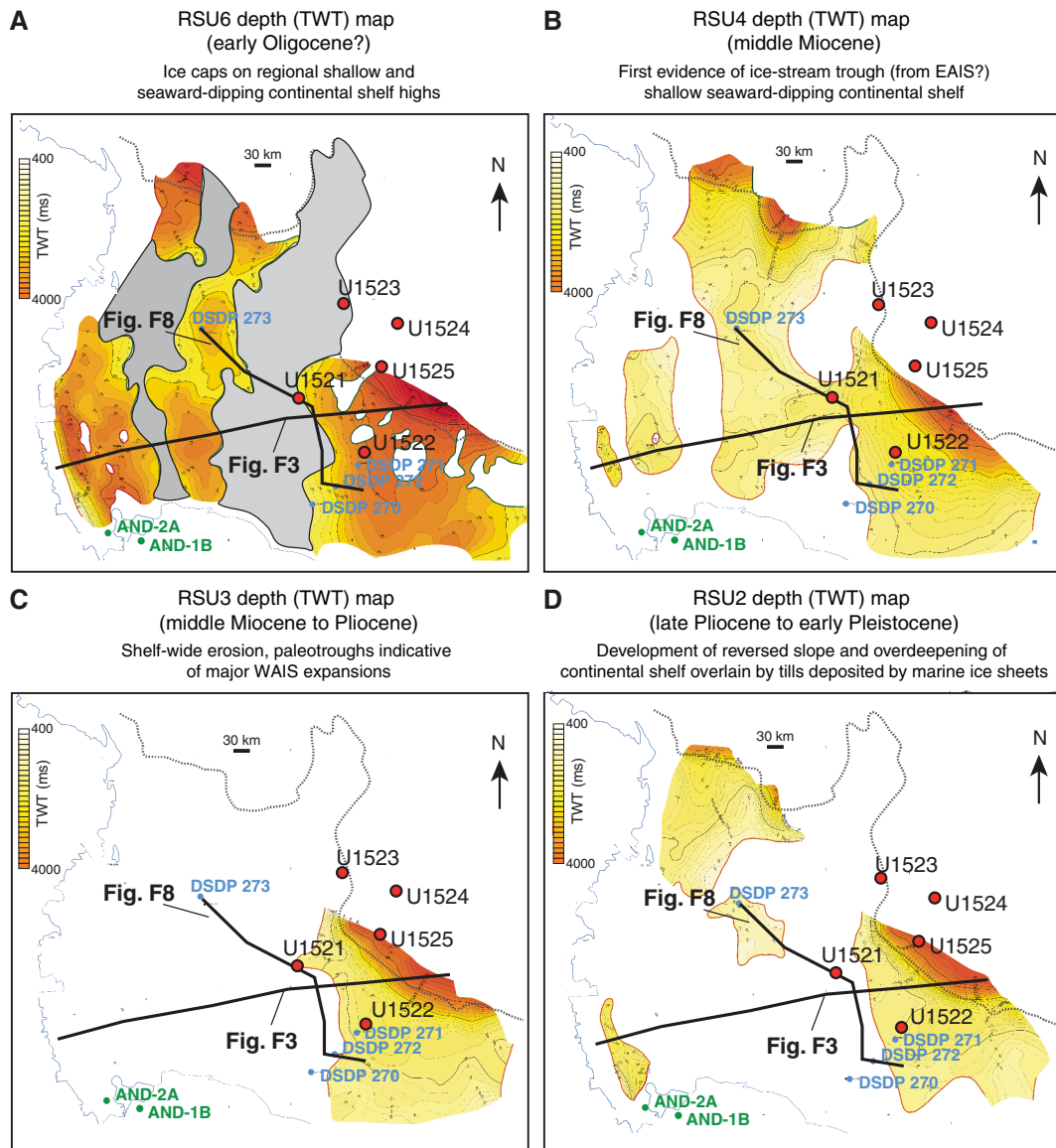


Figure F8. Composite seismic cross section of Lines PD90-34, PD90-35, and PD90-36 (after Anderson and Bartek, 1992; De Santis et al., 1995) showing a transect across the central Ross Sea that includes Deep Sea Drilling Project (DSDP) Sites 272 and 273 and Site U1521. The seismic profile and age constraint from the sites document that this area was filled with glacial sediments (~250 ms TWT thick) during the early Miocene, suggesting ice advance from the south or southwest. The green reflector on top of the glacial unit is interpreted to be the RSU4 unconformity carving a large southeast–northwest-oriented trough across the central Ross Sea (see Figure F7 for transect line). Site U1521 records sediment below and above Unconformity RSU4, providing information of ice-volume growth and retreat during the early Miocene cooling, the middle Miocene, and the Middle Miocene Climatic Transition. Seismic lines are single-channel reflection seismic profiles (air gun 2.6 l) collected by Rice University, TX (USA), in 1990 (Anderson and Bartek, 1992). SP = shotpoint.

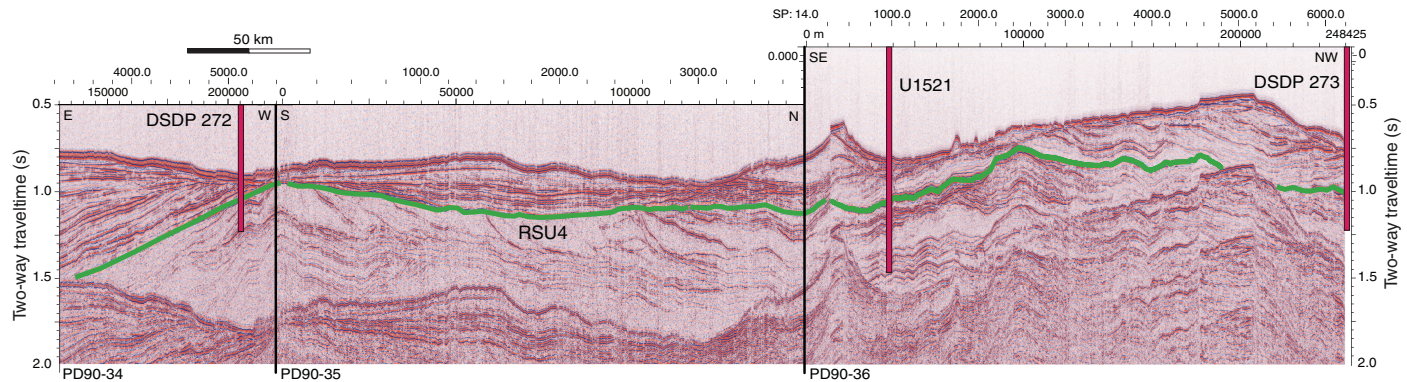


Figure F9. Bathymetric map with locations of Site U1521, other Expedition 374 sites, Deep Sea Drilling Project (DSDP) Leg 28 sites, and Antarctic Geological Drilling Project (AND) drill cores. Red box = location of inset map with Site U1521 on seismic profile Line PD90-36 (Figure F10). Bathymetry from Arndt et al., 2013.

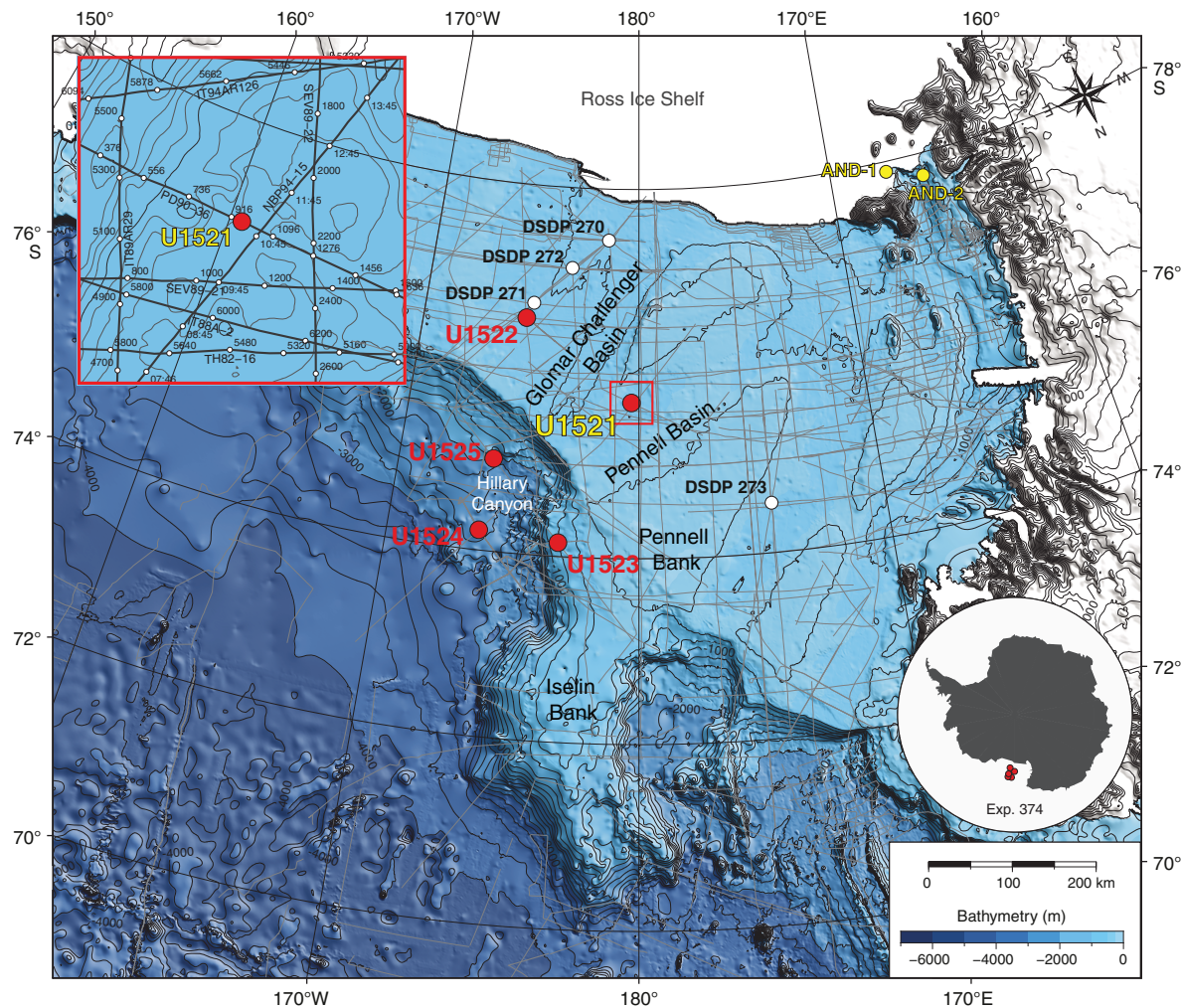


Figure F10. A. Single-channel seismic profile Line PD90-36 across Site U1521 (see inset in Figure F9) and Deep Sea Drilling Project (DSDP) Site 273. Profile (air gun 2.4 l) collected by Rice University, TX (USA), in 1990 (Anderson and Bartek, 1992). SP = shotpoint. B. Interpretation of seismic reflectors and Ross Sea seismic unconformity (RSU4) in A. Arrows = reflector termination.

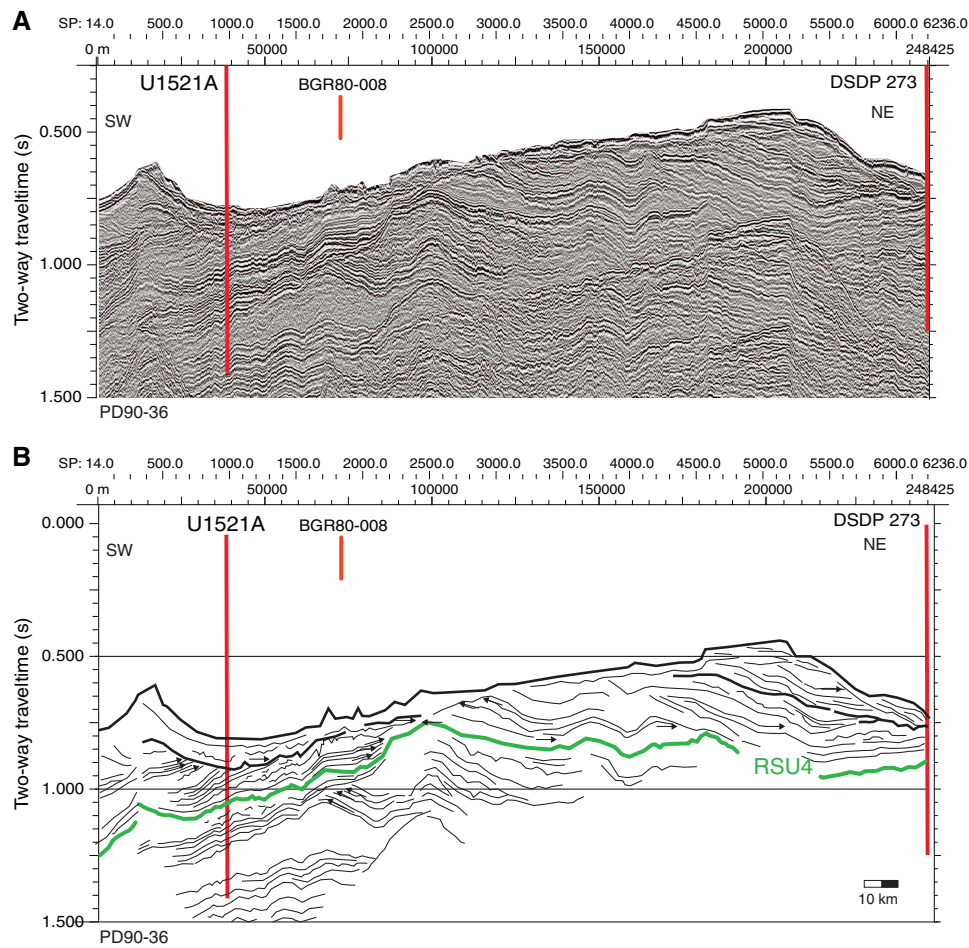


Figure F11. Site U1521 summary. Preliminary environmental interpretation is based on microfossil content. WRMSL = Whole-Round Multisensor Logger, SHMSL = Section Half Multisensor Logger.

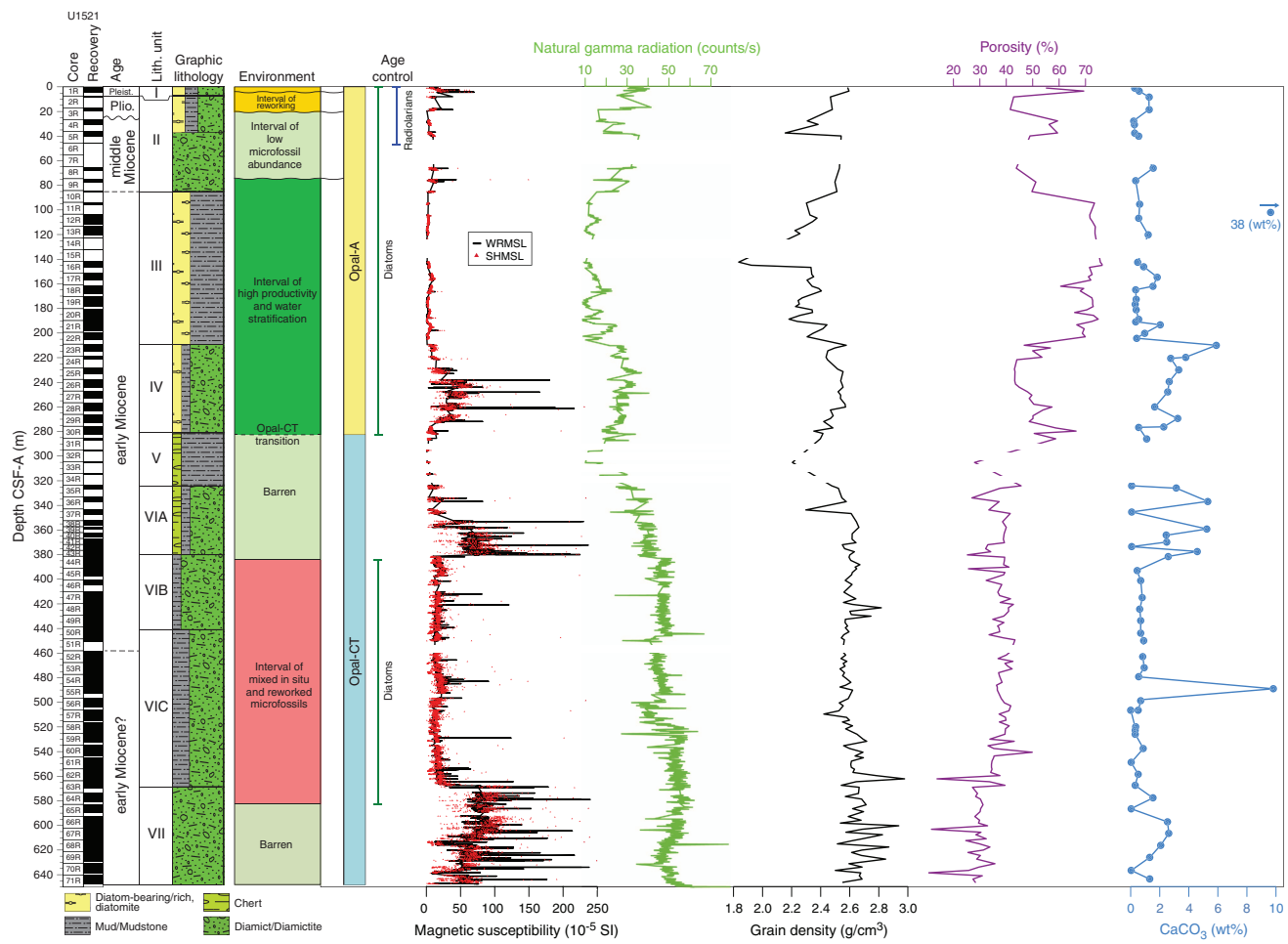


Figure F12. Bathymetric map with locations of Site U1522, other Expedition 374 sites, Deep Sea Drilling Project (DSDP) Leg 28 sites, and Antarctic Geological Drilling Project (AND) drill cores. Red box = location of inset map with Site U1522 on seismic profile Line I06290-Y2 (Figure F13). Bathymetry from Arndt et al., 2013.

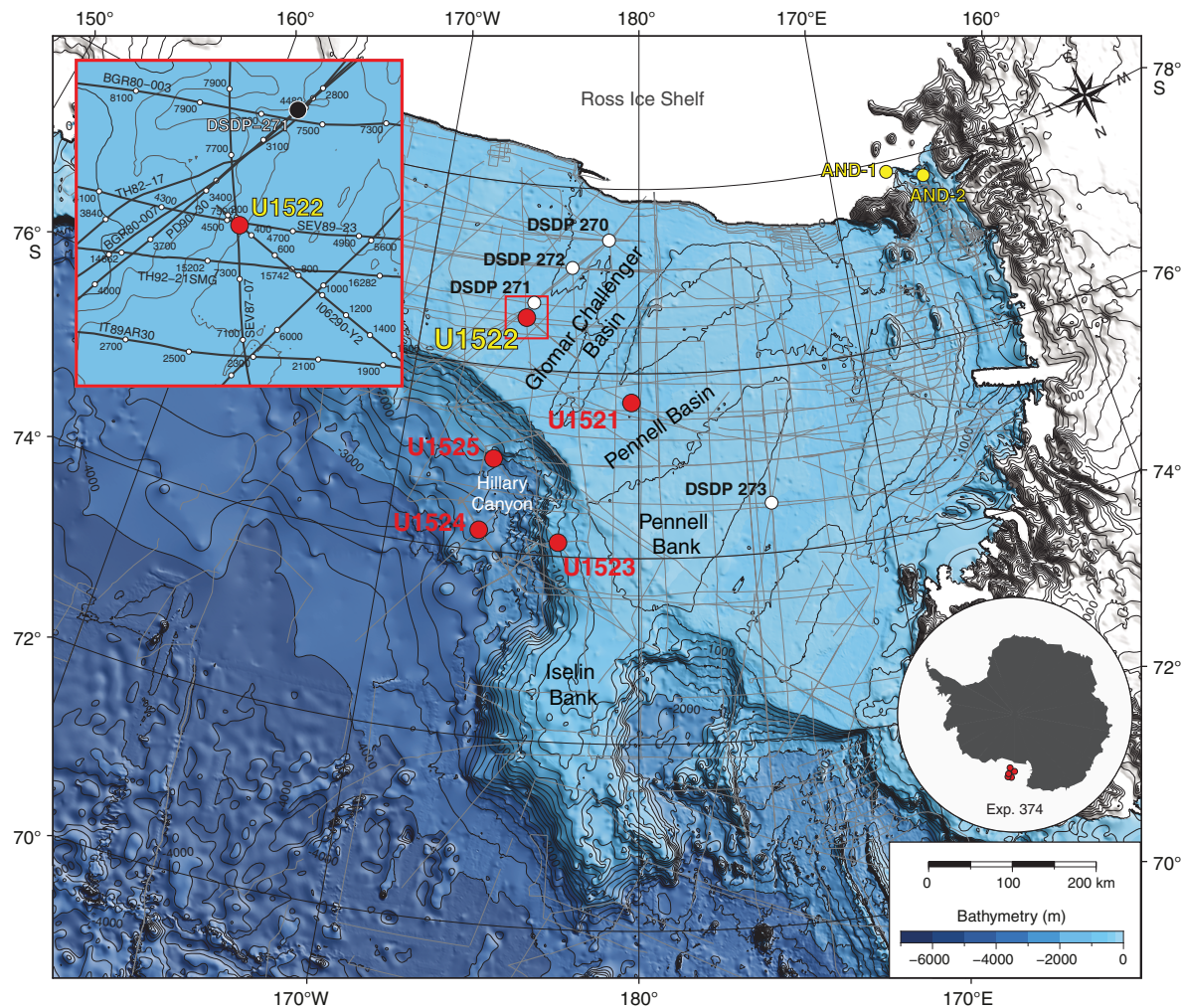


Figure F13. A. Multichannel seismic profile Line I06290-Y2 across Site U1522 (see inset in Figure F12). Profile collected by Istituto Nazionale di Oceanografia e Geofisica Sperimentale (Italy) under Programma Nazionale delle Ricerche in Antartide in 2005–2006 (Böhm et al., 2009). The source used was a 2 × air gun array (11.6 l), and data were acquired with a 600 m streamer (48 channels; first offset = 50 m and last offset = 650 m). SP = shot point B. Interpretation of key seismic reflectors and Ross Sea seismic unconformities (RSU1–RSU3) in A.

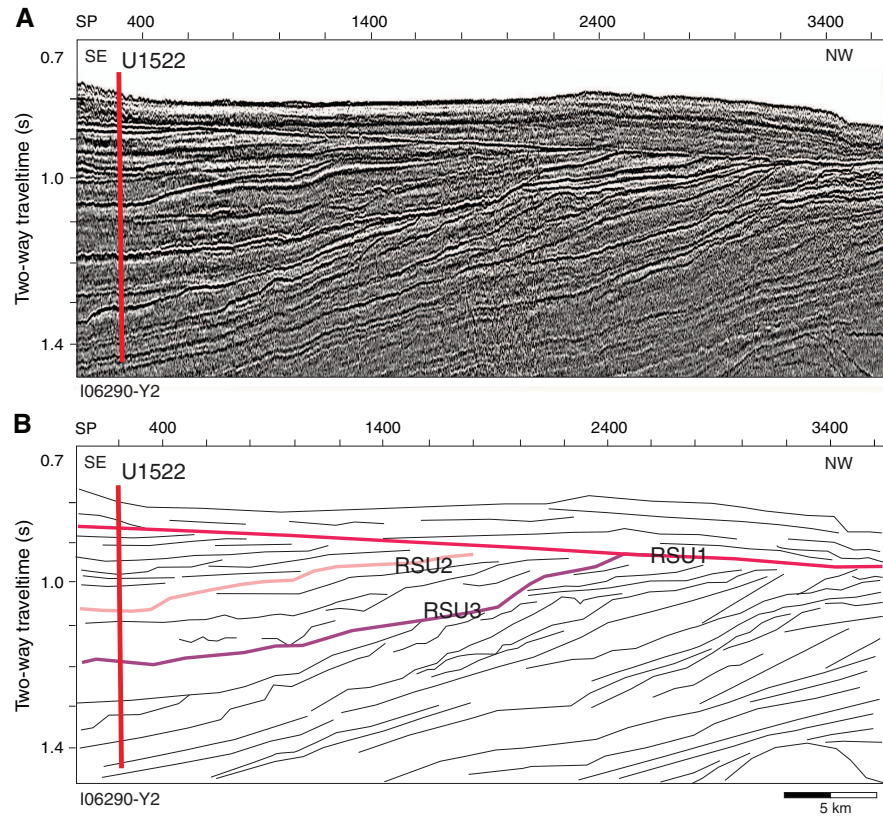


Figure F14. Site U1522 summary. Preliminary environmental interpretation is based on microfossil content. WRMSL = Whole-Round Multisensor Logger, SHMSL = Section Half Multisensor Logger.

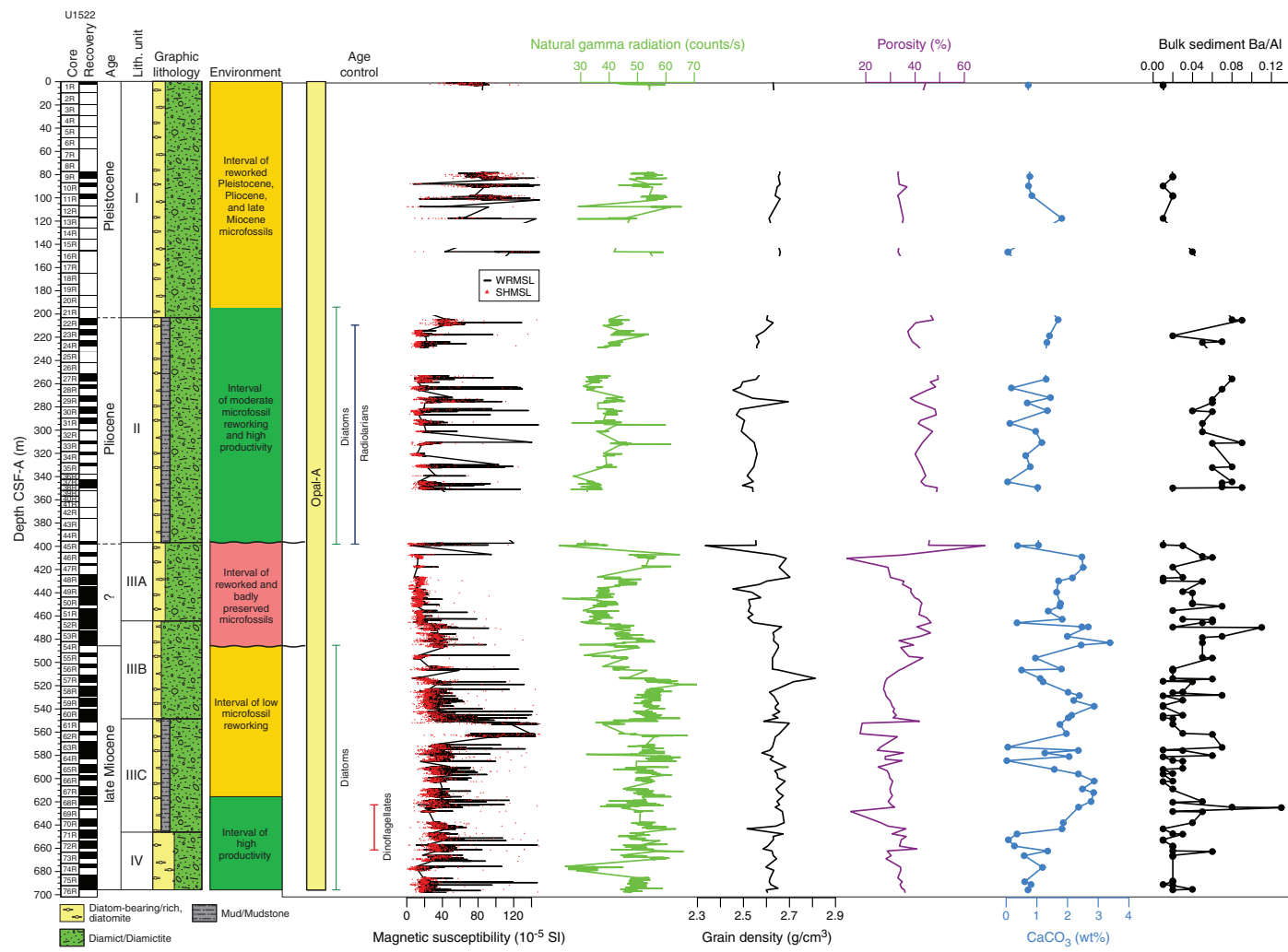


Figure F15. Bathymetric map with locations of Site U1523, other Expedition 374 sites, Deep Sea Drilling Project (DSDP) Leg 28 sites, and Antarctic Geological Drilling Project (AND) drill cores. Red box = location of inset map with Site U1523 at the intersection of seismic profile Lines IT17RS-301 and IT94AR-127A (Figure F16). Bathymetry from Arndt et al., 2013.

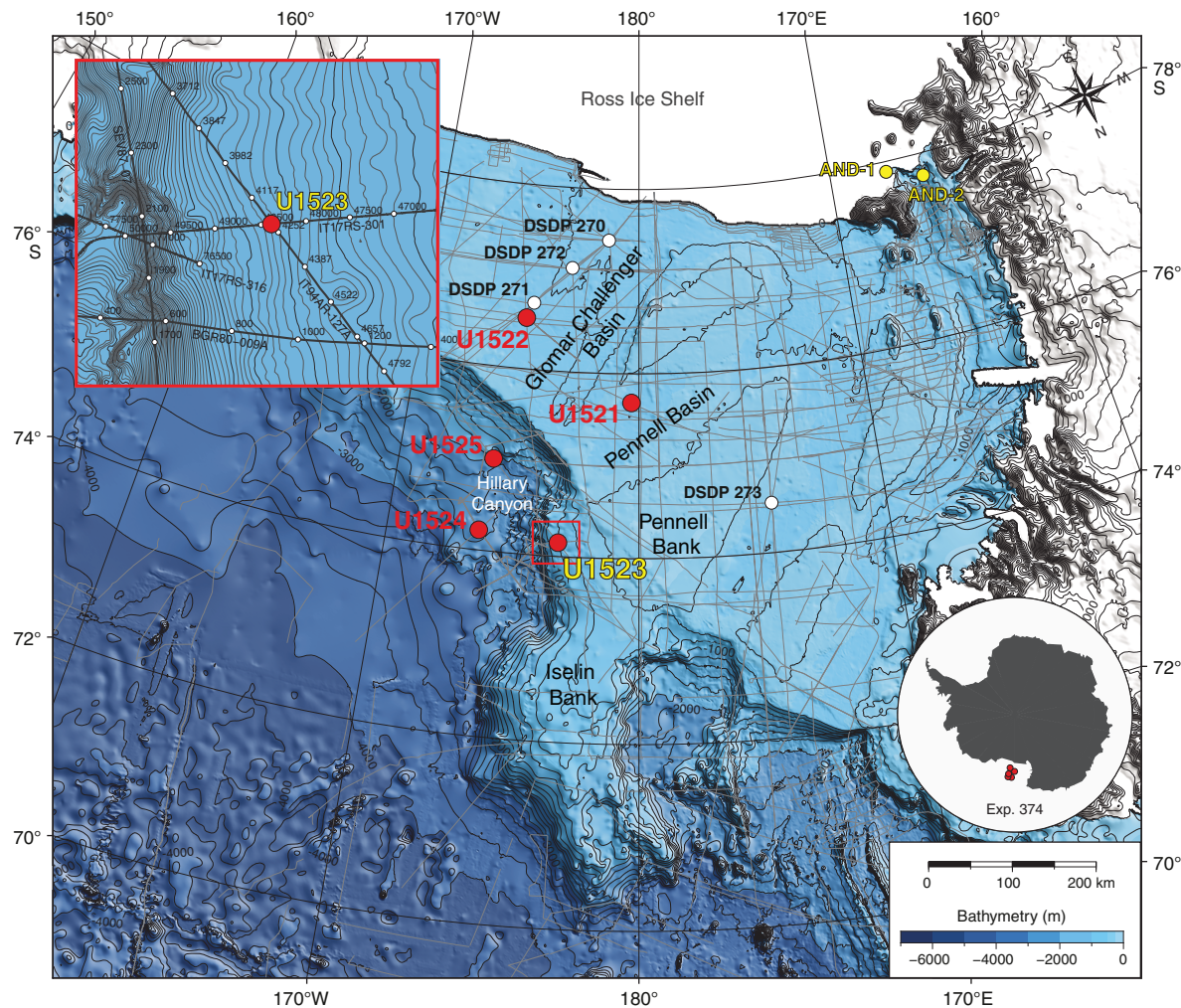


Figure F16. Multichannel seismic profile Line IT94AR-127A with location of Site U1523 at the cross point with Line IT17RS-301 (see inset in Figure F15). Profile collected by Istituto Nazionale di Oceanografia e Geofisica Sperimentale (OGS; Italy) under Programma Nazionale delle Ricerche in Antartide in 1994 (I. Finetti et al., unpubl. data). Seismic stack profile is available through the Antarctic Seismic Data Library System for scientific purposes. The source used was a 2×20 -air gun array (74.8 l), and data were acquired with a 1500 m streamer (120 channels; first offset = 164 m and last offset = 1664 m). Reprocessing of Line IT94AR-127A for Expedition 374 was done by Riccardo Geletti (OGS). SP = shotpoint.

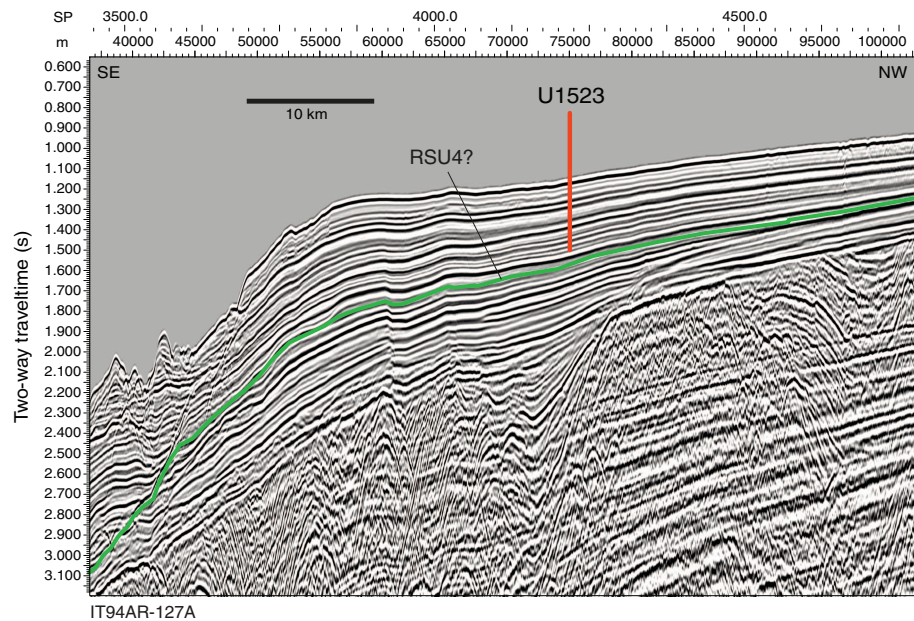


Figure F17. Site U1523 summary. Preliminary environmental interpretation is based on microfossil content. WRMSL = Whole-Round Multisensor Logger, SHMSL = Section Half Multisensor Logger.

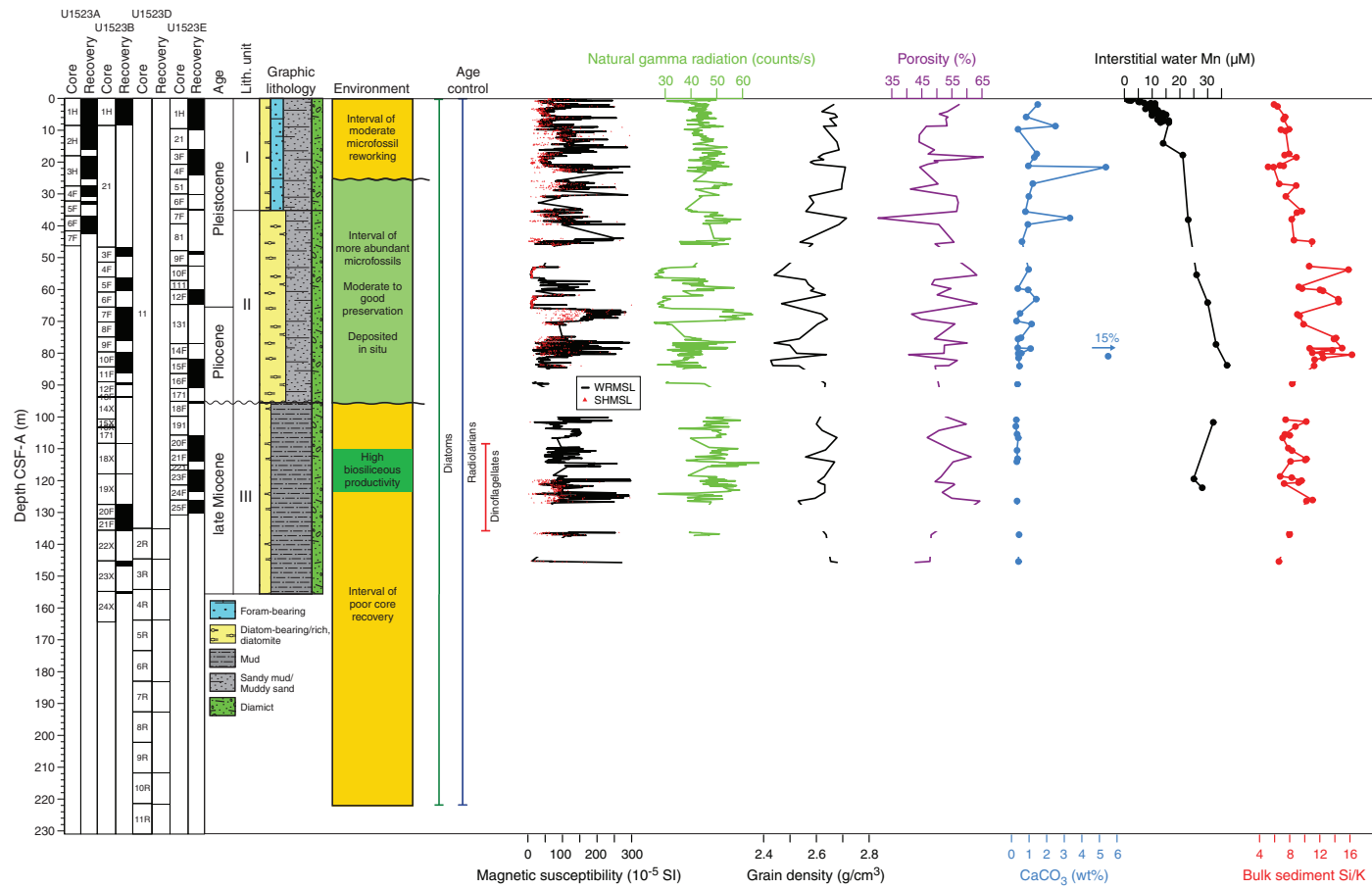


Figure F18. Bathymetric map with locations of Site U1524, other Expedition 374 sites, Deep Sea Drilling Project (DSDP) Leg 28 sites, and Antarctic Geological Drilling Project (AND) drill cores. Red box = location of inset map with Site U1524 on seismic profile Lines TAN0602_08 (Figure F19) and IT17RS-303B. Bathymetry from Arndt et al., 2013.

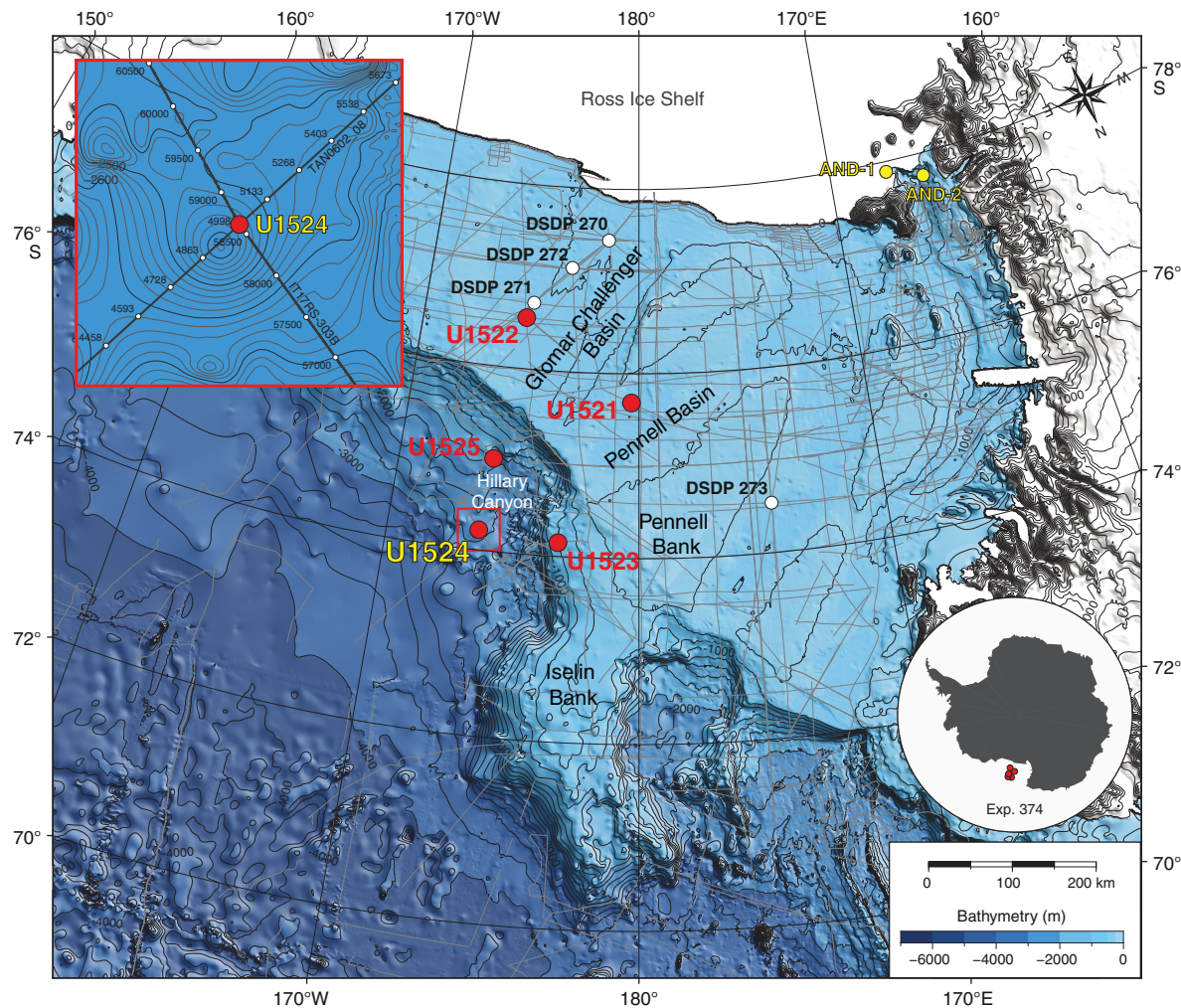


Figure F19. A. Multichannel seismic profile Line TAN0602_08 with location of Site U1524 at the intersection of Line IT17RS-303B (see inset in Figure F18). Seismic profile collected by NIWA and GNS Science in 2006 using the RV *Tangaroa* (Lindeque et al., 2016). The source used was a 4-air gun array (9.8 l), and data were acquired with a 300 m streamer (48 channels; near offset nominally 129 m and far offset = 422 m) towed at a nominal depth of 10 m. SP = shotpoint. B. Interpretation of key seismic reflectors in Line TAN0602_08.

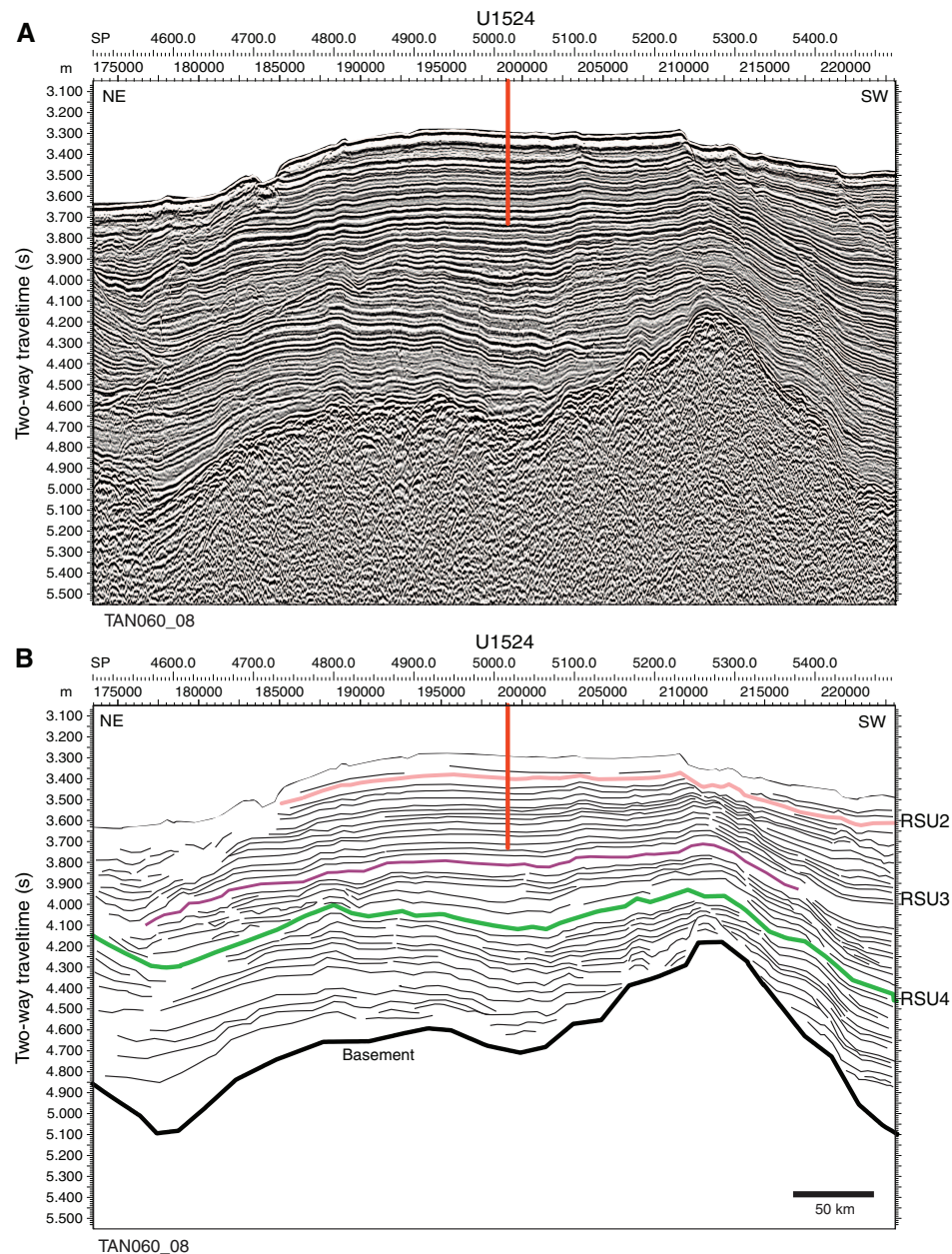


Figure F20. Site U1524 summary. Preliminary environmental interpretation is based on microfossil content. WRMSL = Whole-Round Multisensor Logger, SHMSL = Section Half Multisensor Logger.

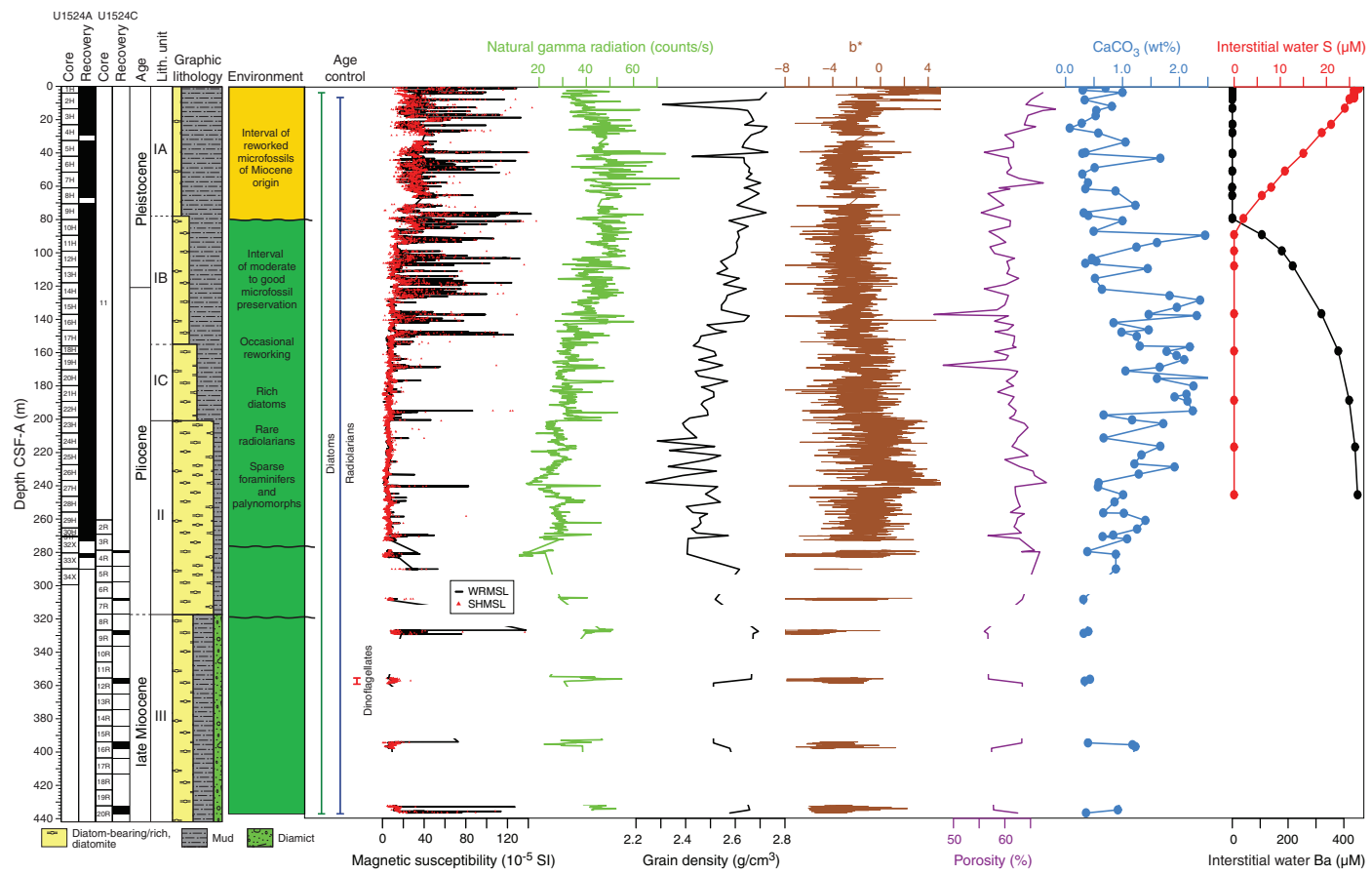


Figure F21. Bathymetric map with locations of Site U1525, other Expedition 374 sites, Deep Sea Drilling Project (DSDP) Leg 28 sites, and Antarctic Geological Drilling Project (AND) drill cores. Red box = location of inset map with Site U1525 on seismic profile Line IT94AR-127 (Figure F22). Bathymetry from Arndt et al., 2013.

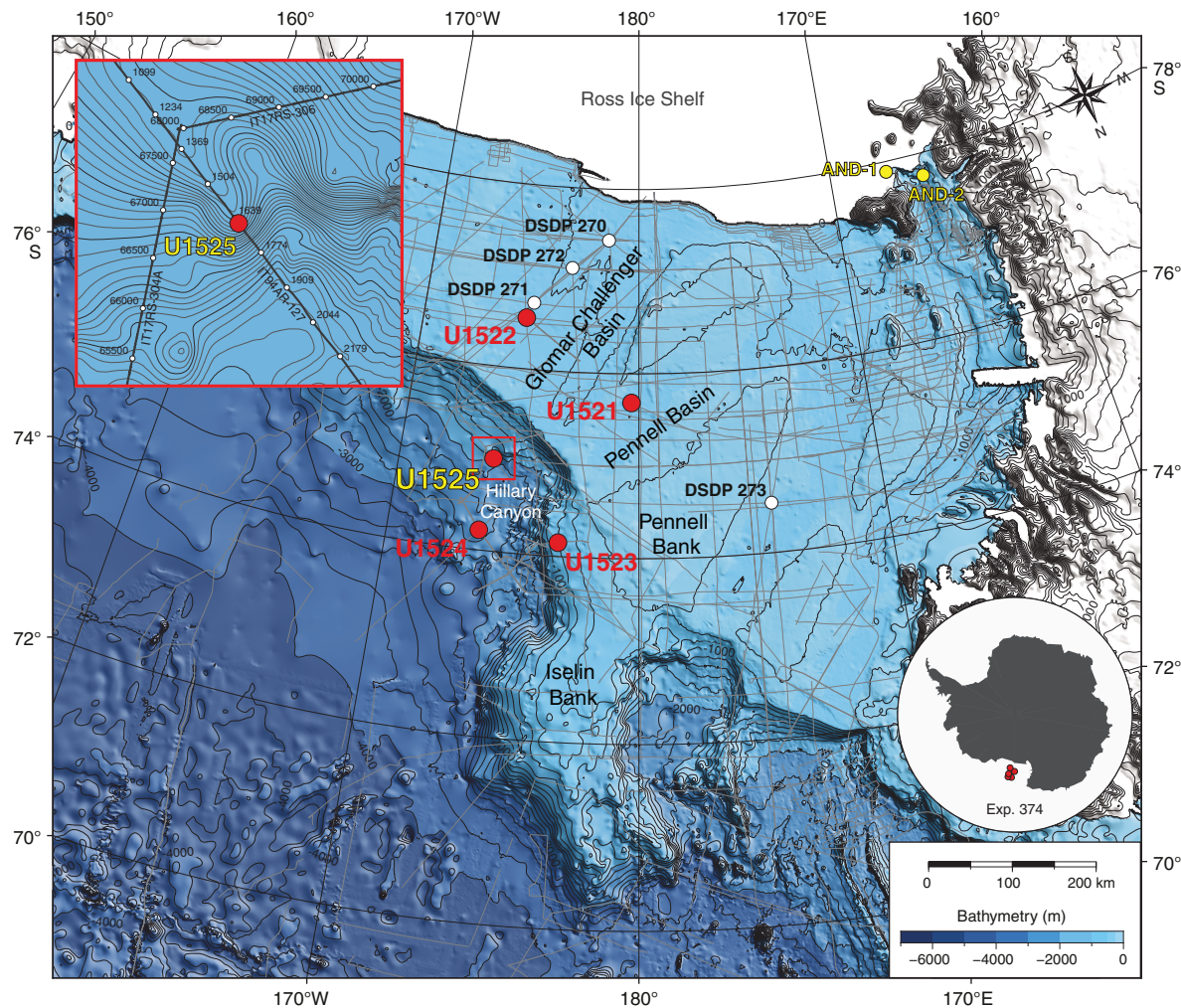


Figure F22. A. Seismic profile Line IT94AR-127 across Site U1525 (see inset in Figure F21). Multichannel reflection seismic profile collected by Istituto Nazionale di Oceanografia e Geofisica Sperimentale (OGS; Italy) under Programma Nazionale delle Ricerche in Antartide in 1994 (I. Finetti et al., unpubl. data). The seismic stack profile is available through the Antarctic Seismic Data Library System for scientific purposes. The source used was a 2×20 air gun (74.8 l), and data were acquired with a 1500 m streamer (120 channels, first offset = 164 m and last offset = 1664 m). Reprocessing of seismic Line IT94AR-127 for Expedition 374 was done by Riccardo Geletti (OGS). SP = shotpoint. B. Interpretation of key seismic reflectors in Line IT94AR-127.

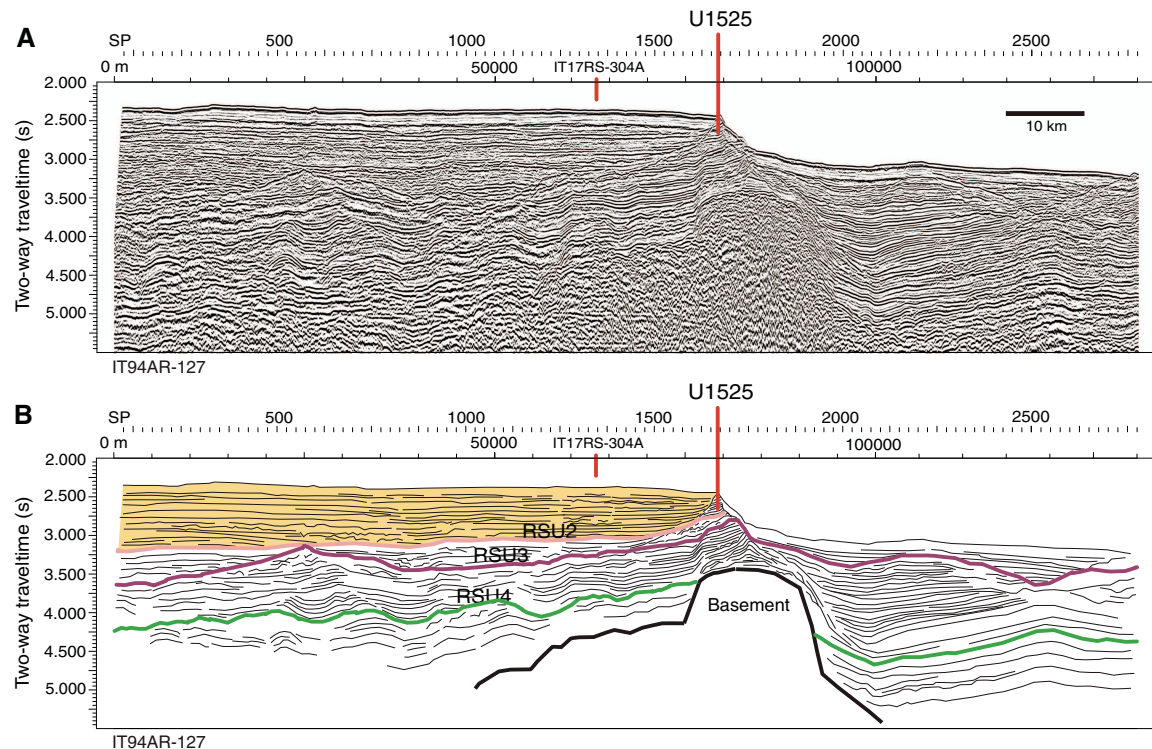


Figure F23. Site U1525 summary. Preliminary environmental interpretation is based on microfossil content. WRMSL = Whole-Round Multisensor Logger, SHMSL = Section Half Multisensor Logger.

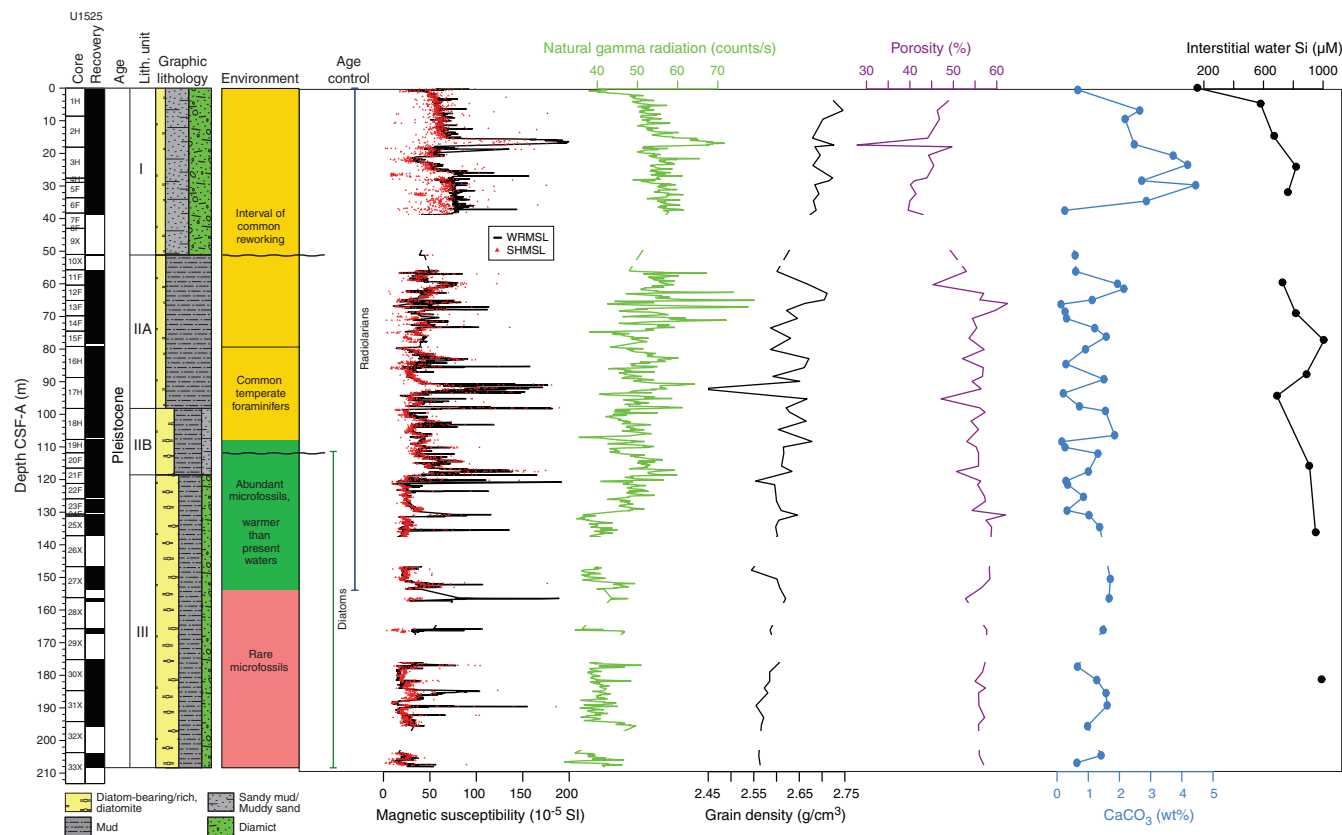


Figure F24. Composite seismic cross section showing transect approach from the continental shelf to the slope and rise. The seismic data have different resolutions and penetration depths because they were collected by several nations with different parameters and targets. Line BGR80-007 (24-air gun array 23.45 l) was collected by Bundesanstalt für Geowissenschaften und Rohstoffe (Germany) in 1980, Line ATC-208 (bolt-type air gun 35.58 l) was collected by the Institut Français du Pétrole (France) in 1982, and Lines IT94-127A (2 × 20-air gun array 74.8 l) and IT17RS-303B (air gun 3.44 l) were collected by Istituto Nazionale di Oceanografia e Geofisica Sperimentale (Italy) under Programma Nazionale delle Ricerche in Antartide in 1994 and 2017, respectively. DSDP = Deep Sea Drilling Project.

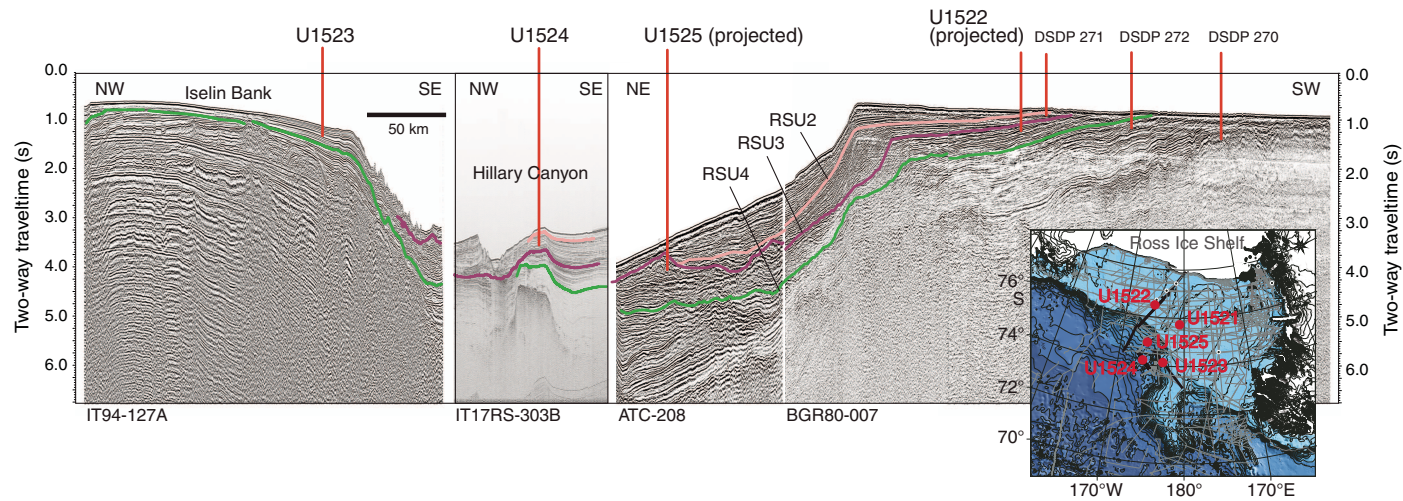


Figure F25. Microfossils from Ross Sea sediments, Expedition 374. Specimen sizes = ~20–200 µm. Diatoms: A. *Thalassiosira vulnifica* (U1523B-10F-CC). B. *Actinocyclus karstenii* (U1523B-10F-CC). C. *Actinocyclus* sp. B of Harwood and Maruyama (1992) (374-U1523E-16F-CC). D. *Actinocyclus maccollumii* (U1523E-10F-CC). Radiolarians: E. Actinomimid radiolarian (Hole U1523A mudline). F. Spongodiscidid radiolarian fragment (Hole U1523A mudline). G. *Spongoplegma* (?) spp. (Hole U1523A mudline). H. *Spongopyle* spp. (Hole U1523A mudline). Foraminifers: I. *Cibicidoides grossepunctatus* (U1523B-11F-CC). J. *Globocassidulina biora*, pustulose form (U1522A-2R-CC). K. *Globoconella inflata* (U1525A-16H-CC). L. *Nonionella iridea* (U1521A-21R-CC). Dinoflagellates: M. *Selenopemphix* sp. 1 (U1525A-27X-CC). N. *Selenopemphix bothrion* (U1523B-20F-CC). O. *Lejeuneacista* sp. cf. *L. communis* (U1523B-22F-CC). P. *Operculodinium? eirikianum* (U1521A-16R-CC).

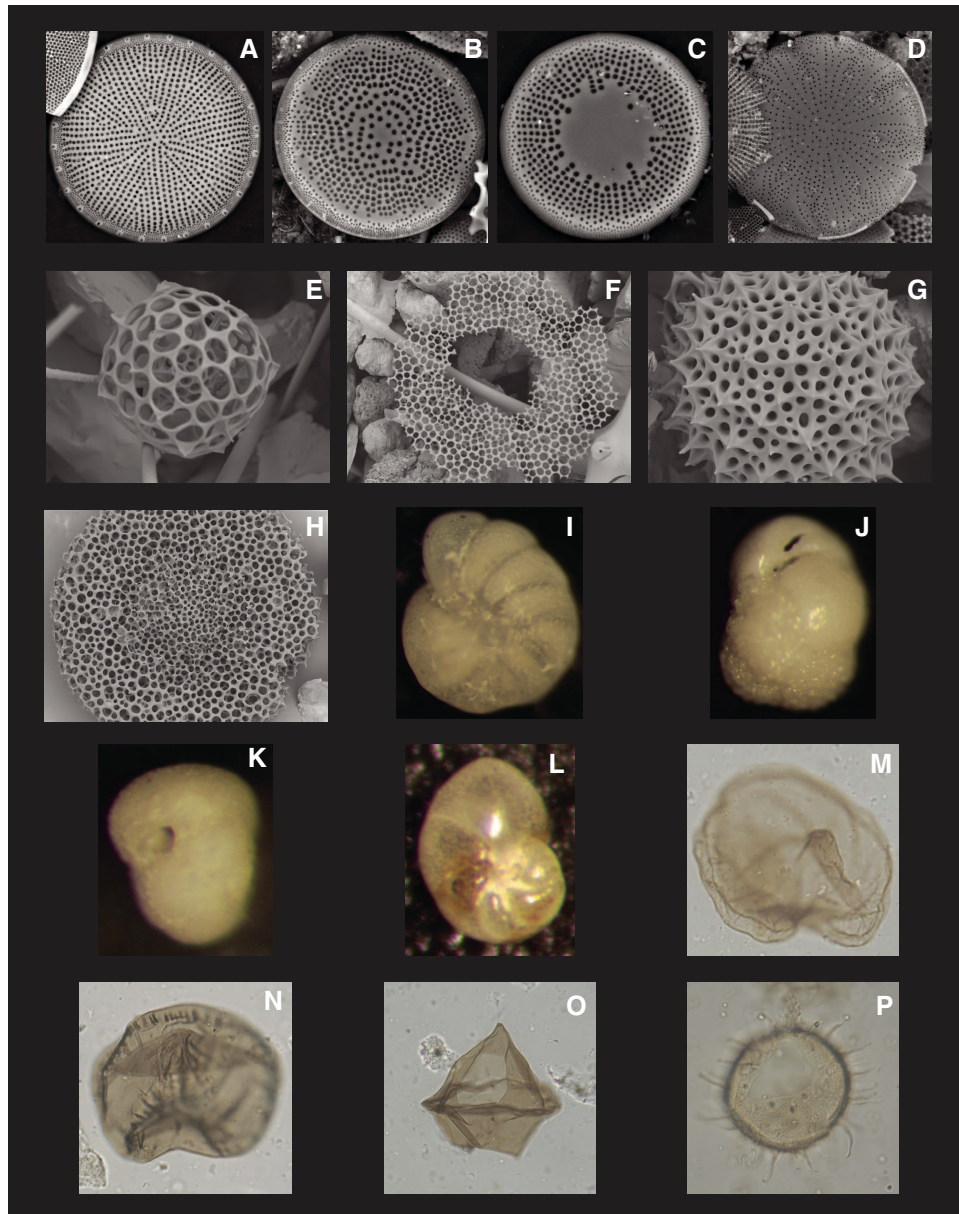


Figure F26. Diatom specimens from Ross Sea sediments, Expedition 374. A–F. *Actinocyclus karstenii*. (A, D: U1523E-10F-CC; B–E and F [interior view]: U1523B-10F-CC). G. *Actinocyclus* sp. B of Harwood and Maruyama (1992) (U1523E-16F-CC). H. *Stellarima microtrias* (U1523B-10F-CC). I–K. *Actinocyclus maccollumii* (U1523E-10F-CC; I [interior view]). L. *Thalassiosira striata* (U1523E-16F-CC). M, N. *Thalassiosira vulnifica*, M with corroded valve (U1523E-10F-CC). O. *Thalassiosira webbi* (U1523B-10F-CC). P. *Thalassiosira kolbei* U1523B-10F-CC). Q, R (internal view), S, T. *Thalassiosira torokina* (Q, R: U1523E-10F-CC; S, T: U1523E-16F-CC).

